Università degli Studi di

DIPARTIMENTO DI INGEGNERIA INDUSTRIALE DII
Corso di Laurea Magistrale in Ingegneria Chimica e dei Processi Industriali

Tesi di Laurea Magistrale in
Ingegneria Chimica e dei Processi Industriali

Experimental investigation on horse manure drying for an efficient and self-supporting combustion

Relatore:
Prof. Paolo Canu

Correlatore:
PhD Luca Da Lio

Laureando:
Giovanni Nardin
Matricola 1210008

Anno Accademico 2019/2020

Abstract

This work investigates the horse manure drying process to make it suitable for an efficient combustion. Customized furnaces will be required, where drying and burning are integrated. Several drying devices having different air-manure contact configuration have been experimentally designed, assembled and tested. They include an aerated hopper, a fixed packed bed dryer and a rotary dryer in both through-circulation and cascade configuration. Up to the desired moisture content (30%) a constant drying rate often prevails. It is proved that static dryers do not assure an homogeneous drying within the volume, because the drying air follows preferential paths, controlled by the bed porosity distribution. Conversely, dynamic dryers (drums) enhance the particle-air contact by continuously mixing the material and achieve a more uniform moisture content. Consequently, the investigation focuses on variables influencing the drying process in rotary dryers. The coupled effect of the rotation speed and the number of flights on the air-material contact is explored. The drying process is affected mainly by the air temperature and the air flow rate. In addition, it is shown that hot (and wet) flue gasses can be directly used as drying stream without significant performance decline. Finally, a 0D predictive drying model and preliminary scale-up indications for a real industrial application are developed.

Riassunto

Questo lavoro di tesi indaga il processo di essiccazione dello stallatico di cavallo al fine di rendere tale biomassa adatta a una combustione efficace. Saranno necessarie fornaci dedicate, dove le operazioni di essiccazione e combustione sono integrate. Sono stati sperimentalmente progettati, costruiti e testati quattro essiccatori caratterizzati da diverse configurazioni di contatto aria-solido. In particolare, essi sono una tramoggia aerata, un essiccatore a letto fisso e un essiccatore rotante implementato secondo le configurazioni a "flusso attraverso il materiale" e a "cascata". L'essiccazione del materiale avviene prevalentemente a velocità costante fino al raggiungimento del contenuto di umidità desiderato (30%). Viene dimostrato che gli essiccatori statici non garantiscono un'essiccazione omogenea all'interno del loro volume perchè l'aria essiccante segue cammini preferenziali controllati dalla distribuzione della porosità del letto. Al contrario, gli essiccatori dinamici (tamburi) assicurano il contatto aria-materiale attraverso il continuo mescolamento dello stallatico e garantiscono un contenuto di umidità più uniforme. Di conseguenza, l'indagine sperimentale si concentra maggiormente sulle variabili che influenzano il processo di essiccazione negli essiccatori rotanti. Viene dunque esplorato l'effetto accoppiato della velocità di rotazione e del numero di mescolatori interni sul contatto aria-materiale. L'essiccazione è particolarmente sensibile alla temperatura dell'aria e alla portata dell'aria. In più, viene dimostrato che i fumi di combustione, caldi e umidi, possono essere utilizzati come flusso essiccante senza che si verifichi una diminuzione di prestazioni. Infine vengono sviluppati un modello predittivo 0D e delle indicazioni preliminari finalizzate al passaggio dalla scala pilota a quella finale.

Contents

Introduction

In Veneto region, there are over a hundred horse stables. The horses housed there in are fed with hay and each of them produces between 8 and 14 tons of manure per year. Horse manure is an heterogeneous mixture composed of horse solid and liquid dejections and bedding materials such as straw, wood shavings, sawdust with different percentage depending on the stall management. Manure is regularly removed from the stables and the bedding material is replaced. The removed manure management, concerning duration and arrangement (out/indoor) of the storage, could significantly alter the dry matter, thus the energy content.

Usually, the material is disposed of in fields and in landfill. The recovery and landfill disposal costs may vary between different local waste disposal companies but they can be significant for large horse stables.
An interesting alternative to the above mentioned possibilities is the energy exploitation in furnaces for heat production. However, since the manure is porous and hygroscopic, it has an high moisture content that prevents the manure combustion as collected from the stables. Instead, once properly dried it burns effectively like a woody biomass. This is the reason why the drying is a crucial step for the energetic use of this poor biomass.

Scopes and goals

In this work an experimental investigation on horse manure drying is performed in order to make it suitable for an efficient combustion. Customized furnaces will be required, where drying and burning are integrated.

The attention is focused on the selection of the proper drying device and on the effect of the design variables on drying performances. Thus, four different dryers (i.e., aerated hopper, packed fixed bed, through-circulation rotary dryer and cascade rotary dryer) are designed, engineered and assembled in pilot-scale. A sensitivity analysis on drying performance with respect to air conditions (i.e., temperature,

flow rate, absolute humidity) and the air-solid contact intensity is performed.
The final goal is to integrate the drying process within a manure-fired furnace in order to produce the dry manure in real-time for the furnace. According to the author's knowledge, the leader manufacturers of biomass boilers are not able to burn the manure without a substantial addition of wood chips to compensate the presumed "poor" fuel quality.
The dryer design guidelines are:

- High performances: short drying time, little air flow rate;
- Compactness: small space needed;
- Simplicity: in the manufacturing and in the operating perspective;
- Cost reduction: little capital and operative costs;
- Turn-key: completed, integrated and ready-to-use.

Thesis structure

The thesis is drawn up in five different Chapters.
Chapter 1 is a critical overview of the drying phenomenon and of the batch and continuous industrial technology that are available on the market.
Chapter 2 presents the materials and the devices developed and built to carry out the experimental investigation. Moreover the analytical instrumentations, the experimental methods are described too.
Chapter 3 critically analyses all the results obtained from the experimental tests.
Chapter 4 presents the rotary dryer numerical methods and evaluates the numerical results.
Chapter 5 draws the conclusions and takes stock of the effectiveness of the dryers.

Chapter 1

Critical overview

This Chapter summarizes with the fundamentals of drying process. Firstly porous hygroscopic and non-hygroscopic materials are presented and then different types of moisture are explained. In particular, hygroscopic materials are those with high quantity of bounded water whereas non-hygroscopic have a negligible amount of physically bounded water. The description of the drying process is deeply investigated through the drying curve and the main limiting factors in drying process are discussed as well. Finally, the most important batch and continuous industrial drying operations are investigated: the former is suitable for small production and valuable material, the latter is used when higher productivity is required.

1.1 Hygroscopic and non-hygroscopic materials

The material interaction with the water is extremely important to understand how the moisture can be removed in a proper way. The attention is focused on the water which is retained inside a porous solid. The bound moisture in a solid exerts an equilibrium vapour pressure lower than that of pure water at the same temperature, while the unbound moisture is the moisture contained by a solid which has the same vapour pressure of the pure water at the same temperature. A wet solid might be non-hygroscopic or hygroscopic.

Non-hygroscopic materials are characterized by pores full of water, when the material is saturated, or full of air when it is dry. The amount of physically bounded water is negligible. The vapour pressure of water is only function of temperature. Over a certain moisture content, every material behaves like the non-hygroscopic. Some typical non-hygroscopic materials are sand, polymeric granules and glass spheres.

Hygroscopic materials have a high quantity of bounded water. The vapour pressure of the internal water is smaller than the one of the pure water and it

Table 1.1: Definitions of properties commonly used in drying literature.

Term/symbol	**Meaning**
Adiabatic saturation temperature, T_{as}	Equilibrium gas temperature reached by unsaturated gas and vaporizing liquid under adiabatic conditions. (Note: For air/water system only, it is equal to the wet bulb temperature, T_{wb}).
Bound moisture	Liquid physically and/or chemically bound to solid matrix so as to exert a vapor pressure lower than that of pure liquid at the same temperature.
Constant rate drying period	Under constant drying conditions, drying period when evaporation rate per unit drying area is constant (when surface moisture is removed).
Dew point	Temperature at which a given unsaturated air-vapor mixture becomes saturated.
Dry bulb temperature	Temperature measured by a (dry) thermometer immersed in vapor-gas mixture.
Equilibrium moisture content, X*	At a given temperature and pressure, the moisture content of moist solid in equilibrium with the gas-vapor mixture (zero for non-hygroscopic solids).
Critical moisture content, X_c	Moisture content at which the drying rate first begins to drop (under constant drying conditions).
Falling rate period	Drying period (under constant drying conditions) during which the rate falls continuously in time.
Free moisture, X_f	Moisture content in excess of the equilibrium moisture content (hence free to be removed) at given air humidity and temperature.
Humid heat	Heat required to raise the temperature of unit mass of dry air and its associated vapor through one degree ($J\,kg^{-1}\,K^{-1}$ or Btu $lb^{-1}\,{}^{\circ}F^{-1}$).
Humidity, absolute Y	Mass of water vapor per unit mass of dry gas (kg_{vap} kg^{-1}_{d-air} or lb_{vap} lb^{-1}_{d-air}).
Humidity, relative	Ratio of partial pressure of water vapor in gas-vapor mixture to equilibrium vapor pressure at the same temperature.
Unbound moisture	Moisture in solid which exerts vapor pressure equal to that of pure liquid at the same temperature.
Water activity	Ratio of vapor pressure exerted by water in solid to that of pure water at the same temperature.
Wet bulb temperature, T_{wb}	Liquid temperature attained when large amounts of air-vapor mixture is contacted with the surface. In purely convective drying, drying surface reaches Twb during the constant rate period.

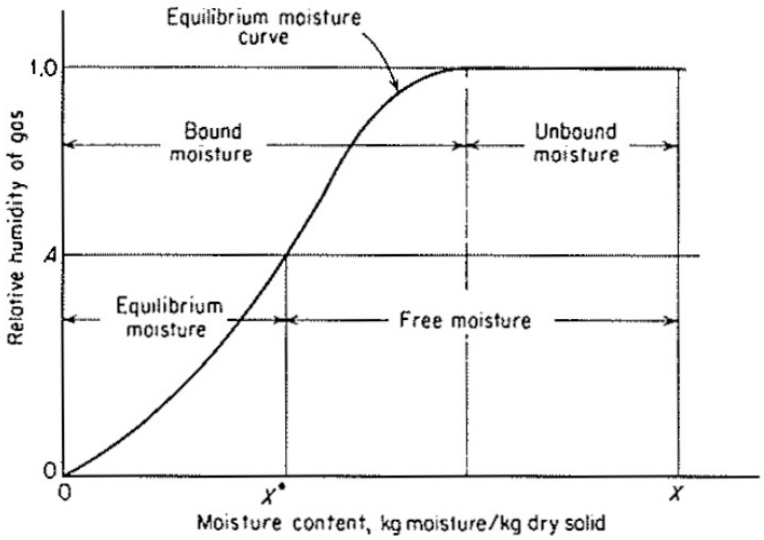

Figure 1.1: Types of moisture [1].

is not only function of the material and the temperature but also of the moisture content. Typical hygroscopic materials are zeolites, wood shavings and sawdust.

In Figure 1.1 the equilibrium moisture curve is reported. It is a graphical description of the relation between the solid moisture content X and the relative humidity of the drying air supplied at constant conditions.

The moisture content of the solid X is the moisture to dry mass ratio which can assume values greater than 1.

$$X = \frac{m_m}{m_d} \tag{1.1}$$

The relative humidity of the drying air (RH) is the ratio of the vapour pressure of the water vapor in the air and the one of the pure water. If a wet solid is exposed to continuously supplied drying air with a relative humidity A, the solid releases moisture by evaporation until the concentration reaches the equilibrium curve at X^*. The excess of moisture from the equilibrium content is the free moisture, which is the evaporated one. The solid still contains an amount of water that can be removed using dryer air. Note that the above curve depends on the thermo-hygrometric characteristic of the drying air, i.e., temperature and specific humidity. When air temperature is increased, the curve shifts to the left reaching lower values of moisture content for the same air relative humidity [2].
For the sake of clarity, Table 1.1 summarizes all these concepts.

The equilibrium curve of the specific material also depends on the particle size and the specific surface distribution [1].

There are different metrics to express the moisture content. The mass fraction of the moisture in the wet solid (u) is the ratio of the mass of the moisture in the solid to the total mass of the solid which is always less than 1.

$$u = \frac{m_m}{m_m + m_d} \tag{1.2}$$

The ratio between the actual material mass m and the initial one m_0 is known as W/W_0 and is widely used to describe the variation of the material weight during time.

$$W/W_0 = \frac{m}{m_{@t=0}} \tag{1.3}$$

Relationships among the above variables are:

$$u = \frac{X}{1+X} \qquad X = \frac{u}{1-u} \tag{1.4}$$

$$u = 1 - \frac{(W/W_0)_{t=\infty}}{W/W_0} \qquad W/W_0 = \frac{1}{(1-u)\cdot\left(1+\frac{u_0}{(1-u_0)}\right)} \tag{1.5}$$

1.2 Process of drying

The drying process aims to reduce the moisture content in a solid matrix often porous. This process was widely studied long ago by W.K. Lewis [3] and by W.R. Marshall [4]. Depending on the available energy source, the drying processes are classified in low and high temperature ones.

1.2.1 Low-temperature drying

One of the most diffuse drying technique is the low temperature convective drying. It consist on drying of wet material by a forced low RH air flow while the solid temperature is kept lower than the boiling point of water. The energy required for the moisture evaporation is supplied by the airflow in convective regime. In order to describe the physical phenomena occurring during the drying process, let's consider a batch drying test in a cabinet, where a generic granular material is dried using air under constant drying conditions. The test must record the weight loss due to the evaporation during time. Figure 1.2a shows the expected moisture content vs time. This representation is useful to evaluate the drying time. Four zones can be

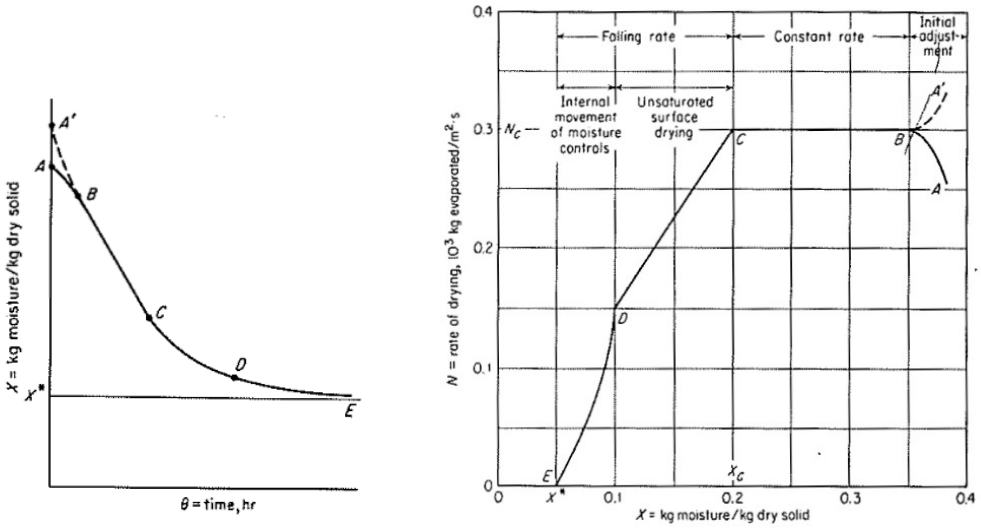

(a) (b)

Figure 1.2: Batch drying test at constant drying conditions [1]: drying curve (a); drying-rate curve(b).

distinguished from the initial moisture content to X*, the equilibrium one 5. These zones have different drying-rates (N).

$$N = -\frac{m_d}{A} \cdot \frac{\Delta X}{\Delta \theta} \tag{1.6}$$

Where m_d is the mass of the dry solid, A is the cross sectional area of the bed to the airflow and the ratio $\Delta X/\Delta\theta$ is the average derivative of the moisture content with respect time. Since the ratio is negative there has to be a minus sign in order to obtain a positive velocity. N is the mass drying-rate per unit of surface ($\mathrm{kg\,m^{-2}\,s^{-1}}$).

In Figure 1.2b, the drying-rate N as a function of the moisture content X is shown. It is read from right to left. The initial adjustment AB is often neglected because it is small compared to the others periods. In this period the system varies his temperature until it reaches the equilibrium temperature. The velocity increases if the surface temperature is lower than the equilibrium one (AB) and vice versa (A'B).

In the BC interval, the drying-rate is fairly constant. In fact, heat and vapour transfer occurs only on the external surface of the material because of the continuous diffusive rise to the surface of unbounded water from the internal pores that act like moisture reservoirs. This phenomena is caused by the gradient in concentration between the inner and external part or by capillarity if the material is porous. Through BC, a thin layer of moisture covers the external surface of the material. The surface of the particle is wet enough to saturate the layer of air adjacent to it

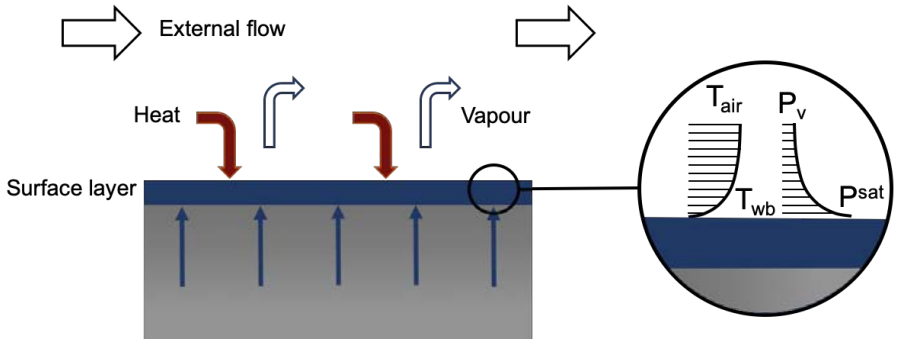

Figure 1.3: Constant drying-rate period.

[2]. A schematic representation of this physical mechanism is shown in Figure 1.3. Here, the heat flux is used for the moisture evaporation without increasing the temperature. The particles behave like the wet bulb of a wet thermometer. Thus their temperature is the wet bulb temperature of the gas stream and it is constant. During this stage, the drying rate depends on the medium properties (e.g. pore size and permeability) and on the external conditions such as air temperature, relative humidity, velocity, and flow configuration [6]. The drying-rate is kept constant until liquid is provided to the external surface at higher rate than the evaporation one [1].

The decreasing drying-rate period CD starts when the dry spots appear on the surface. The vapour pressure is now less than the saturation one. For this reason, the vapour flux decreases and the heat provided by the airflow to the medium is higher than the one required to evaporate the external moisture. Consequently, the exceeding heat increases the temperature of the material surface, while decreasing the moisture content [6].

In the DE interval, the curve of the drying-rate changes its slope. It starts when the liquid water is unable to reach locally the surface since before it evaporates. The drying phenomenon is now inside the particle. Two zones can be observed in the material: an inner zone, where liquid capillarity prevails, and an external one, where dominates the vapour flux due to molecular diffusion [5]. The inner zone reduces as the drying proceeds. The process ends when the inner temperature is equal to the external one and the moisture content is the equilibrium one, X^*.
The low-temperature drying is widely used in processes where the wet material is a secondary raw material, such as biomass intended for combustion process. Accordingly, the experimental investigation carried out in this work deals with low temperature drying methods.

1.2.2 High-temperature drying

When the temperature of the wet porous material is kept higher than the boiling point of the water, the process is called high-temperature drying. It is generally faster and higher energy consuming than the previous one but some material can degrade by the exposure to high temperature.
The internal evaporation of water also causes an overpressure inside the material. The gradient of pressure further supports the moisture transport, both in the vapour and in the liquid phase, to the external surface. The temperature of the porous medium has to be higher than 100 °C for a certain time, at atmospheric pressure, to get an overpressure. This is the case of those material that are not damaged by high temperature such as sludge, coal and beet pulp. It is possible to reduce the required temperature decreasing the external pressure. In this way the water boiling point decreases and the material can be dried in a less critical condition. This is the principle of vacuum drying, particularly useful for lumber, food and pharmaceuticals that would be damaged by high temperature levels. In these cases, the external surface is saturated of water and the overpressure is enough to let the moisture exit in a liquid phase.

1.3 The limiting factors for drying performances

In any drying process, the aim is to dry the material in the shortest time. In order to reach this goal, the key of the process optimization is to identify (possibly measuring specific material properties) the drying limiting mechanism. The limiting factors of a generic drying process can be grouped in two classes [7]:

- heat and mass transfer limitations;
- equilibrium condition.

Heat and transfer limitations appear when it is not supplied enough heat to the evaporation process. Such limitations depends on solid characteristics (e.g. porosity), the inlet and outlet moisture content, the heat rate, the temperature of the drying air and the heat losses [7]. A typical example of heat and mass transfer limitation is when the airflow heat content is insufficient to provide the evaporation latent heat, which is required by the wet solid to evaporate. The air flow rates or its temperature needs to be improved. Heat and mass transport limits the process when the solid residence time is too short. Material structure, particle size and temperature affect the drying kinetic. For instance, increasing the hot air rate, the heat given is suitable but the solid residence time in the dryer is still too small.
Finally, the equilibrium moisture content is the minimum achievable using a specific

air flow (fixed temperature and relative humidity of air). The equilibrium moisture content increases with the relative humidity of the air, as shown in Figure 1.1 or with a decrease of air temperature. So that, depending on the external air conditions, the material shifts the equilibrium moisture content. That is the reason why the material can regaining moisture during the storage.

1.4 Batch operations

Drying operations can be broadly classified according to whether they are batch or continuous [1]. In both these configurations the gas stream continuously flows, so that the difference between them lays only on the solid material being dried. The batch processes are suitable for small-scale operations where valuable material are dried.
Batch equipment is operating intermittently or cyclically under un-steady-state conditions: the dryer is charged with the wet material which remains in the dryer until dried. Finally, the material is unloaded. Then a new cycle begins.
It is a relatively expensive operation and it is consequently limited to pilot plant or for those material that are little influenced by added expenses in the discontinuous drying operation.

The tray dryer, also called cabinet, is a widely diffused drier, Figure 1.4. It is used to dry solid materials that need to be supported on a tray. The cabinet has different trays where the material is spread. Once the trays are charged, the cabinet is closed and the hot air blown by a fan flows across and between the trays. It is blown by a fan. When the drying is completed, the cabinet is opened, the tray is extracted and replaced by a new batch.
The dryer must be insulated from the external for two reasons: the reduction of the

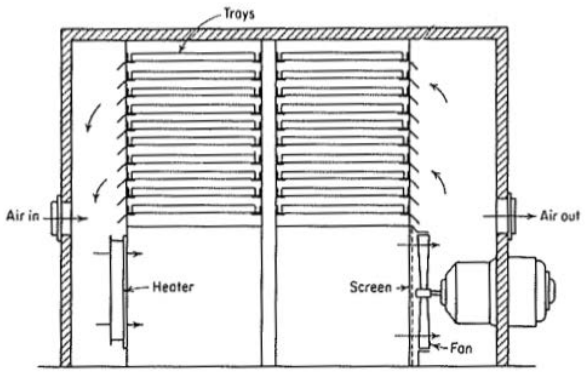

Figure 1.4: Typical tray drier [1].

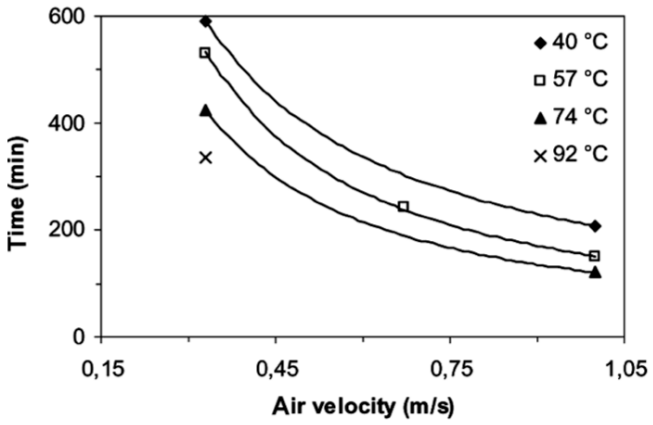

Figure 1.5: Total drying time versus air velocity for various air temperature in the wood chips drying runs [8].

heat losses and the maintenance of the internal wall at temperature above the dew point of the air to prevent the condensation of the moisture upon the wall.
In this dryer the mechanism of drying is the cross-circulation drying. The drying rate is established by the flux that reaches the solid surface. The drying occurs from the upper surface. The drying surface receives heat by convection from the gas stream which flows over the trays and by conduction through the solid [1].

Another batch dryer is the packed fixed bed dryer in which the drying medium flows through the wet solid bed. This is a low temperature process.
The exchange of heat and moisture does not take place in the whole bed, but it is limited to a finite zone called the drying zone. The drying zone moves through the bed following the airflow direction. In the drying zone, moisture and temperature gradients are present in both the gas and solid phase. Wet material is present at the front of the drying zone, where no drying occurs since the air is more or less saturated by moisture. Behind the drying zone, where the drying is completed, the material has reached a state of equilibrium with the hot drying air [9].
Many studies[10], [8],[6][11],on this configuration, were carried out on wood chips. The most important parameters which affect the drying process are: air temperature, velocity, relative humidity, bed height and pressure drop through the bed.
The characteristics of the drying medium have a strong impact on the process. As shown in Figure 1.5, as soon as the air temperature is increased, the total drying time decreases. Increasing the air velocity, the heat and mass transfers are improved so the drying time decreases.
The relative humidity of the air is the driving force of the process. The farther the air is from the saturation, the greater the driving force.

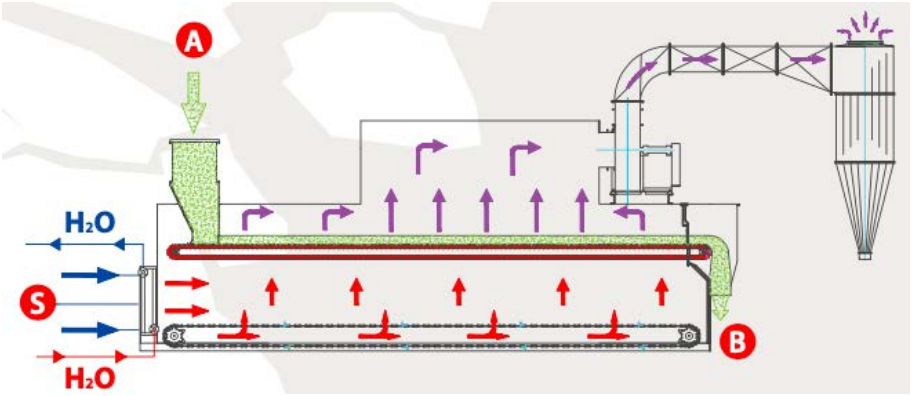

Figure 1.6: Packed moving bed dryier by Scolari s.r.l.

The bed height impacts on the drying time and also on the operative costs. The higher the bed height, the higher pressure drop across the bed and the greater blowing costs [11].

A solution, inspired by the packed bed is an aerated hopper, also considered in this thesis work. It is used in the drying of polymeric pellets. This configuration provides the air inlet in the hopper through louvers placed on the sloping sides. The air flows through the material as in the through-circulation configuration. The hopper has some great advantages to reduce the overall volume of the drying unit and to allow for storage and drying in the same static device. The material can be discharged thanks to gravity.

1.5 Continuous operations

Compared to batch solutions, continuous drying offers many advantages: the needed equipment is smaller with respect to the productivity; it allows for continuous operation avoiding intermediate storage; the product has a more uniform moisture content and the costs of drying per unit of product are lower [1].

Continuous industrial drying is carried out in different ways according to the operative requirements and the material characteristics. The most common used technologies are packed moving bed, through-circulation rotary dryer and cascade rotary dryer.

A packed moving bed (PMB) dryer is shown in Figure 1.6. Here the wet biomass in (A) is fed from a hopper to a moving bed. The conveyor belt is perforated to allow the air inlet (S) to flow through the bed. Before contacting the material, the airflow is preheated through an exchanger with a hot fluid (often H_2O). The dry

biomass is collected in point (B).

The drying air path may be different according to the design. Fans blow heated air through the solid, usually upward through the wet solid and downward after the initial drying has occurred. In this way a more uniform moisture concentra-tion throughout the bed is obtained [1], [6], [8].

The advantages of the PMB dryer include its relatively simple structure, low capital cost, and high drying efficiency with the recycling of the drying air. However, this type of dryer has difficulties in using a high temperature air and thus it is only suitable for required final biomass moisture content above 15% [12].

Rotary dryer is one of the most important group of dryers. The rotary dryer is relatively expensive compared to the other drying devices [6] but it is suitable for high productivity that can be achieved at higher temperature [12].
It is a long cylindrical drum that rotates around its axis. The wet material is fed from one side of the rotary drum and it proceeds through it thanks to the small angle inclination of the axis. Hot air flows through the drum either co-current with the solids or counter current to them. This is usually an high temperature process, carried out up to 500 °C for sand, concrete and other inert materials. In order to avoid the biomass ignition inside the dryer, the material in the outlet must not be overheated, in fact, the air temperature must be lower than the auto ignition temperature and the co-current arrangement is suggested.
The rotary dryer can be divided into three sections: two of them are static while the other one rotates. In the inlet section there is a chute that feeds the wet particles to the drum and also feeds the connection with the hot air duct. The outlet section separates the dry solid from the gas stream. The outlet gas are sent to a cyclone and to a bag filter in order to separate the dust (fine entrainments) and limiting the particulate emission. The drying section is the core of the dryer because the drying take place in it. Depending on the contact between the wet material and the airflow in the drying section, two main classes can be distinguished: through-circulation rotary dryer and the cascade rotary dryer.

Through-circulation rotary dryer is shown in Figure 1.7. The dryer section is characterized by a slowly revolving tapered drum with louvers to permit entrance of the hot gas stream beneath the solid [1]. The gas is admitted only to those louvers which are underneath the bed of solid. Solid showering does not appears and the dust is limited. It combines the capacity of the rotary dryer that keeps the material moving, avoiding aggregation, with the one of the through-circulation that forces the overall air to flow through the material.

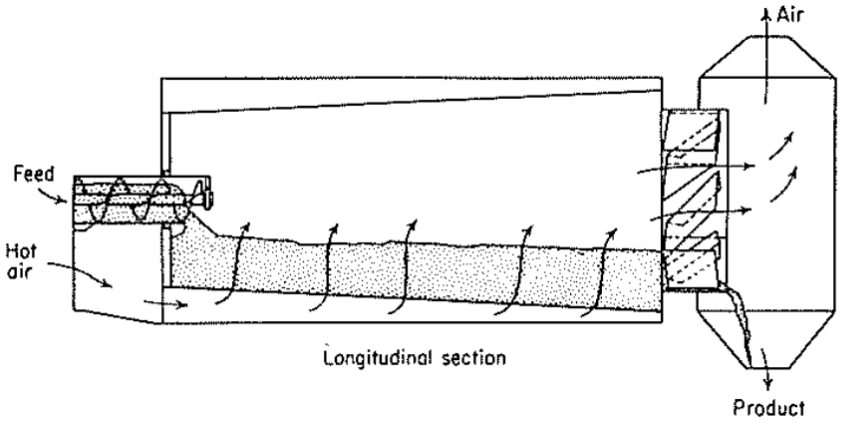

Figure 1.7: Through-circulation rotary dryer [1].

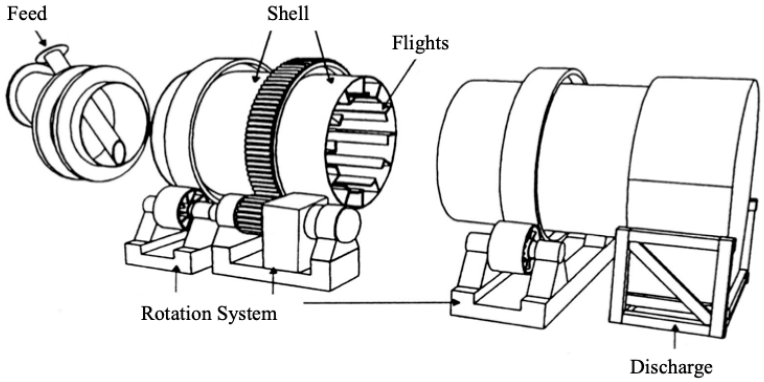

Figure 1.8: Cascade rotary dryer for biomass drying [14].

Cascade rotary dryers are characterized by lifting flights extending from the cylinder wall for the full length of the dryer that lift the solid and shower it down in a curtain through the air. The air flows in axial direction and they are effective for both sawdust and chips [13]. They are deeply investigated in the following.

1.5.1 Cascade rotary dryer

In the cascading rotary dryer, Figure 1.8, the particles are mechanically fluidized thanks to the coupled effect of the rotation and the flights [15]. Generally, to achieve this configuration, the ratio between the centrifugal and gravitational forces acting on the particle ν should be into the range 0.0025 - 0.04

$$\nu = r_e \frac{\omega^2}{g} \tag{1.7}$$

where r_e is the distance of the flight from the axis, ω is the rotation speed and g the gravity constant. The flights are fin-like structures on the drum wall that lift

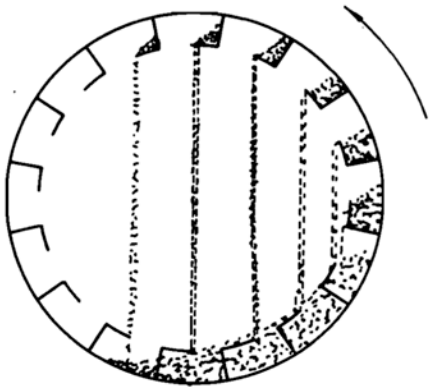

Figure 1.9: Drum cross-section [15].

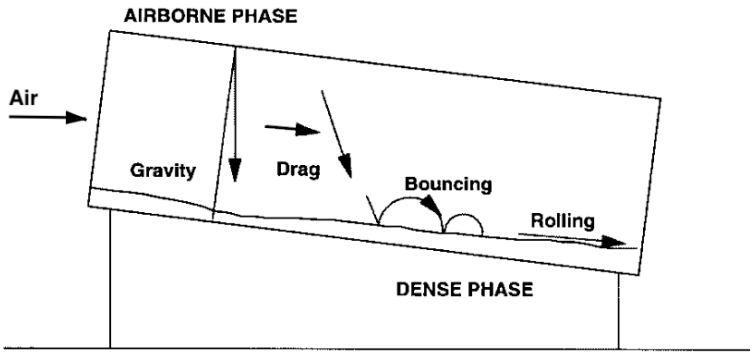

Figure 1.10: Mechanisms of particle movement along the drum [7].

up the material to shower it later through the hot gas stream as a raining curtain. This process is fundamental because there is a strong interaction between the wet particles and hot air, so that a high heat and mass transfer is guaranteed. This solution provides a better heat and mass exchange than with in a packed bed dryer. Moreover, all particles have an homogenous moisture distribution in the same cross-section since they are exposed to the gas stream for the same amount of time.

Figure 1.9 shows a number of cascades of particle falling down from the flights on the cross sectional area of the dryer. The shower can be improved acting simultaneously on the rotating speed and the flights number and shape.
The particles have an intermittent motion, being continuously lifted up by flights and falling in the cascade. During the shower they are exposed to the hot gas stream, in orthogonal paths. Since the drying mostly takes place during the particle cascade [2] this continuous motion is extremely important.

The axial motion depends on several variables related to the axis inclination, as sketched in Figure 1.10. Gravity is the main force, it acts on the airborne phase, combined with the air drag on the raining curtains. Then there is the bouncing

Table 1.2: Typical design specification [6],[16].

Design variables		
Mean air–vapor velocity counter-current (m/s)	v_{air}	2
Mean air–vapor velocity co-current (m/s)	v_{air}	3
Total holdup to volume fraction (%)	H/V	5 - 15
Length to diameter fraction (-)	L/D	2 - 20
Number of flights to diameter fraction (1/m)	n_f/D	5 - 10
Centrifugal to gravitational forces on the particle (-)	ν	0.0025 - 0.04

which occurs when the particles impact with the bottom of the dryer and the rolling when the particles slide down the sloping floor of the dryer. [7]

A typical problem affecting rotary dryer is the particle entrainment in the air stream which influences the residence time of the particle. It depends on different factors.

The first undesired phenomena is the drag which affects the falling particles in the drum. The air drags the particles in the flow direction changing the solid mass flow rate from the specification. Indeed in a co-current configuration, the air drag may cause a reduction in the particles residence time increasing the outlet mass flow rate and avoiding to reach the moisture content specification. While in the counter-current configuration, the air flow drags particles in the opposite direction to their desired one. Hence the particle axial motion is slowed down. The drag may determine an increase of the residence time and so the particle inside the drum may dry more than the required.

The second undesired phenomena occurring in the rotary dryer is the rolling of the particles in the bed at the bottom of the dryer. The rolling phenomena is more evident when the drum is overloaded: the flights are not able to lift up all the material, so a fraction of particles rolls over to the exit. The rolling bed increases the particle axial mobility because particles tend to slide on each other over the top of the bed [6].

All the above considerations result in some practical design rules based on industrial past experience. Among them the most useful for a first rough design are: the length to diameter fraction L/D and the total holdup to volume fraction H/V. The former is related to the particle residence time inside the drum and to the particle axial velocity. The latter is related to the possibility to have enough time and space to fly in the cascade and to reduce rolling phenomena. These practical design rules are collected in Table 1.2.

A common indicator of dryer performances is the evaporated mass flow rate per volume of dryer: typical values are 50, 60, 70 $\mathrm{kg\,h^{-1}\,m^{-3}}$ [17].

Chapter 2

Materials and experimental methods

The aim of this Chapter is to present the materials considered in the drying process and the devices developed and built to carry out the experimental investigation. Firstly, the materials are presented: manure, which is an heterogeneous wet mixture including horse faeces and wood shavings alone. Then, an economic preliminary estimation of the power from horse manure combustion is discussed to demonstrate the feasibility of the manure energetic use. The description of the drying equipments is deeply investigated including the aerated hopper and the rotary dryer. A detailed description of the oven for the manure emissions follows. The analytical instrument to monitor the weight loss and the front of evaporation during the drying process are presented too.

2.1 Materials

Horse manure is an heterogeneous mixture composed of horse solid and liquid dejections and bedding materials such as straw, wood shavings, sawdust with different percentage depending on the stall management (Figure 2.1). The bedding materials are used to keep the horse boxes dry and clean. Wood shavings is the main fraction, especially in the north of Italy and in Europe while in the south of Italy straw is preferred. The manure consistency resembles that of dirt, what's more the smell is not unbearable.

One of the key characteristic of horse manure with respect to combustion purposes is the high moisture content which is generally in the range 55-65%. The bounded moisture is mainly inside the solid dejections whose moisture content is greater than 75%. Additional parameters to characterize manure are summarized in Table 2.1.

Figure 2.1: Horse manure.

The manure is generally stored outdoor in big heaps where it is subjected to variable weather conditions. The storage duration can modify the moisture content and reduce the organic components while most of the ammonia content is released into the atmosphere. The manure mechanical handling is complex because of the material heterogeneity and the variable moisture content that makes it sticky. Moreover, the material can drastically increase its density if it is compressed and consequently the porosity of the bulk (empty volume over bed volume) can be very different from the local bed porosity.
The wet manure can be disposed of in three ways:

- used as fertilizer in their own ground;
- sold to a different farm, according to the fertilizers sale normative (Dlgs n75/2010) and previous registration at the fertilisers producers register;
- given to a certified company that collects, transports and disposes of the material in the authorized centre.

Since 2009 manure is a by-product suitable for energy production, in agreements to the Veneto region deliberation 2272 of 28/07/2009 and to the following European regulation 1262/2017 related to combustion of farm animals manure.

Table 2.1: Manure physical properties.

ρ_{bulk}	$\mathbf{u}_0$	$\mathbf{HHV}_{db}$	$\mathbf{LHV}_{db}$	$\mathbf{LHV}_{wb}$	$\mathbf{m}_{wb}$	$\mathbf{T}_{ai}$
kg/m^3	$\frac{kg_m}{kg_m+kg_d}$	MJ/kg	MJ/kg	MJ/kg	$\frac{\text{ton}}{\text{year horse}}$	°C
280	0.55 - 0.65	16 - 20	14 - 15	2 - 4	8 - 14	210

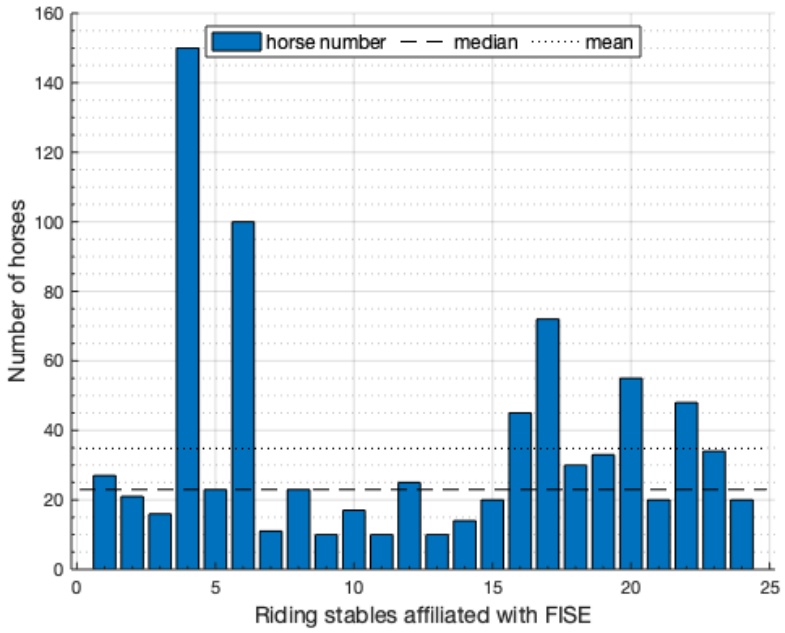

Figure 2.2: Horse number for each riding stable affiliated with FISE Veneto.

In order to produce energy by combustion, the heating value (HV) is a crucial parameter to the process cost-effectiveness. In Table 2.1 the mean values of HV measured during previous studies [18], [19] on different horse manure samples are reported. The manure lower heating value on dry basis is comparable to the one of non-wooden biomass (14-15 $\mathrm{MJ\,kg^{-1}}$) [18] [19] while the one on wet basis is extremely small (2-4 $\mathrm{MJ\,kg^{-1}}$), due to the large moisture content. In the following, the LHV on dry basis equal to 14 $\mathrm{MJ\,kg^{-1}}$ is considered. The dry manure auto ignition temperature (T_{ai}) in ambient atmosphere is 210 °C [18]. This is important to avoid an undesired combustion inside the ducts which leads to the furnace.
Also, the manure production rate per horse is a key parameter to estimate the energy potential of this biomass.
To determine the real potential of the manure in the energy production, a direct survey is carried out. It turned out that the mean production of manure for each horse is 8 to 14ton per year, in accordance with literature studies [20]. Moreover collecting information about the number of horses per stable allows to evaluate the most suitable size of the furnace. As shown in Figure 2.2 a common number of horses per stable is 23 (25 horse stables).

The stall management deeply influences the manure composition and, in turn, its properties. In fact, depending on the cleaning frequency of the stall, the faeces-bedding ratio changes. Since the wood shavings (Figure 2.3) are 80% on volume basis of the manure, more clean, more hygienic, easier to handle and more homogeneous

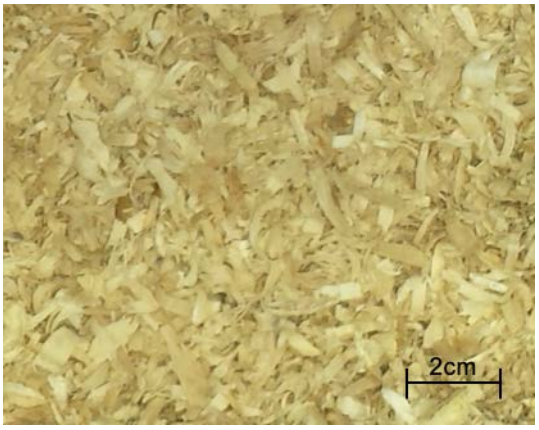

Figure 2.3: Wood-shavings.

than manure, they are used in the first part of the experimental campaign to get preliminary indications about manure behaviour. Considering that the wood shavings initial moisture content is equal to 9% they are rehydrated with water up approach the manure moisture content (60%).

2.2 From the horse number to a thermal power

For a manure fueled furnace and without storage, the manure availability in the stable determines the furnace size. In fact, the dry manure is the fuel that permits the combustion: the higher the manure production rate, the higher the furnace power.
In the following, a simple relation between the furnace power and the horse number is derived. The lowest values of LHV_{db} and manure production rate in Table 2.1 are considered. The weekly manure production $\dot{m}_{wb}$ ($kg_{wb}\ week^{-1} n_{horse}^{-1}$) is obtained by simple conversion:

$$\dot{m}_{wb}^{w} = \dot{m}_{wb}^{y} \cdot \frac{1000}{n_{w/y}} \tag{2.1}$$

where $\dot{m}_{wb}^{y} = 8\ \mathrm{ton}_{wb}\ \mathrm{year}^{-1} n_{horse}^{-1}$ is the mass manure production for each horse in a year, and $n_{w/y}$ is the number of weeks per year.

The amount of dry solid $\dot{m}_{d}^{w}$ ($\mathrm{kg}_{db}\ \mathrm{week}^{-1}\ \mathrm{n}_{horse}^{-1}$) is obtained as:

$$\dot{m}_{d}^{w} = \dot{m}_{wb}^{w} \cdot (1 - u_0) \tag{2.2}$$

where $\dot{m}_{wb}^{w}$ is obtained by Equation 2.1 and u_0=0.6 is the initial moisture content.

The heat power depends on the mass flow rates and the lower heating value, thus:

$$P = \dot{m}_d \cdot LHV_d \cdot n_{horse} = 1.4(\mathrm{kW\ horse}^{-1}) \cdot n_{horse} \tag{2.3}$$

Table 2.2: Furnace design variables for a 50 horse stable.

Horses	**P**	$\dot{m}_{db}$	$\dot{m}_{SP}^{out}$	$\dot{m}_{wb}^{in}$	$\dot{V}$
#	kW	kg/h	kg/h	kg/h	m^3/h
50	**70**	18	25.71	45	0.16

where P is the power (kW), $\dot{m}_d$ is the mass flow rates on dry basis ($kg\,s^{-1}$ $horse^{-1}$) and LHV_d is the lower heating value on dry basis (kW). Accordingly, the furnace power depends linearly on the horse number in a stable (Figure 2.4).
It is possible to find out, for a desired furnace power, the needed manure flow rate required at the target moisture content of u=30% at the furnace inlet, which is also the flow rate at the drying process outlet:

$$\dot{m}_{SP}^{out} = \frac{P}{LHV_d} \cdot \frac{1}{(1 - u_{SP})} \tag{2.4}$$

Finally the inlet flow rate for the drying process is obtained:

$$\dot{m}_{wb}^{in} = \frac{\dot{m}_{SP}^{out} \cdot (1 - u_{SP})}{(1 - u_0)} \tag{2.5}$$

The minimum number of horses to make manure fueled furnace economically attractive can be considered equal to 50. The results of the calculations for 50 horses, then 70 kW, are summarized in Table 2.2. A mass flow of 45 kg $h^{-}1$ on wet basis is required or 18 kg $h^{-}1$ on dry basis, which implies 17 kW to reduce the moisture.

In addition, riding stables are allowed to give the manure to another farm, without restrictions, as given by Annex A to Dgr. n.1349 of 03/08/2011. In fact, they are willing to improve their disposed strategy: approx 42% is interested in the opportunity of installing furnace and up to 83% finds the transfer of manure to other sites attractive. These data come from poll given to 25 riding stables affiliated to FISE Veneto.

2.3 Equipment description

In this Section the devices used to investigate drying processes at the lab scale are described: most of them were custom designed and modified (aerated hopper and the rotary dryer), others are standard laboratory equipments (quartz tubular reactor heated by electrical oven).

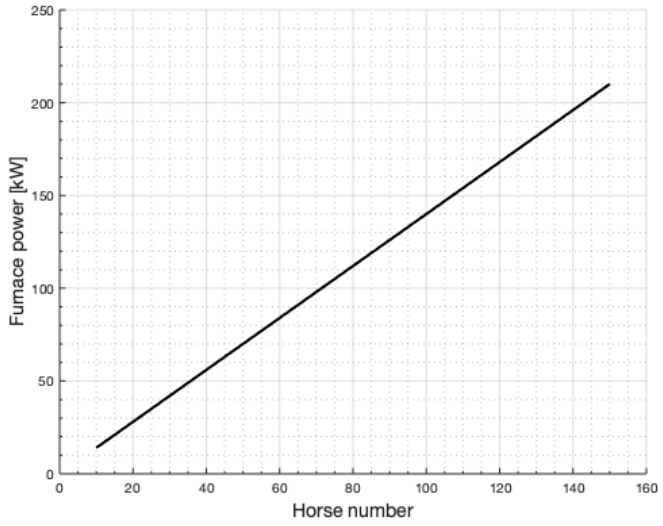

Figure 2.4: Furnace power in function of the horse number.

2.3.1 Aerated hopper

The aerated hopper is a metal storage vessel equipped with louvres that allow the injection of air. The drying process occurs thanks to the air forced to flow through the packed manure inside the hopper from the bottom to the top. This configuration is really inexpensive, compact and robust. Indeed, it has some great advantages to reduce the overall volume of the drying unit and to allow for storage and drying in the same static device. In fact, the wet material enters the hopper from the top and exits dried at the bottom due to gravity action. Moreover this device is easy to design and manufacture and it is completely static.

Figure 2.5a shows the pilot scale hopper used for the experimental campaign. The tested bin is 15 l volume, 0.40 m height and wedge-shaped so the upper part has constant squared section with depth of 0.20 m, while the lower part (hopper section) has a rectangular variable cross section. The hopper ends with a discharge drawer, that can be opened to empty the dryer. The two sloped wall have five louvre that allow air flow. In this way the air is initially forced to reach the bottom and then rises upward throughout the bed.
Air is delivered to the hopper inlet by two 6 cm ID aluminium tubes, connect the hopper by the T-joint from which the air is fed, Figure 2.5b. A thermocouple is placed in one of the two air inlet tubes. Metal clamps assure the sealing. A fan blows air from the ambient air and pushes it inside a canvas PVC tube of 6 cm to the T-joint. A small sampling tube (4 mm diameter) allows to connect the canvas PVC tube to a pressure probe for pressure drop measurements.

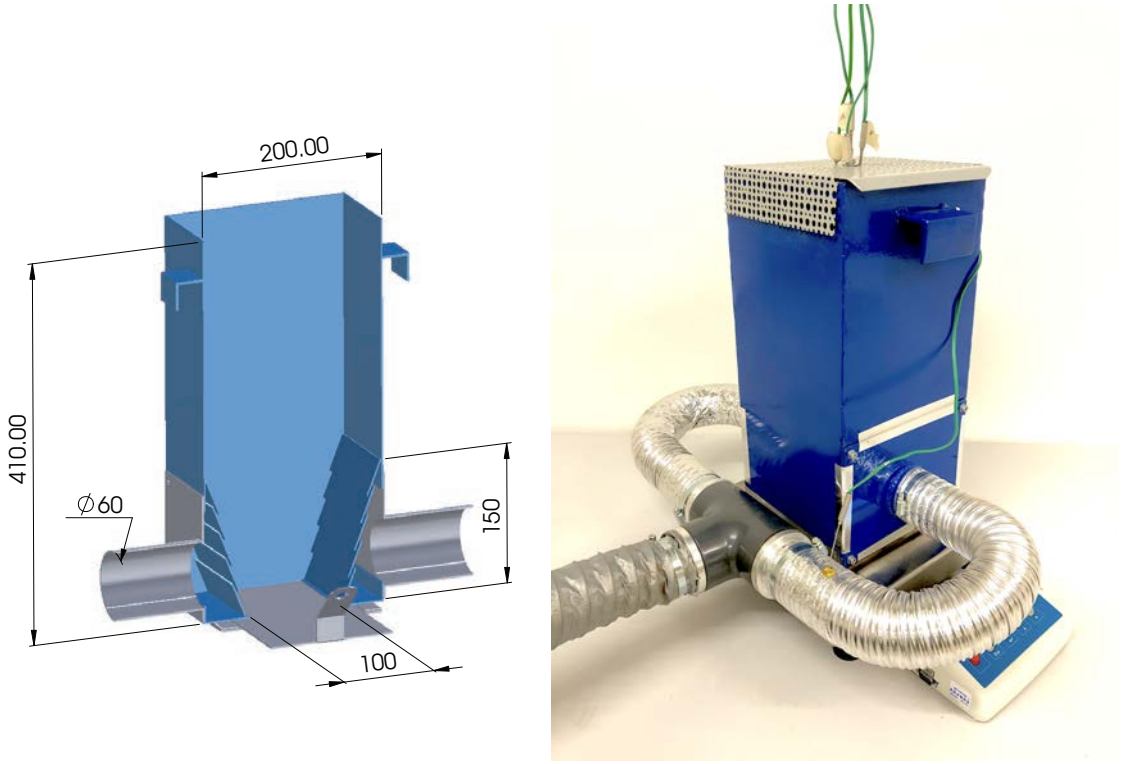

(a) *(b)*

Figure 2.5: Aerated hopper: internal section representation (a); photography of the experimental device (b).

A metal perforated plate is placed on the hopper top to avoid entrainments and to support many thermocouples located inside the material. The aerated hopper weight is about 10 kg.

The blower (MAPRO CL 34/1) is shown in Figure 2.6. An inverter (Siemens Micromaster) allows to vary the rotational speed of the electric motor and, in turn, the flow rate. The flow rate for each rotational speed is estimated by the fan characteristic curves (Figure 2.7), which have been derived from manufacturer data by the turbo-machine similarity laws for incompressible fluids. The pressure difference Dp across the fan is directly measured by a differential pressure probe (SICRAM).

2.3.2 Pilot-scale rotary dryer

The rotary dryer consist of a drilled cylinder with diameter equal to 0.30 m and length of 0.60 m kept horizontal position, see Fig.2.8. The rotational motion is provided by a variable speed DC electrical motor. The pilot-scale dryer is operated batch wise. The drying air is injected in the drum either radially along the cylinder

Figure 2.6: Blower with its inverter.

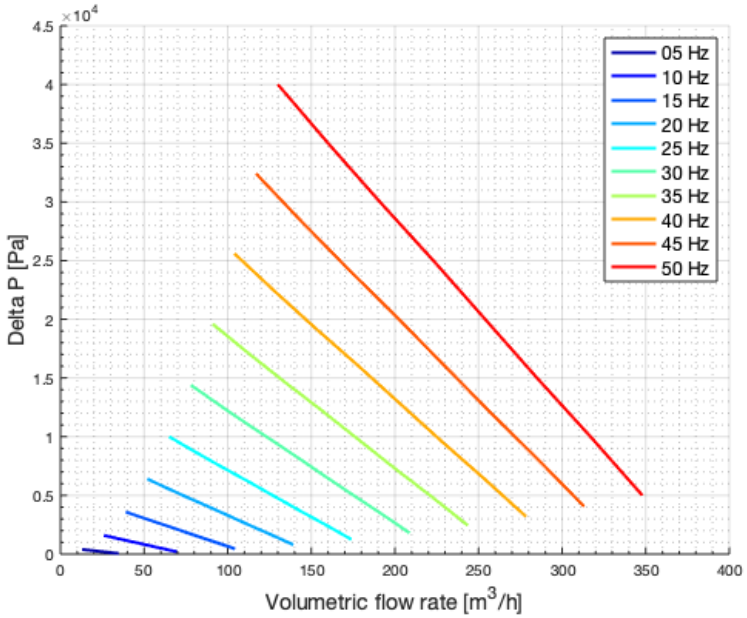

Figure 2.7: Fan characteristic curve as a function of the frequencies, at 20 °C *and* 101.3 kPa.

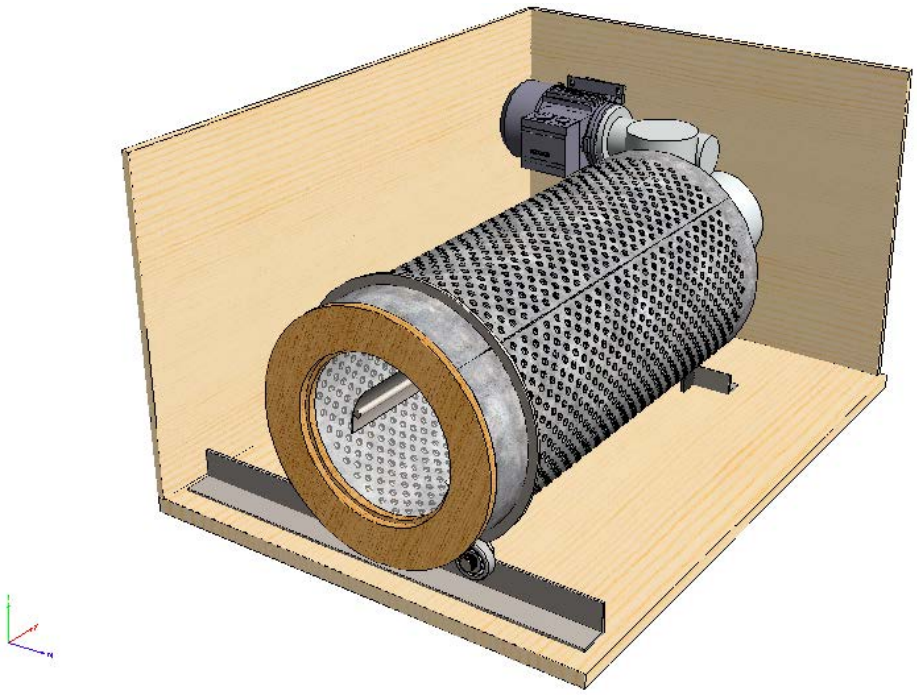

Figure 2.8: Rotary dryer scheme, in its wooden case.

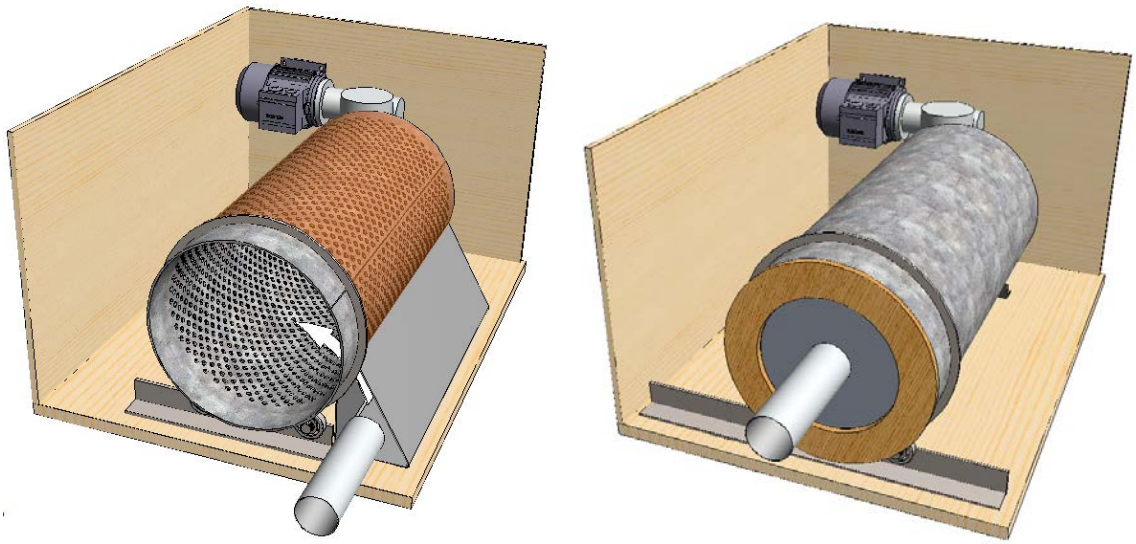

(a) *(b)*

Figure 2.9: Rotary dryer configurations: radial with air-blade (a), axial (b).

(a) (b)

Figure 2.10: Hot air production: pellet stove with conveyor (both the dry hot air and the flue gas can be used) (a); Heat gun (b).

length by means of a tailored conveyor (air blade), or axially, through the circular inlet opening.

In the radial configuration (Figure 2.9a), a fixed PE film surrounds the cylinder external surface to ensure the injection of the air only in correspondence of the air blade, which is fixed too. The air enters in radial direction through the material and then exits in axial direction.

In the axial configuration (Figure 2.9b), the whole external surface is sealed with a PE or aluminium film to avoid leak of air.

The drum and the electric motor are put in a wooden case that gives structural support to the drum bearings and make transportation easier. The whole assembly weights 46 kg mainly because of electric motor.
The fan and the canvas tube are the same used in the tests with the hopper.

Heated drying air is generated by (i) a pellet stove at almost fixed flow rate and temperature ($\dot{V}_{air}$= 50 or100 $m^3\,h^{-1}$, T_{air}= 65 or 75 °C) or (ii) a heat gun at variable flow rates and temperatures ($\dot{V}_{air}$=15 - 30 $m^3\,h^{-1}$, T_{air}= 150 - 380 °C). Test using the flue gasses from pellet combustion were also performed ($\dot{V}_{air}$=30 $m^3\,h^{-1}$, T_{air}=150 °C). These devices are shown in Figure 2.10.

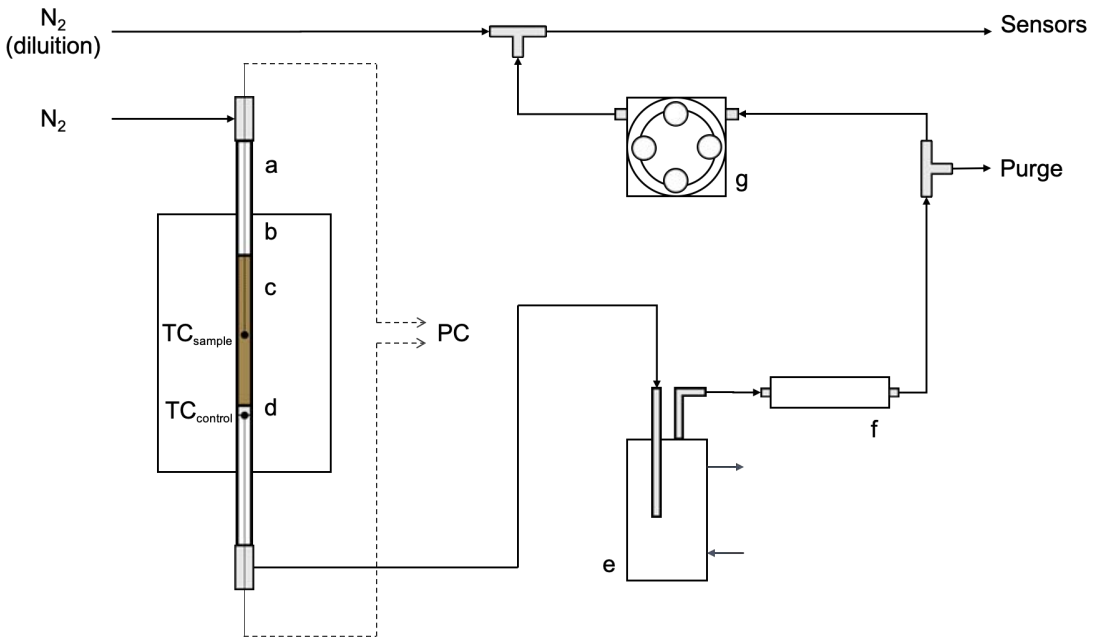

Figure 2.11: Setup for the analysis of manure emissions during the drying: a-quartz tubular reactor; b-electrical oven; c-manure sample; d-quartz wool sustain; e-condenser; f-filter; g-peristaltic pump.

2.3.3 Oven for manure emission

Emissions during the manure drying process play a crucial role with respect the environmental impact. Among others, ammonia emission could be problematic because of the very high nitrogen content (0.9%) in the manure [21]. Accordingly, ammonia emissions were measured and compared to the corresponding stack emissions limit (250ppm). In addition, the formation of flammable gas during drying was also investigated, to evaluate the fire hazard. With this regard, the manure is heated inside a packed bed reactor, as shown in Figure 2.11, and the resulting emissions are analysed. The reactor is a 16 mm diameter, 450 mm length quartz tube (a). A layer of quartz wool (d) supports the material bed (c). The air enters in the reactor from the top and exits at the bottom with 4 mm diameter tubes. The quartz reactor is set vertically, inside a cylindrical oven (b) that heats the material under a clear thermal policy. The heat is provided by an electrical resistance. The oven (Watlow) is 300 mm height and its diameter is of 20 mm. A digital flow meter measure the required inert gas flow rate (N_2). Two K-thermocouples are present too: one inside the bed (TC_{sample}) and the other one under the quartz wool support ($TC_{control}$). A condenser (e) and a cotton filter (f) are located right after the reactor. The condenser, cooled by water, traps the bio oil and the cotton filter avoids the entrainments of particulate. Then a fraction of the stream is purged while a defined flow rate is pumped by a peristaltic pump (g) to the electrochemical sensors (NH_3,

H_2, CO). This stream is diluted with N_2 before flowing through the sensors to match their range.

2.4 Analytical instrumentation

(a) *(b)*

(c)

Figure 2.12: Analytical instrumentations: Radwag WLC/F1/R scale (a); Moisture analyzer Radwag MA 50/1.R (b); DataLogger HD31 (c).

Balance

A balance with a squared weighing pan of 30 cm (Radwag WLC/F1/R) was used for drying tests in the hopper. The device, shown in Figure 2.12a, has a weighing range equal to 30 kg with a resolution of 0.5 g. The RS232 port allows the communication between the scale and the computer, to record continuously the weight during drying.

Moisture analyser

A moisture analyser designed to measure the relative moisture content in small samples was used (Radwag MA 50/1.R). The device, shown in Figure 2.12b, ensures a fast and precise process of determination of water content in a tested sample.
The heat is provided by an halogen lamp and IR emitter causing humidity evaporation from the sample. The heating stops when the evaporation is completed.
The moisture analyser was set to provide a step in temperature up to 125 °C and kept it constant until the end of the drying process. The process stops when the weight is stable for 25 s.

DataLogger

Delta OHM DataLogger HD31 is a portable multifunction instrument, Figure 2.12c. It has three independent inputs which can be connected to SICRAM probes. They can be singular or multifunction to measure multiple physical quantities such as temperature, relative humidity, atmospheric or differential pressure, air velocity etc. The probes calibration is done by the producer and it is kept in memory by the probe. Connecting a coupled relative humidity and temperature probe, the instrument is able to calculate the variables coming from the relative humidity such as dew point, wet bulb temperature, absolute humidity etc.

The coupled temperature and relative humidity sensor is composed by a capacitive probe to measure the relative humidity and by a Pt100 probe for the temperature. Starting from these two measurements the DataLogger determines the saturation vapour pressure, the vapour partial pressure, the mixing ratio between the vapour and the dry air, the enthalpy, the absolute humidity, the dew temperature and the wet bulb temperature. The operating range is from -20 to 80 °C with ± 0.1 °C accuracy and from 0 to 100 % RH with $\pm 1.5\%$ accuracy.

The pressure probe is a differential one (SICRAM). Its maximum measurable difference is 1100 Pa with 1 Pa resolution and the operating temperature range is

between -10 and 60 °C. The sensor have two tubes of 4 mm of diameter from which the pressure is sampled.

Thermocouple

The thermocouple is a temperature transduction. The used thermocouple are K type, their operability range is 0 to 900 °C with a sensitivity of $41\,\mu V\,°C^{-1}$. The thermocouples signal is acquired by Picolog which is a device that measures eight TC and sends the measurement to a computer thanks to a USB.

Electrochemical Sensors

Electrochemical sensors have been used to measure manure emissions. CO-AE Carbon Monoxide Sensor and H2-BF Hydrogen Sensor are used. The sensor consists of a pyroelectric detector which give in output a voltage signal proportional to the gas concentration. It is important that the flow rate through the sensor is sufficient to avoid the gas diffusion to the front face of the sensor. The suitable flow rate for CO and H_2 sensors is between 300 and 500 mL/ min. The operating range for CO and H_2 is 0 to 10 000 ppm.

Chapter 3

Experimental results

This Chapter presents and analyse the results of the experimental tests. The drying performances in the aerated hopper, the packed fixed bed and the rotary dryer configuration are evaluated. Brief consideration about manure emissions are made too.
In the aerated hopper both the wood shavings and the manure are tested. The attention is focused on the effect of the air flow rates and of the air temperature on the drying curve. What's more, the drying front is tracked by temperature measurement inside the material for both the aerated hopper and the packed bed arrangement.
The rotary dryer performances are experimentally evaluated on manure in both the through-circulation and the cascading configuration. As for the cascading configuration a sensitivity analysis on variables influencing the drying time (air velocity and temperature, rotation speed and number of flights). It is seen that the air temperature and flow rates have a strong impact on drying performance while the rotation speed and the number of flights affect the cascading regime. Among these variables, the number of flights is less influential. Experimental results are used to tune the numerical model and to provide a rough rotary dryer design.

3.1 Preliminary investigation on manure emissions

The preliminary investigation about manure emissions deal with two different thermal conditions: the drying in the dryer and the drying approaching the furnace. This test aims to simulate two stages: in the former the the ammonia emissions are observed to evaluate the need of a post-dying air treatment, while in the latter, attention is posed on the formation of explosive emissions to prevent fire hazard.
The manure (10 g)is placed inside the quartz reactor where $500\,\mathrm{ml\,min^{-1}}$ N_2 flows through it. The thermal policy is $10\,^{\circ}\mathrm{C\,min^{-1}}$ up to $105\,^{\circ}\mathrm{C}$ then the reactor is kept

isotherm for an hour to obtain dry manure. After that, the system is heated up to 750 °C at 10 °C min^{-1}. The emissions are collected, diluted and analysed.
During the drying stage there are not any ammonia emission issue as shown in Figure 3.1. In fact, the dry manure starts to emit ammonia at 200 °C. The material temperature never reaches that level inside the dryer since its auto ignition temperature is extremely close to that. The ammonia peak occurs at 325 °C: in this condition the material is already in the furnace. In the dryer there are not harmful emissions so the drying off-gas treatment is not required and emissions can be vent in the atmosphere or used as secondary air in the furnace.
In the ramp of temperature the CO and H_2 are detected by the sensors as shown in Figure 3.1. The manure releases hydrogen starting from 480 °C, reaching its peak in concentration (1.7%vol) at 645 °C. It is always under its lower flammability limit of 4%vol. While the carbon monoxide shows two higher peaks at 310 °C (2.7%vol) and 710 °C (2.5%vol) without exceeding the lower flammability limit 12.5%vol. The CO signal is affected by hydrogen cross sensitivity, so the second peak might be lower than measured.
To sums up, the drying process is not affected by ammonia emissions but same consideration cannot be done for the furnace flue gas since the ammonia will be present there. These emissions can be partially controlled decreasing the air-fuel ratio.
Moreover, the manure emits flammable gasses at high temperature and in concentrations lower than the hazardous one. These temperatures are expected only in the combustion chamber where these gasses are not an issue.

3.2 Aerated hopper

The aerated hopper investigation aims to analyse the drying process with the continuous measuring of the sample weight. The progression of the drying front is evaluated, as well.
Tests are carried out with the following procedure:

- The hopper is filled with material up to 5 cm from the top (h_{bed} =35 cm). The bed has a volume roughly equal to 12.9 l. It is regularly lightly packed with a metal load to make it replicable and as homogeneous as possible.

- The charged device is placed on the scale and the air inlet tube must be supported by ensuring the discontinuity between the hopper on the scale and the surroundings.

- The air is ambient air. It undergoes to the daily variations of temperature and

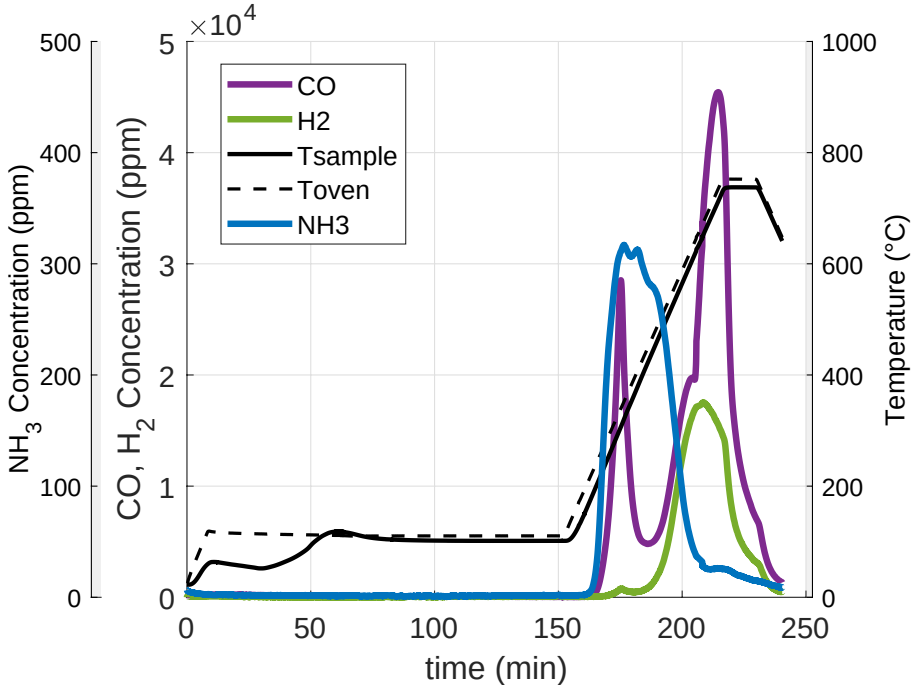

Figure 3.1: Manure emissions at $10\,^{\circ}\mathrm{C\,min^{-1}}$ *up to* $105\,^{\circ}\mathrm{C}$*, 1 h isotherm and* $10\,^{\circ}\mathrm{C\,min^{-1}}$ *up to* $750\,^{\circ}\mathrm{C}$*.*

specific humidity but tests belonging to the same group are done in the same day.

- The pressure drop through the bed needs to be checked before starting the test, in order to determine the air flow rates using Figure 2.7.

3.2.1 Effect of the air flow rate

The air flow rate aims to ensure the mass transfer and provide the energy for the moisture evaporation in a competitive time. In addition, the air has to flow homogeneously through the bed without breaking through it or even fluidising it. Two air flow rates are tested: 100 and $180\,\mathrm{m^3\,h^{-1}}$. Wood shavings are used with moisture content similar to manure one.
In Table 3.1 the tests conditions are reported. They are carried out at constant temperature of $26\,^{\circ}\mathrm{C}$.

These flow rates are chosen as the minimum and the maximum flow rates. These represent the range in which it is possible to observe drying phenomena in a reasonable time. The upper limit is physical, in fact, the through circulation configuration is not ensured for higher values. Higher flow rates lift the entire bed then break through it creating preferential air paths and eventually the air drags the dry wood shaving particles out of the hopper.

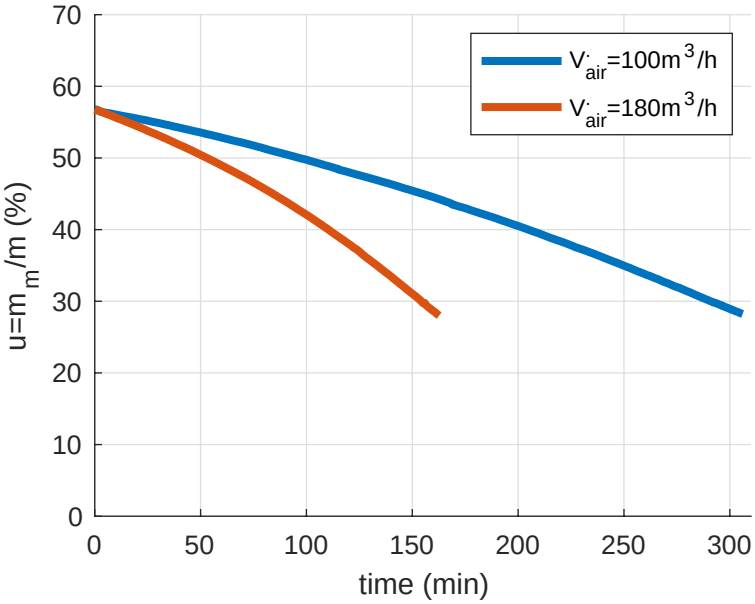

Figure 3.2: Effect of the air flow rates on the wood shavings moisture content u at 26 °C, h_{bed}=35 cm.

Figure 3.2 shows the wood-shaving moisture content (u) during time. The drying process reaches the set point when u=30%. The required time is between 2.5 and 5 hours depending on the air flow rates. The performances could appear very poor, but, on the other hand, ambient air (or slightly warmed air) is available in large quantities without costs. The higher flow rate dries the material in a shorter time. In order to better explain the effect of the air Figure 3.3 is shown. Here the moisture content ratio X is reported in time. In particular, both the experimental curves have a linear behaviour in the whole drying process. They are therefore fitted by the dots straight lines. According to Equation 1.6 the derivative of X in time is the drying rate. Being the function a straight line, the drying rate is constant. The slopes of the curves are different: at the high air flow rate corresponds an high slope and an high drying rate too. In Table 3.1 the corresponding values of the constant drying-rate for each test are reported. Increasing the air flow rates at 26 °C of 80%, the

Table 3.1: Experimental conditions for the investigation of air flow effect in aerated hopper.

Test	**Material**	$\mathbf{w}_0$ g	$\mathbf{u}_0$ $\frac{kg_m}{kg_m+kg_d}$	$\dot{V}_{air}$ m^3/h	$\mathbf{T}_{in}$ °C	$\mathbf{Y}_{in}$ $\frac{kg_m}{100kg_{da}}$	$\mathbf{t}_{SP}$ min	**N** $kg_m/(m^2h)$
A	wood-shavings	2417	0.57	100	26	1.1	290	4.7
B	wood-shavings	2421	0.57	180	26	1.2	153	8.9

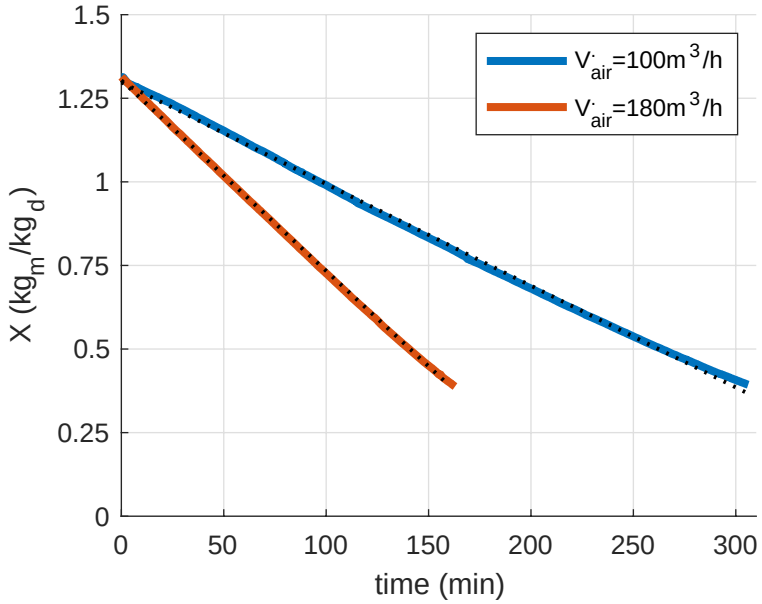

Figure 3.3: Effect of the air flow rates on the wood shavings moisture content X at 26 °C, h_{bed}=35 cm.

constant drying-rate is almost doubled.

(a) *(b)* *(c)*

Figure 3.4: Moisture distribution on the hopper cross-section at the end of the test B: z=10 cm (a); z=20 cm (b); z=30 cm (c).

At the end of the test, on the top of the material bed, a central circular dark zone surrounded by a light one is clearly visible. These colours differ the wet and the dry wood shavings. Hence, the moisture content in the hopper bed is not homogeneous within a cross section. The drying proceeds through the bed creating a front of drying that prefers the peripheral zones. In fact, it does not progress from the bottom to the top homogeneously across the hopper cross section. In Figure 3.4

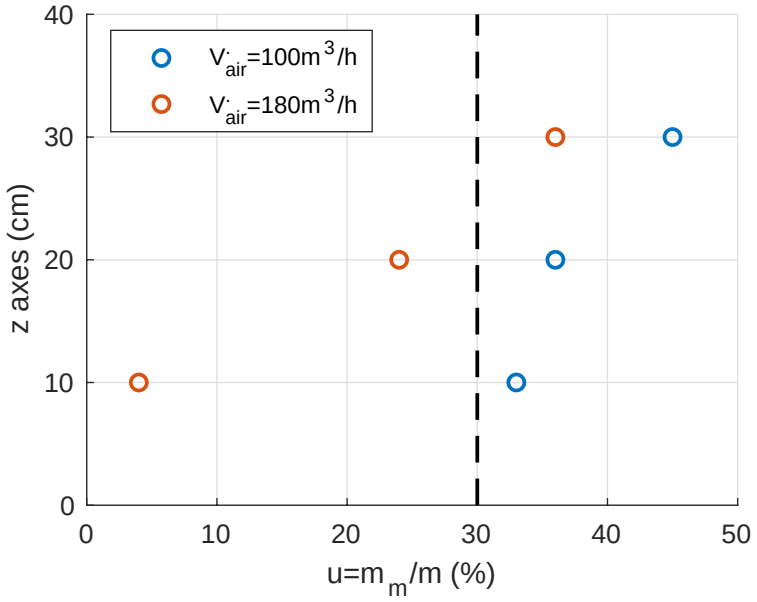

Figure 3.5: Moisture content among the z axis at u_{end}=28%, 26 °C.

the photos of the material at different heights in the bed (z=10, 20, 30 cm from the bottom) in test B are reported. Moreover, the central material for each of these planes is sampled and tested in the moisture analyser. The result is shown in Figure 3.5. When the mean of the material reaches the set point, the central zone of the bed is still wet.
If the process continuously runs this can not be a problem since the material proceeds from the top to the bottom meeting dryer air. .
In order to investigate the progression of drying, inside the hopper, a number of thermocouples are placed in it. Note that during the constant rate period the temperature is constant and equal to the web bulb temperature. When the constant rate ends at a certain position the temperature starts to increase and the front of drying proceeds. This will be further investigated in Section 3.2.3.

3.2.2 Effect of the air temperature

The drying air temperature has a strong impact on the drying process. Three temperature are evaluated in wood shavings drying: 26 °C, 29 °C, 32 °C.
The tests are carried out keeping constant all the other variables: the air flow rates 180 $m^3\,h^{-1}$, the bed height is 35 cm and the dry solid mass is around 1000 g. The experimental conditions are summarized in Table 3.2.

Figure 3.6 shows the moisture content u in time for the different air temperatures.

Table 3.2: Experimental conditions for the air temperature investigation in aerated hopper.

Test	**Material**	$\mathbf{w}_0$ g	$\mathbf{u}_0$ $\frac{kg_m}{kg_m+kg_d}$	$\dot{V}_{air}$ m^3/h	$\mathbf{T}_{in}$ °C	$\mathbf{Y}_{in}$ $\frac{kg_m}{100kg_{da}}$	$\mathbf{t}_{SP}$ min	$\mathbf{N}$ $kg_m/(m^2h)$
C	wood-shavings	2972	0.65	180	26	1.3	246	9.2
D	wood-shavings	2906	0.64	180	29	1.3	189	11.4
E	wood-shavings	2571	0.63	180	32	1.4	137	13.4

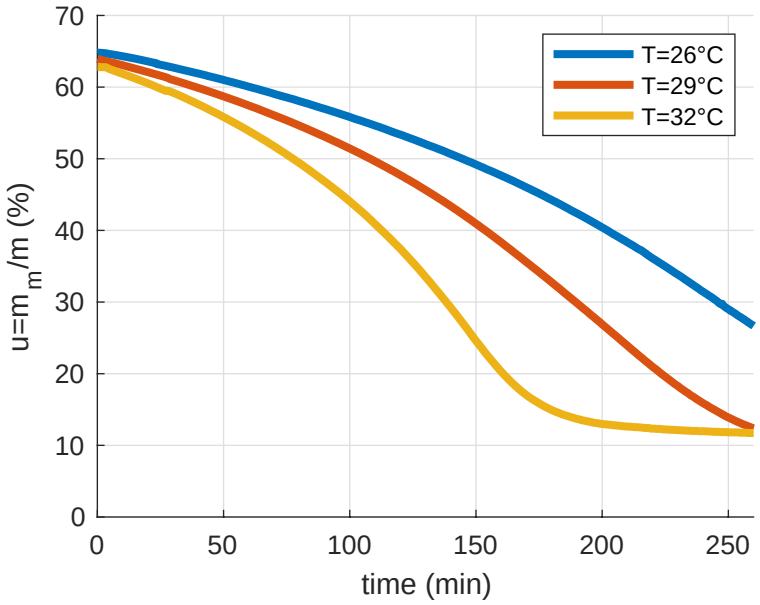

Figure 3.6: Air temperature effect on the wood shavings moisture content u at $180\,m^3\,h^{-1}$ *and* h_{bed}=35 cm.

Increasing the air temperature of only 3 °C the time required to reach the set point decreases of 50 min. In this range of operability there are probably heat and mass transfer limitations as the heat provided to the wet solid is low. From an analytical point of view, the temperature enters in the equation of drying in the air enthalpy (Equation 4.4) and in the driving force of the mass transfer since the saturated moisture content follows the Antonie's law 4.10.
The moisture content X in each test decreases linearly until the set point as shown in Figure 3.7. The constant drying rate increases almost linearly with the temperature in this range. In the final part of the tests, when the curve reduces its slope, the decreasing drying rates stars.

The ambient air is characterized by high variability between day and night and even more between different seasons. This variability affects the drying rate in a strong way. Since this investigation focuses on air around 30 °C, it is evident that

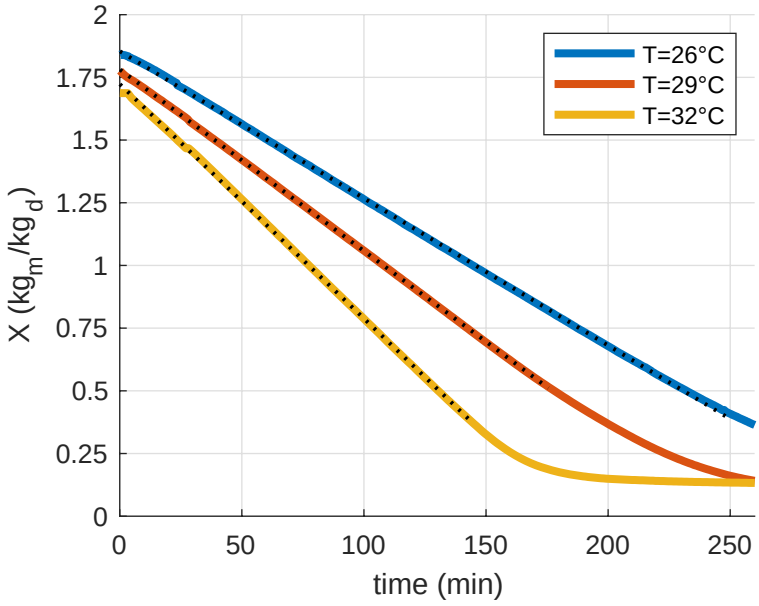

Figure 3.7: Air temperature effect on the wood shavings moisture content X at $180\,\mathrm{m^3\,h^{-1}}$ *and* h_{bed}=35 cm.

when the furnace works in winter, the air needs to be lightly heated up to 30 °C. This is not a big deal from an industrial point of view. The control of the air temperature becomes crucial to design an effective drying unit.

3.2.3 Monitoring of the front of drying

Since the drying process, until the design point humidity, occurs completely at the constant drying rate, in a fixed point, the temperature is kept constant until the front of drying overcomes it. When the temperature increases the drying is considered completed because it reaches rapidly the temperature of the drying air. In order to monitor the temperature, seven thermocouples are introduced inside the bed in different positions. This investigation aims to have a rough picture of the moisture distribution over time inside the hopper volume. The temperature samplings along two vertical lines are made at first: one at 2.5 cm from the hopper wall, the other at 2.5 cm from the central axis.

The peripheral zone is investigated in test D, Table 3.2. Five thermocouples are used to observe the air-wall effect while the others two are set at 2.5 cm far from the centre, as shown in Figure 3.8. Table 3.3 summarizes the thermocouples pattern inside the hopper.
The global behaviour is reported in Figure 3.9a. The effect along x direction in the

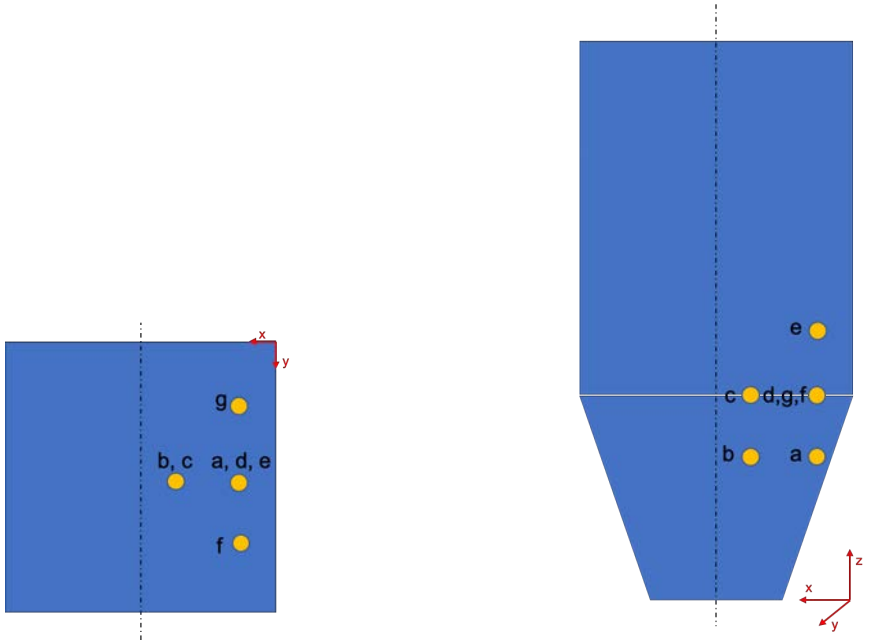

(a) *(b)*

Figure 3.8: Thermocouples positions in the aerated hopper, test D : top view (a); front view (b).

lower section of the hopper (z=10 cm) is shown in Figure 3.9c. The front of drying reaches point b after two hours from point a even though point b is relatively close to the air inlet. When point b is dried all the material in the hopper is close to the set point (u=35%). Moreover only a fraction of the air flows through this cross sectional area because the louvres for air inlet are from z=0 cm up to z=15 cm. This direction is a tough path for the airflow. The drying of points a and b occurs initially at higher temperature than the others. Hence they meet an hotter and drier airflow but at the same time the flow rate is lower.

On the opposite, at z=15cm, the front of drying moves from d to c rapidly, Figure 3.9d. The fact that across this plane flows all the volumetric flow rates may be the reason why the front of drying proceeds so fast.

Along the y direction, the thermocouples are fixed in d, f and g. Figure 3.9b shows a symmetric behaviour between d and f while g is late. This inhomogeneity might be due to the heterogeneity of the material.

In the periphery, along z direction, shows a clear wall effect, Figure 3.9e. The airflow runs away in this direction and the front of drying proceeds rapidly from a to e passing through d. This behaviour is in accordance with the photos on page 35. On the other hand, in the central zone the front of drying proceeds slowly from point c to b, as shown in Figure 3.9f. The bottom zone is not easily reached by the airflow so that the air is stagnant there. Indeed, in the bottom there is a dead zone,

Table 3.3: Position of thermocouples in test D.

TC	**x** cm	**y** cm	**z** cm
a	2.5	10	10
b	7.5	10	
c	7.5	10	15
d	2.5	10	
f	2.5	15	
g	2.5	5	
e	2.5	10	20

it may be due to the low effective air injection. Moreover the louvres allow the air inlet from the bottom up to z=14 cm so that only 70% of the airflow interests the hopper plane z=10 cm.

The investigation on the front of drying at the hopper central axis is carried out in test E, Table 3.2. Six thermocouples are placed along the axis starting at 5cm from the bottom up to 30cm with regular intervals of 5cm. The result is shown in Figure 3.10 where the bar are red when the temperature is kept constant (i.e. drying in progress), while becoming green when the temperature raises (i.e. drying is concluded).
The aerated bin can be divided in two zones: the bottom (hopper) and the top one. The former shows a criticality in the drying process. The front of drying proceeds from the top to the bottom. This result confirms the presence of the dead zone which is difficult to access by the air. In fact, at z=5 cm the material is dried more than 40 minutes later than the set point. The latter is characterised by a progressive drying among the vertical direction.

To sum up, inside the aerated hopper the front of drying is not homogeneous and it does not proceed from the bottom to the top. This behaviour is mainly affected by the strong wall effect that preferentially lets the airflow to pass near the wall without flowing through the material itself. Also the way in which air is injected, has an important role: the louvres direct the airflow in an ineffective way to the bottom and in any case the material in the core of the hopper cannot be easily reached due to the bed permeability. Finally the intrinsic heterogeneities of the material contribute to the creation of air preferential paths even thought the bed is packed in the same way.

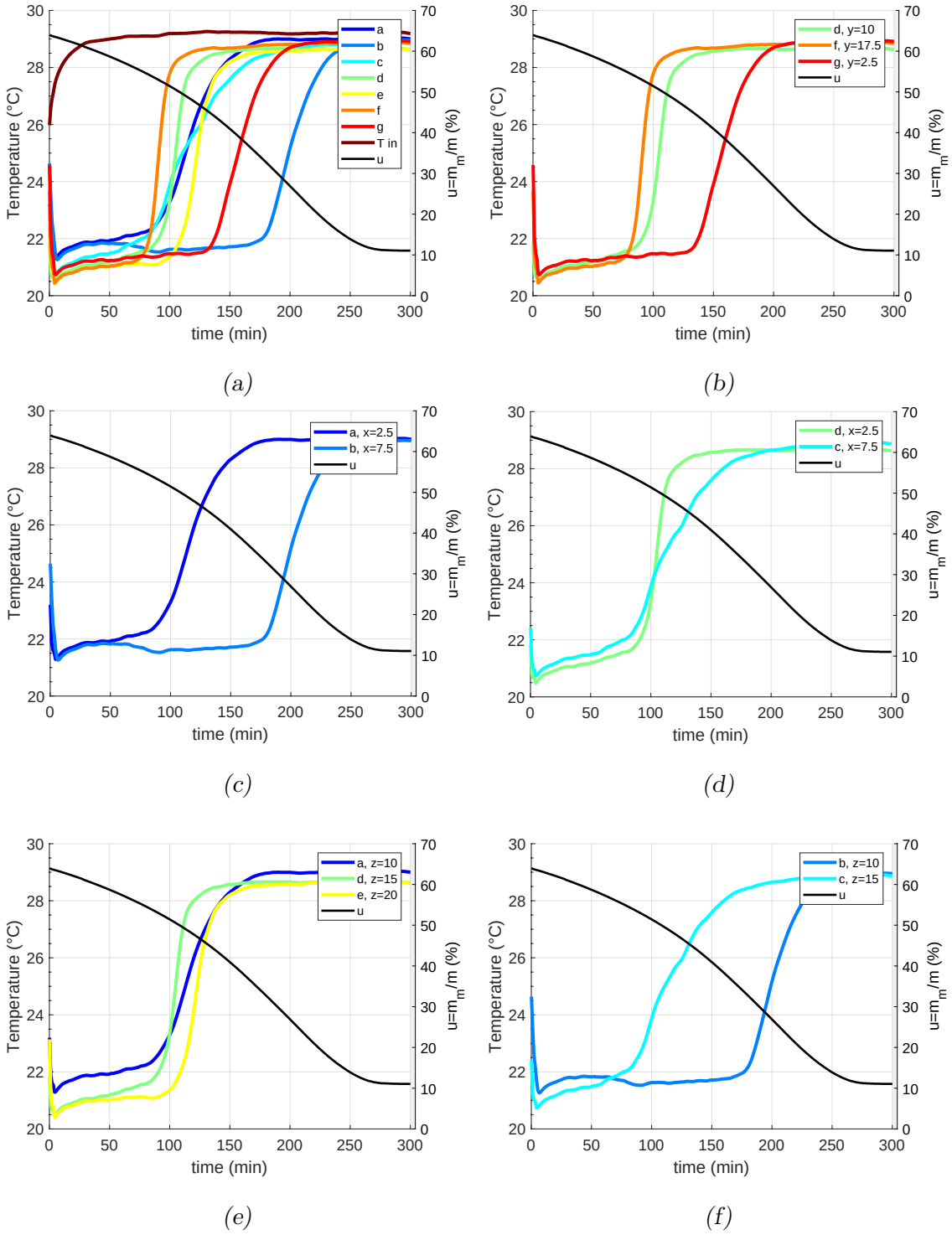

Figure 3.9: Front of drying investigation on Test D at $180\,\mathrm{m^3\,h^{-1}}$, T_{air}=29 °C, h_{brd}=35 cm*: Overall behaviour(a); along y direction, z=15cm, x=2.5cm (b); along x direction, z=10cm, y=10cm (c); along x direction, z=15cm, y=10cm (d); along z direction, x=2.5cm, y=10cm (e); along z direction, x=7.5cm, y=10cm (f).*

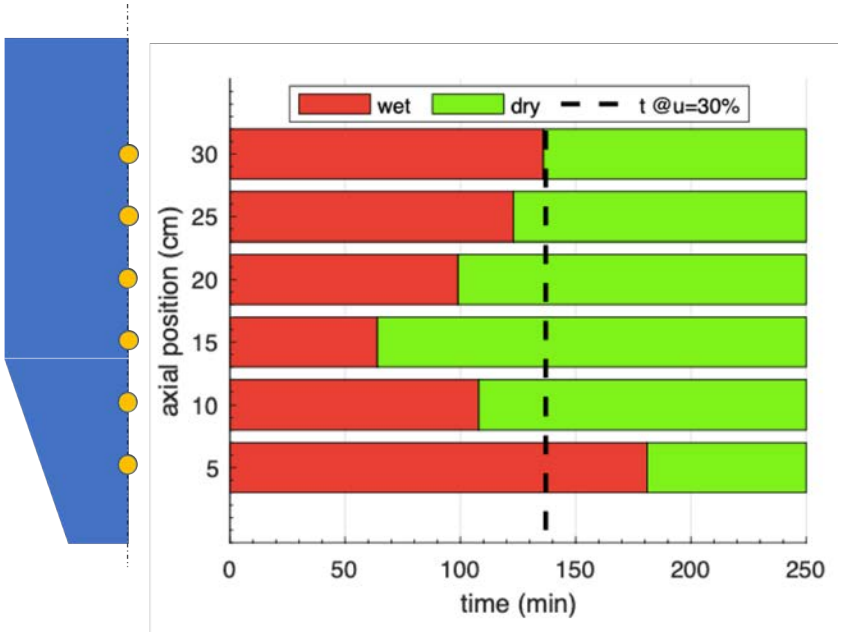

Figure 3.10: Front of drying investigation on Test E along the z direction (x=10cm, y=10cm) at 180 $m^3\,h^{-1}$, T_{air}=32 °C, h_{bed}=35 cm

3.2.4 Manure behaviour

After the investigation on the wood-shavings it is necessary to focus on the manure. The bed in the hopper is 35 cm height and the temperature along the hopper axis is recorded with 6 thermocouples placed starting from 5 cm from the bottom up to 30 cm with regular intervals of 5 cm. The manure is tested at two different air flow rates: 57 $m^3\,h^{-1}$ and 135 $m^3\,h^{-1}$. These flow rates are lower then the one performed in the wood shavings study because the manure bed has a lower permeability. The wet manure has an high tendency to pack itself, increasing the resistance to the airflow. Higher flow rates break through the bed without obtaining the desired through-circulation configuration.
The tests are carried out at ambient air at 30 °C and RH_{amb}=40%. The manure initial moisture content is u_0=55%. The test experimental conditions are collected in Table 3.4.

Table 3.4: Experimental conditions for the manure drying investigation in aerated hopper.

Test	**Material**	$\mathbf{w_0}$ g	$\mathbf{u_0}$ $\frac{kg_m}{kg_m+kg_d}$	$\dot{V}_{air}$ m^3/h	$\mathbf{T}_{in}$ °C	$\mathbf{Y}_{in}$ $\frac{kg_m}{100kg_{da}}$	$\mathbf{t}_{SP}$ min	**N** $kg_m/(m^2h)$
F	manure	2840	0.54	135	30	1.0	175	9.4
G	manure	2834	0.54	57	30	1.0	474	3.9

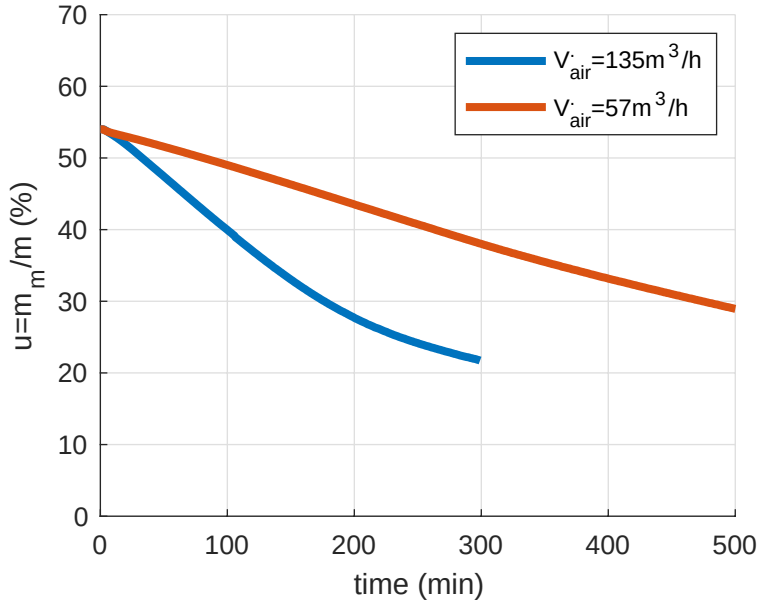

Figure 3.11: Effect of the air flow rates on the manure moisture content u at 30 °C, h_{bed}=35 cm.

The air effect is significant also on the manure, as shown in Figure 3.11. At this temperature, the best performance is 3 h achieved by the highest flow rate while at a lower flow rate the set point is reached in 8 h. These tests have comparable drying time to the wood shaving one.
Figure 3.12 shows that the moisture content behaviour can be linearly fitted only at high X values(u¿38%). So, the constant drying rate is 60% of the total drying time. The constant drying rate is N_F=9.2 kg m^{-2} h^{-1} in test F, comparable with the one of test C and D on the wood shavings, while is N_F=3.9 kg m^{-2} h^{-1} in test G. The decreasing drying rate starts at higher moisture levels than wood shavings. This behaviour is due to the high hygroscopic characteristics of the manure. In fact, the moisture is strongly retained inside the manure and and the moisture transport by capillarity and diffusion is more difficult.

The front of drying is even more inhomogeneous. Figure 3.13 shows the axial profile in z direction at bin centre of test F. Similar to what already observed for the wood shavings, the hopper bottom is hardly reached by the air flow, while in the upper section the front of drying regularly proceeds upward along the z direction. The bottom of the hopper is still critical. At the set point (t=180 min) three positions are already dried while the others are still wet. The mean moisture content is at the set point but since the hopper section is still wet, this means that in different position the material must be drier than the set point. Moreover, as in the wood shavings case, in a generic z plane, the central material is wetter than

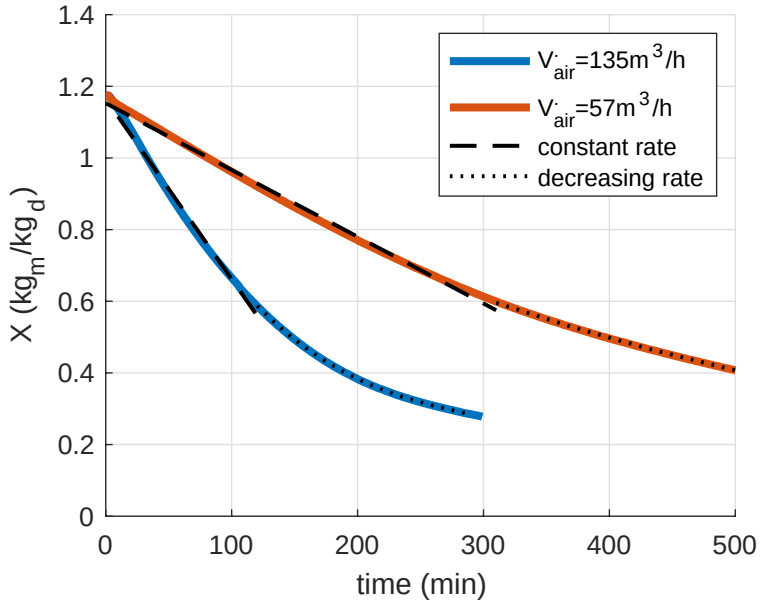

Figure 3.12: Effect of the air flow rates on the manure moisture content X at 30 °C, h_{bed}=35 cm.

the peripheral one. The moisture gradient at fixed z depends on the internal air distribution, that is the material permeability.

At the end of the drying test, the hopper discharge capability is tested by opening the discharge drawer. When it is removed the dry material does not exit on its own: it is self-supporting as shown in Figure 3.14, despite the hopper angle is very low (18°). This behaviour is mainly due to cohesive and mechanical forces, showing that the dry material is extremely far from the free-flowing behaviour. In addition, the intrinsic manure heterogeneity and the change of its properties with the moisture content make the situation worse.

In particular, it is observed that initially the manure is extremely wet and sticky, so it is easily self-packed inside the hopper. Conversely, at the end of the drying process, it results in a unique solid mass like a monolith, impossible to discharge. Generally the hopper discharge angle is designed in function of the characteristics of the material but when they are strongly variable it is extremely difficult or even more impossible building an effective device in which the discharge flow rate is assured by the gravity. Accordingly, the idea to use an hopper for the simultaneous drying and storage of the manure is unsuccessful, because the material not only experience a non homogeneous drying, but also does not flow naturally.
This device will not find any industrial application thus its study is left. The material

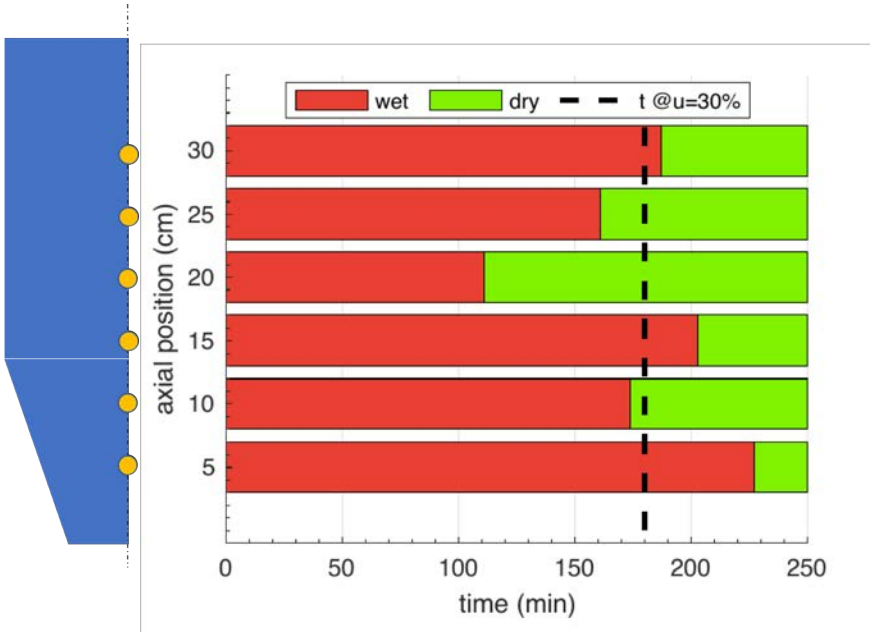

Figure 3.13: Front of drying investigation on Test E along the z direction (x=10cm, y=10cm) at $135\,\mathrm{m^3\,h^{-1}}$, T_{air}=30 °C, h_{bed}=35 cm

handling is a crucial point which has to be considered along with the drying itself.

3.2.5 Conclusions

The aerated hopper is a device that has the ambition to store and dry in the same static device, meeting the reduction of the size required. Since it is a static device, it is easily manufactured. Ambient air is forced to flow from a plenum through the bed inside the hopper without dispersions but its path is not homogeneous on the hopper cross section. In fact, the air follows a preferential path strongly affected by

Figure 3.14: Self-supporting dry manure inside the aerated hopper.

Table 3.5: Experimental conditions for wood shavings drying investigation in packed fixed bed, h_{bed}=20cm.

Test	Material	$\mathbf{w_0}$ g	$\mathbf{u_0}$ $\frac{kg_m}{kg_m+kg_d}$	$\dot{\boldsymbol{V}}_{\boldsymbol{air}}$ m^3/h	$\mathbf{T}_{\boldsymbol{in}}$ °C	$\mathbf{Y}_{\boldsymbol{in}}$ $\frac{kg_m}{100kg_{da}}$	$\mathbf{t}_{\boldsymbol{SP}}$ min	**N** $kg_m/(m^2h)$
H	wood-shavings	1737	0.61	180	31	1.0	87	16
I	wood-shavings	1740	0.61	180	31	1.0	91	15.8

the wall effect and the material inhomogeneity. Indeed, the front of drying reaches the zone along the hopper vertical axis with difficulties. Increasing the airflow the drying process is more effective but the drying time is still high in the order of magnitude of the hours. However the flow rates have an upper limit that ensures the bed integrity so the airflow cannot be arbitrarily increased . Other variables need to be investigated to improve the drying performances. In the end, the manure characteristics and their variability do not ensure the discharge of dry material. This makes the hopper useless. The material handling needs to be entrusted by a dynamic device, for instance those used in the agricultural sector (e.i. the manure spreader wagon has rotors that mechanically attack the manure). It is recommended to separate the storage of the wet material and the drying section.

3.3 Packed fixed bed

The investigation on the packed bed dryer aims to reproduce the idea of a packed moved bed in which the drying air is blown from the bottom across a constant section layer. In this way the issues due to the inhomogeneity of air distribution are overcome. Different height of the bed are tested.
For sake of simplicity, the packed fixed bed configuration is obtained by setting a metal grid inside the hopper to divide the bed and the decreasing section. The grid is set at z=15 cm to obtain a bed of squared constant section. The experimental investigation is carried out on wood shavings. The airflow is at ambient conditions, and flow rate is $180\,m^3\,h^{-1}$. Since the device is actually similar to the aerated hopper, the procedure is the same.

3.3.1 Monitoring of the front of drying

Two replicas of the same test are carried out in order to evaluate the repeatability of the phenomena and their experimental conditions are reported in Table 3.5. Moreover the pattern of thermocouples is improved, as shown in Figure 3.15. In

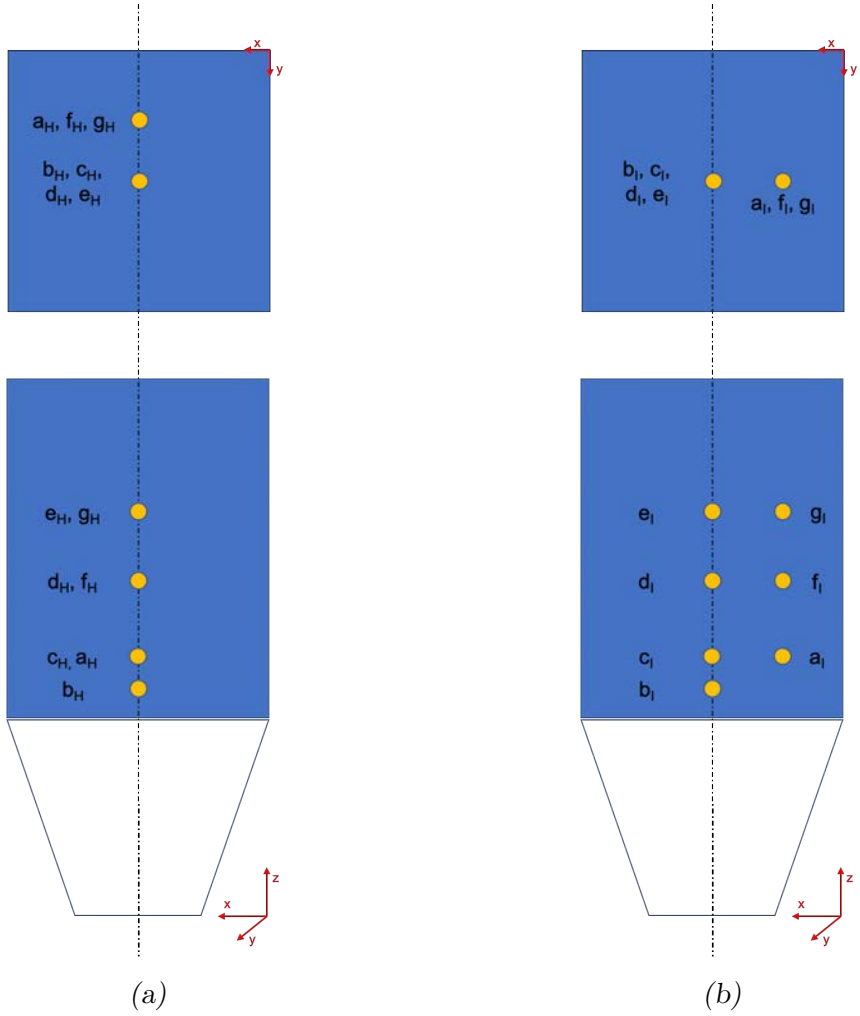

Figure 3.15: Thermocouples positions in the packed bed dryer, h_{bed}=20cm: test H (a); test I (b).

each test the temperatures along the bed axis are investigated at z=2.5, 5, 10 and 15 cm. Also another vertical direction is evaluated in each test between the centre and the walls: on the air louvres side (Test I, x=5 cm, y=10 cm) or on the opposite (Test H, x=10 cm, y=5 cm). The thermocouple positions are summarized in Table 3.6.

The repeatability of the process is shown in figure Figure 3.16 where the moisture content u in time is reported. The two tests are carried out at the same inlet air conditions, initial moisture content and mass of dry solid. The two curves are overlapped. They have the same constant drying rate of $16\,\mathrm{kg\,m^{-2}\,h^{-1}}$. The set point is achieved after 90 min.
The front of drying is observed on different z planes. Figure 3.17a shows the temperature on the plane z=5 cm. The signals of the two axial thermocouples (H(10, 10, 5) and I(10, 10, 5)) are overlapped and they start to increase just before

Table 3.6: Thermocouples position in packed bed reactor: test H and I.

TC	**Test H**	**Test I**
ID	**position (cm)**	**position (cm)**
#	(x, y, z)	(x, y, z)
a	(10, 5, 5)	(5, 10, 5)
b	(10, 10, 2.5)	(10, 10, 2.5)
c	(10, 10, 5)	(10, 10, 5)
d	(10, 10, 10)	(10, 10, 10)
e	(10, 10, 15)	(10, 10, 15)
f	(10, 5, 10)	(5, 10, 10)
g	(10, 5, 15)	(5, 10, 15,)

the peripheral ones. This phenomena could be due to the device configuration: the lower part of the hopper is empty and there the airflow is conveyed in the centre from louvres. In this way, the airflow in the centre has higher flow rates when meeting the fixed bed.

This little mismatch is reduced proceeding along the z direction. On the z=10 cm plane, only the thermocouple on the air louvres side shows 10 min lag, as reported in Figure 3.17b. The front of drying homogenization is almost obtained. It is reached out on plane z=15 cm as presented in Figure 3.17c. The air plug flow is obtained through the bed. This configuration allows a more homogeneous progression than in the aerated hopper and it avoids dead zones.

Finally, the front of drying along the axis is reported in Figure 3.18. It shows a progressive rising of the front of drying through the bed in the airflow direction. There is a long timespan between the global set point and the end of drying in the bottom zone while in the upper one the time lag disappear. This fact is undesirable because the airflow decreases its driving forces drying the bottom part more than the required. According to this consideration, the drying of thin bed can improve the drying because the material placed at the bottom and at the top meet the air with lightly different moisture content. In this way the drying occur simultaneously in the whole thin bed. If a photo of the moisture content along z direction at the set point could be take, a small gradient in moisture content (i.e. from 29 to 31%) will be found. The bottom material is not more dryer than the set point.

This must be highlighted in order to focus on the implementations of the continuous device such as packed moving bed. Quantitative indications about progression of the front of drying i.e. internal moisture distribution, are needed to get some information

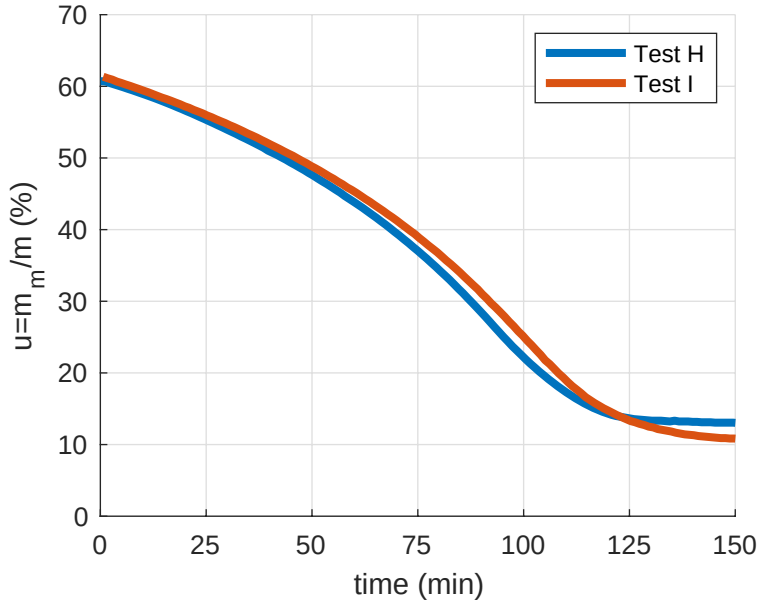

Figure 3.16: Repeatability of drying process on wood shavings moisture content u at $180\,m^3\,h^{-1}$, 31 °C, h_{bed}=20 cm.

about a short optimal bed height, neither too high to avoid large gradient, neither too low to excessively reduce the dryer productivity (or to require excessively large drying surface).

3.3.2 Effect of the bed height

In order to better understand the bed height effect on the drying process, in this Section four bed heights are investigated: 5, 10, 15, 20 cm. The tests are carried out at $180\,m^3\,h^{-1}$ and 31 °C. The temperature signals in the central axis are recorded at z=2.5, 5 and 7.5 cm. Since the cross-section, the density and the initial moisture content are the same in the tests, then the mass is linearly proportional to the bed

Table 3.7: Experimental conditions for wood shavings drying investigation at different bed height in packed fixed bed.

Test	$\mathbf{h_{bed}}$ cm	$\mathbf{w_0}$ g	$\mathbf{u_0}$ $\frac{kg_m}{kg_m+kg_d}$	$\mathbf{\dot{V}_{air}}$ m^3/h	$\mathbf{T_{amb}}$ °C	$\mathbf{RH_{amb}}$ $\frac{kg_m}{100kg_{da}}$	$\mathbf{t_{SP}}$ min	**N** $kg_m/(m^2h)$
H	20	1737	0.61	180	31	1.1	87	16.0
J	15	1341	0.62	180	31	0.8	57	16.3
K	10	891	0.62	180	31	0.8	40	16.3
L	5	433	0.61	180	31	0.8	19	16.2

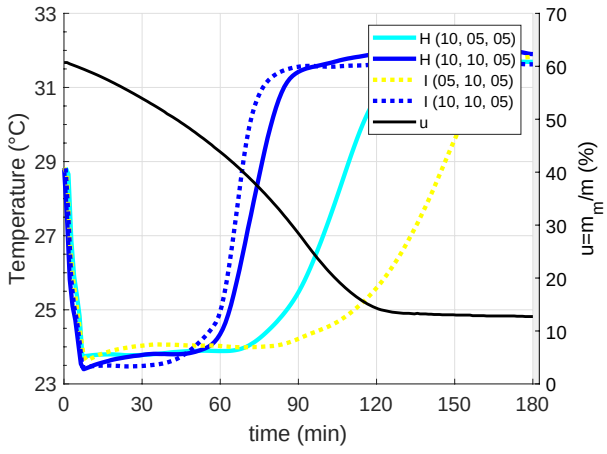

(a)

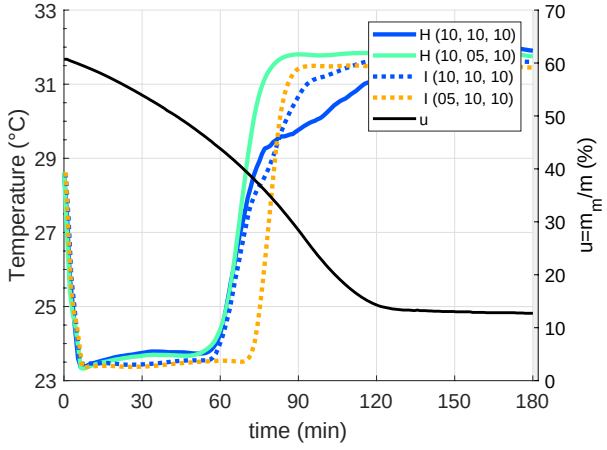

(b)

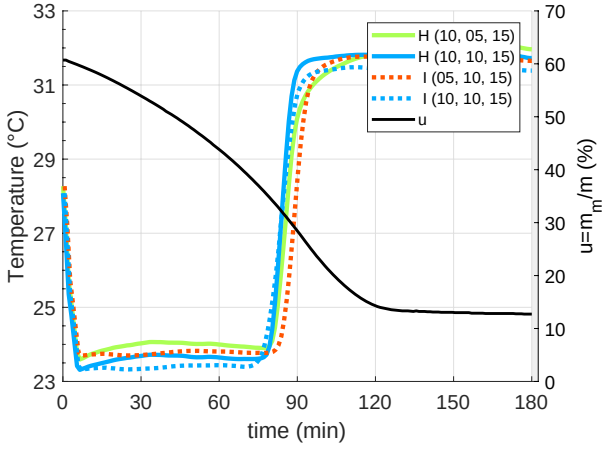

(c)

Figure 3.17: Front of drying investigation on packed fixed bed at $180\,\mathrm{m^3\,h^{-1}}$, T_{air}=31 °C, h_{bed}=20 cm*: on the plane z=5cm (a); on the plane z=10cm (b); on the plane z=15cm (c). Colours and line-style identify position and test ID respectively.*

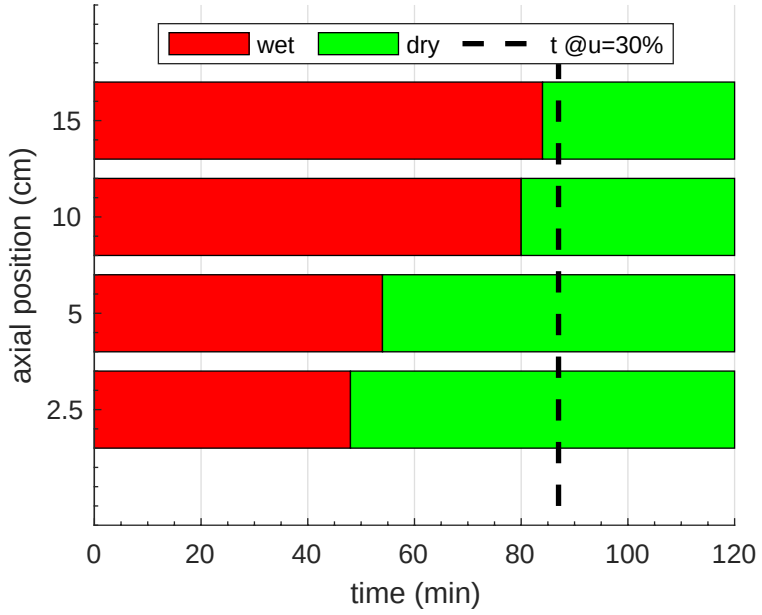

Figure 3.18: Front of drying investigation on Test I along the z direction at the bed centre (x=10cm, y=10cm) at $180\,\mathrm{m^3\,h^{-1}}$, T_{air}=31 °C, h_{bed}=20 cm

height. These conditions are collected in Table 3.7.
The drying curves are reported in Figure 3.19 where the drying time varies from 20 to 90 min by increasing the bed height from 5 to 20 cm. The increase in time is linear with the bed height as shown in Figure 3.20. Thus the drying rate is constant in all the tests (N=$16\,\mathrm{kg\,m^{-2}\,h^{-1}}$). This consideration could be unexpected observing the Figure 3.21 since the slopes of the X curves are different but the drying rate N is independent from the dry mass by definition as opposed to X. This means that the dry manure productivity in the different configurations is independent from the bed height which is $17\,\mathrm{kg\,m^{-2}\,h^{-1}}$.
Consequently, other considerations needs to be done in order to understand what could be the required bed height. Since the productivity is the same, the high bed allows simultaneously the drying and the storage, in addition, the device needs to be charged and discharged less than the lower bed. Moreover the air exiting the bed is at saturation conditions. Whereas the pressure drops through the bed are greater than the lower bed, in turn, the blowing power. Inside the high bed, the zone of active drying is a fraction of the whole bed. This means that the air dries the material until its saturation, then flows through the bed without positive effects. Below the active drying zone there is the front of drying that proceeds in the airflow direction. The inhomogeneity in the moisture composition along the bed is intrinsic in this drying configuration: when the active drying zone is in the middle of the bed, the bottom section is extremely dry (lower than the set point) while the upper

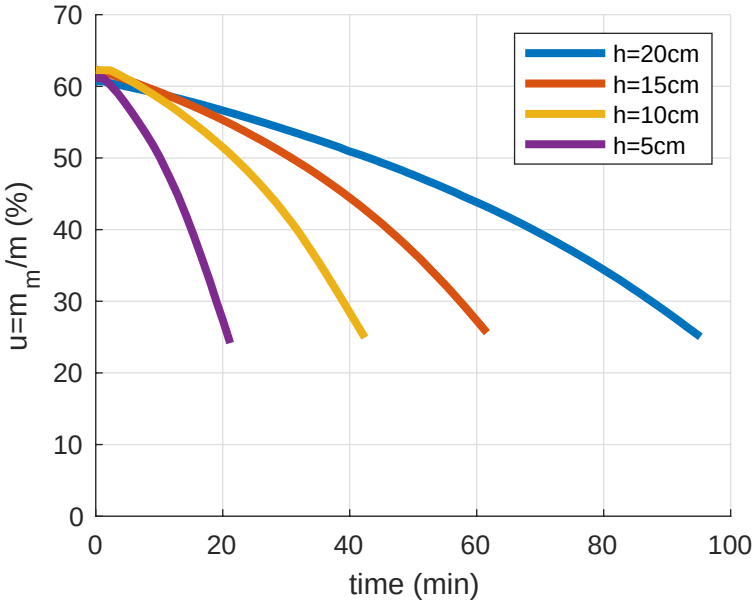

Figure 3.19: Effect of the bed height on the manure moisture content u at $180\,\mathrm{m^3\,h^{-1}}$, T_{air}=31 °C.

one has still the initial content. This phenomenon is shown in Figure 3.22, where the temperature profile on the z axis at test J (h_{bed}=15 cm) is reported compared to the moisture content u. The front of drying reaches z=2.5 cm after 35 min when the moisture content is 47%. At the set point the front of drying has arrived up to half of the bed height (z=7.5 cm). This means that the bottom part is extremely dry while the top is still wet.
It must be underlined that the specification of the product is not the complete dry material but the 30% one. Therefore to have a more homogeneous material it is suggested to perform the drying in a bed where all the height is simultaneously interested by the drying phenomenon. The quality of the product increases and the pressure drop across the bed is reduced. This is the case of test K (h_{bed}=10 cm), where the front of drying does not cross the z=2.5 cm , as shown in Figure 3.23. In fact temperature profile on the z axis is reported: it remains at the wet bulb temperature during the whole process. The active drying zone concerns all the height of the bed, resulting in high moisture content homogeneity .

3.3.3 Conclusions

The packed fixed bed configuration improves the drying performances in terms of air injection and homogeneity of air distribution inside the bed. Moreover the front of drying proceeds as a plug in the airflow direction. Though, the presence of the

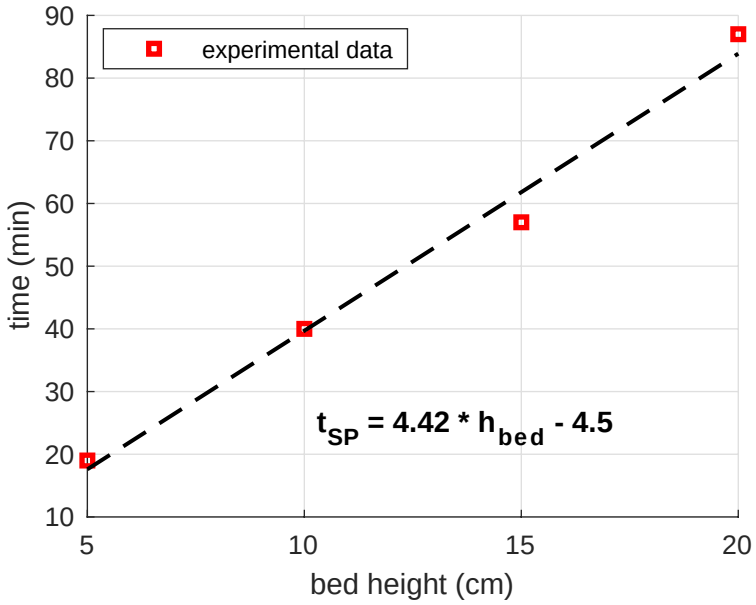

Figure 3.20: Bed height effect on the drying time in packed fixed bed at $180\,\mathrm{m^3\,h^{-1}}$, T_{air}=31 °C.

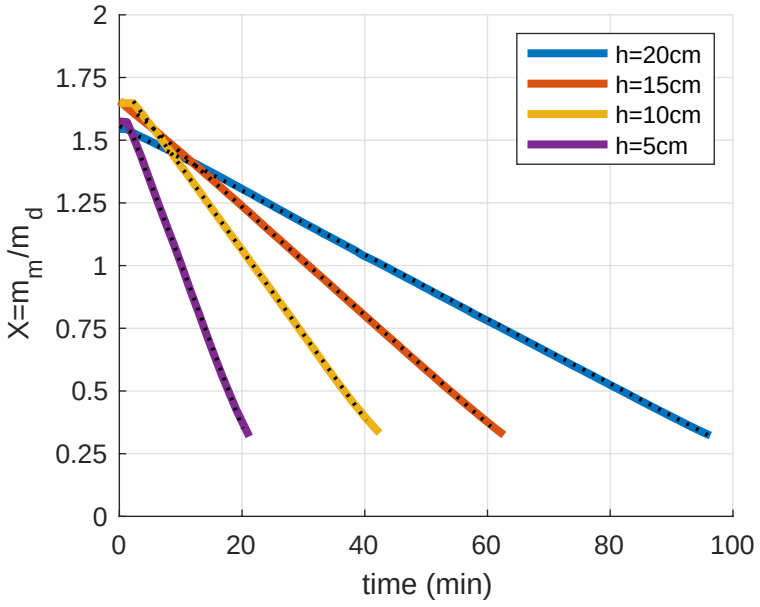

Figure 3.21: Effect of the bed height on the manure moisture content X at $180\,\mathrm{m^3\,h^{-1}}$, T_{air}=31 °C.

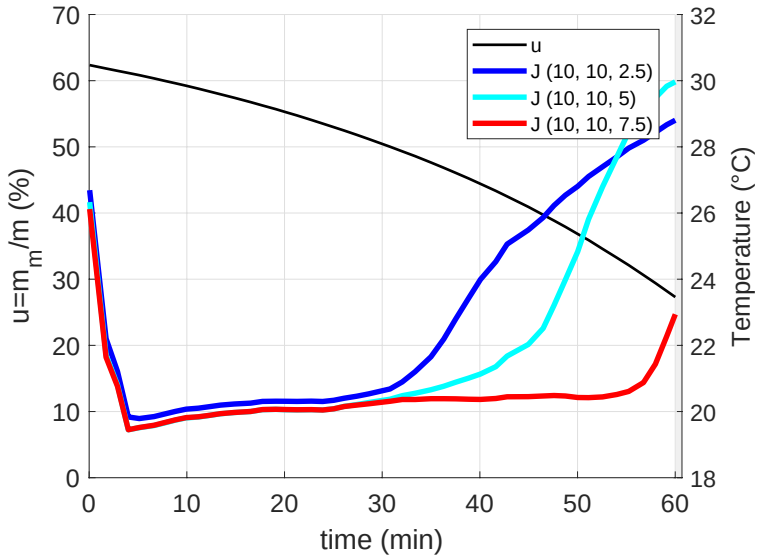

Figure 3.22: Front of drying investigation in the central axis of test J at h_{bed}*=15 cm,* $180\,\mathrm{m^3\,h^{-1}}$*,* T_{air}*=31 °C.*

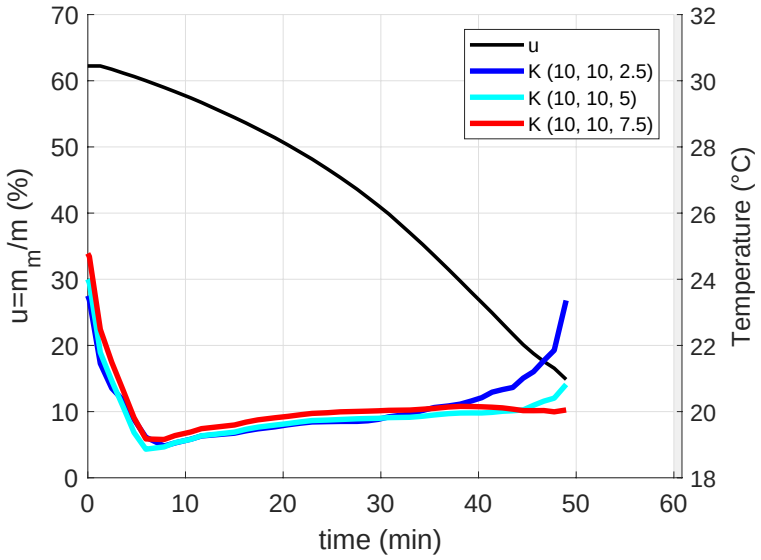

Figure 3.23: Front of drying investigation in the central axis of test K at h_{bed}*=10 cm,* $180\,\mathrm{m^3\,h^{-1}}$*,* T_{air}*=31 °C.*

front of drying generates local inhomogeneity in the bed moisture content, so that, at the set point the lower material will be extremely dried while in the upper one there will still be an offset.
Based on these considerations, it is convenient to design a storage unit that supplies the wet material to the drying unit. Here the drying occurs in a thin layer likewise in the packed moved bed. However, this solution is hardly scalable and requires a large surface for high productivity. They are incompatible with the compactness specification required by the project. In addition, this device would not be cost-effective since its cost could be an important fraction of the whole process capital costs. Therefore, another dryer is investigated. It fits the specification on the costs, the homogeneity of the final material, the proven technology and scalable.
.

3.4 Through-circulation rotary dryer

The following results aim to show the effect of the variables that influence the drying in the rotary dryer.
The desired amount of wet material is charged in the drum, then it starts to rotate. The process is batch so the airflow is blown inside the drum until the moisture composition reaches the set point (u=30%). Sample of about 10 g are analysed in moisture analyser. The material is manually sampled in regular time steps. When the material is sampled, the drum rotation and the air are stopped. In order to have an homogeneous and representative sample of the whole volume in the drum, the drum is divided into three evenly spaced sections from which wet material are sampled. The three samples are then mixed together in order to homogenize the moisture composition. Only 10 g are analysed in the scale, so the others are reintroduced in the dryer and the drying process continues. The discrete sampling introduces a disturbance in the process but the higher effect is on the data collection that are strongly influenced by the sampling points. This is the only way to sample this process because of the large size of the dryer that does not allow a continuous weighting on a scale.

The through circulation rotary dryer is achieved by introducing the air in radial direction through the external drilled surface using a conveyor in the sliding contact which realizes an air-blade. The air-blade injects the air along the whole length of the dryer where the material bed is higher; the dynamic angle of repose for the material is equal to 45° as shown in Figure 3.24. To avoid the air flow dispersions a PE film covers the parts of the external surface of the drum which are not in

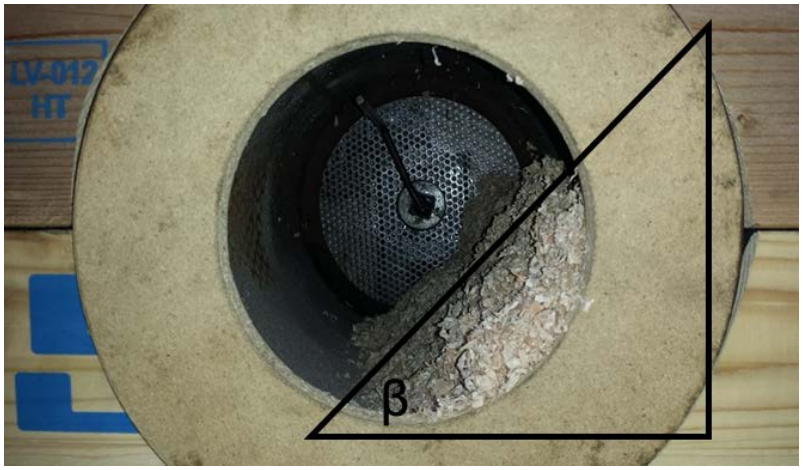

Figure 3.24: Dynamic angle of repose for the wood shavings inside the rotary dryer (H=7%).

contact with the air-blade. The rotating drum slides under the PE film. Moreover the wooden box is closed to allow the exit of air only from the inlet-outlet section of the drum. The air flows through the bed height like it did in the hopper with the advantage that at the end of the process the dry material is not packed, it is easy to discharge and there are not internal gradient in moisture content.
The rotation speed is kept low between 2.4 and 4rpm in order to ensure the material mixing inside the drum with a rolling bed motion in the cross sectional plane.

3.4.1 Effect of the material

The two materials are evaluated in the through-circulation configuration. The drum holdup is of 7% and the rotational speed is equal to 2.4rpm. The air flowing through the bed height is $180\,m^3\,h^{-1}$ at T_{air}=34 °C. The humidity of the wood shavings is equal to the moisture content of the manure. These information are summarised in Table 3.8.
The drying curve is made of the experimental data collected from the discrete sampling. A second order polynomial dotted curve fits these experimental points

Table 3.8: Experimental condition for drying investigation in through-circulation rotary dryer.

Test	**Material**	$\mathbf{w_0}$ g	$\mathbf{u_0}$ $\frac{kg_m}{kg_m+kg_d}$	$\dot{\boldsymbol{V}}_{\boldsymbol{air}}$ m^3/h	$\mathbf{T}_{\boldsymbol{in}}$ °C	$\mathbf{Y}_{\boldsymbol{in}}$ $\frac{kg_m}{100kg_{da}}$	$\boldsymbol{\omega}$ rpm	**H** %	**flights** #	$\mathbf{t}_{\boldsymbol{SP}}$ min	**N** $\frac{kg_m}{m^3h}$
M	wood shavings	893	0.62	180	34	1.5	2.4	7	1	50	12
N	manure	891	0.63	180	35	1.5	2.4	7	1	90	7

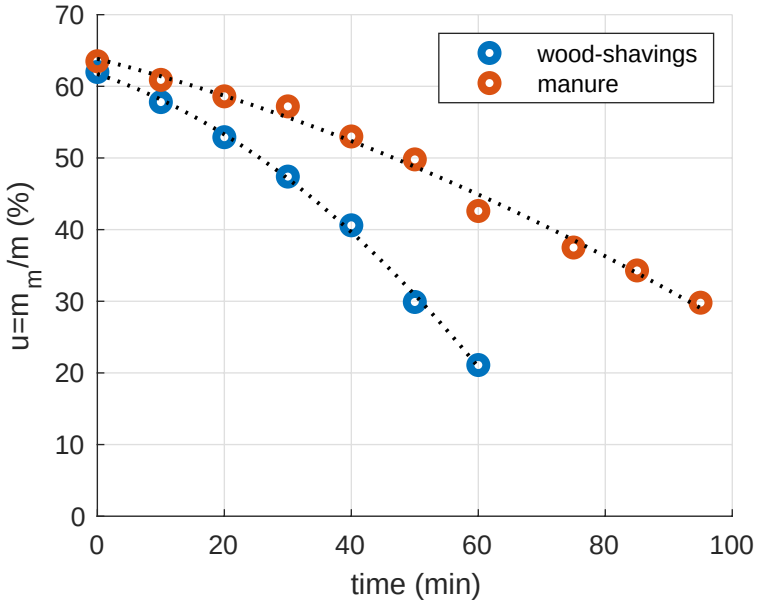

Figure 3.25: Moisture content u in the drying of different materials in through-circulation rotary dryer at $180\,\mathrm{m^3\,h^{-1}}$, $34\,^{\circ}\mathrm{C}$, *H=7%, ω=2.4 rpm.*

to better explain the drying behaviour in time. Figure 3.25 shows the drying curve for manure and wood shavings. Wood shavings reach the set point in 50 min while the same amount of moisture is removed from the manure in 90 min. The drying occurs in constant rate for both materials as presented in Figure 3.26. The slope of the fitting lines provides information about the drying rates, since the dry mass is the same in the two tests: the higher the slope, the higher the drying rate which is expressed per unit of drying volume for the rotary dryer. The manure drying rate is equal to $7\,\mathrm{kg\,m^{-3}\,h^{-1}}$ while the for the wood shavings it is equal to $12\,\mathrm{kg\,m^{-3}\,h^{-1}}$. This difference in the rate of drying depends on the medium properties such as permeability and porosity of the bed. In fact, the manure has a lower porosity and a lower surface area. Moreover the rotational speed ensures a rolling regime in the cross-section plane only for the wood shavings. The manure is in slumping mode in which the dynamic angle of repose varies in a cyclical manner; while in the rolling mode the angle of repose remains constant [22], ensuring a better mixing.

At the end of the drying the materials are not packed and they can be discharged easily. The difference in the two materials is huge in the drying rate and also in the motion inside the drum. The wood shavings are fluffier than the manure while rolling inside the drum. Since the drying process needs to be optimized for the manure and the behaviour of the wood shavings is so different, the following tests focus only on the manure.

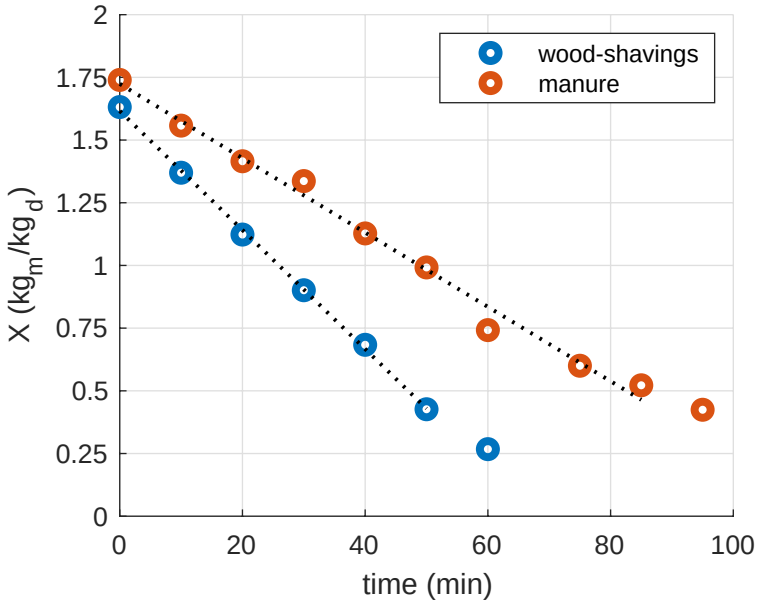

Figure 3.26: Moisture content X in the drying of different materials in through-circulation rotary dryer at $180\,m^3\,h^{-1}$, $34\,°C$, *H=7%, ω=2.4 rpm.*

It is apparent that the manure reaches the set point too long. In order to reduce the drying time the effect of the temperature is investigated in the following.

3.4.2 Effect of the temperature

Table 3.9: Experimental conditions for manure drying investigation in through-circulation rotary dryer.

Test	**Material**	$\mathbf{w_0}$ g	$\mathbf{u_0}$ $\frac{kg_m}{kg_m+kg_d}$	$\dot{\boldsymbol{V}}_{\boldsymbol{air}}$ m^3/h	$\mathbf{T}_{\boldsymbol{in}}$ °C	$\mathbf{Y}_{\boldsymbol{in}}$ $\frac{kg_m}{100kg_{da}}$	$\boldsymbol{\omega}$ rpm	**H** %	**flights** #	$\mathbf{t}_{\boldsymbol{SP}}$ min	**N** $\frac{kg_m}{m^3h}$
N	manure	891	0.63	180	35	1.5	2.4	7	1	90	7
O	manure	900	0.63	180	75	1.2	4	7	1	29	20

The effect of the air temperature is evaluated by the drying curves and by the drying rate. Two different temperatures are tested: 35 °C and 75 °C. The drum holdup is 7%, and the air flow rates is $180\,m^3\,h^{-1}$. The experimental conditions of these tests are reported in Table 3.9.
The effect of temperature on the drying kinetic is impressive, as shown in Figure 3.27. The manure in test N is dried in 90 min while in test O this interval reduces to 29 min. The drying time is reduced of 66% at 75 °C respect to the ambient temperature run. Increasing the temperature means that the mass transfer increases too because the air can load more vapour for dry air mass unit and also the the heat transfer is

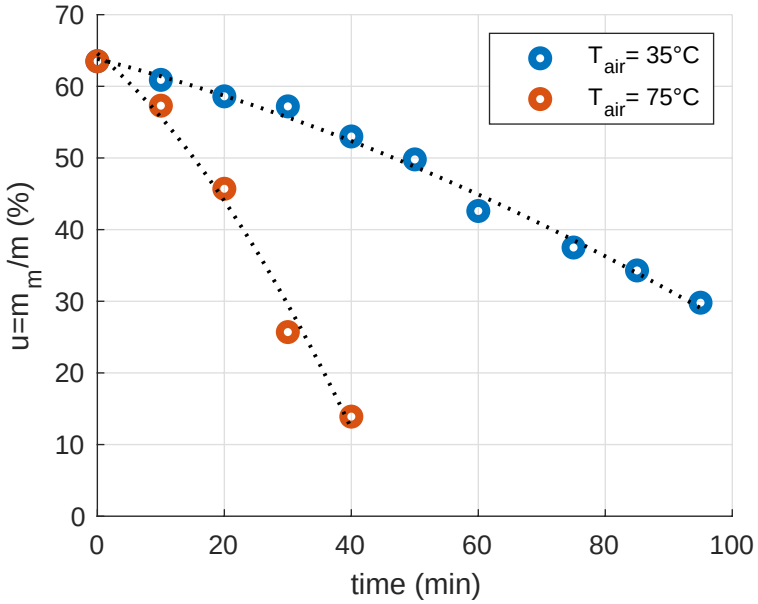

Figure 3.27: Effect of air temperature on manure moisture content u in through-circulation rotary dryer at $180\,\mathrm{m^3\,h^{-1}}$, *H=7%.*

improved.

This effect is shown in Figure 3.28 where the moisture composition X is reported in time. At 75 °C the experimental points can be still linearly fitted so the drying is in constant drying rate. The slope of O test is roughly three times the one of test N consequently the drying rate of O ($20\,\mathrm{kg\,m^{-3}\,h^{-1}}$) is three times the test N ($7\,\mathrm{kg\,m^{-3}\,h^{-1}}$).

The temperature impact on the drying process is remarkable so that it is advisable to keep the temperature high in order to reduce the drying time. However, higher temperature means higher energy used from the furnace and, in turn, less available energy.

3.4.3 Effect of the air injection

The effective contact between the airflow and the material is the core of the heat and mass transfer. Depending on the air injection point it is possible to obtain a through-circulation configuration (T-C) by using the air-blade or a cross-circulation configuration (C-C) by introducing the airflow in axial direction. The former configuration is optimized in several tests already explained while the latter is an intermediate configuration among the through-circulation and the cascade rotary dryer. In particular the material is in rolling regime in the cross section plane, such as in the through-circulation, so that new material is continuously exposed to the airflow on the top

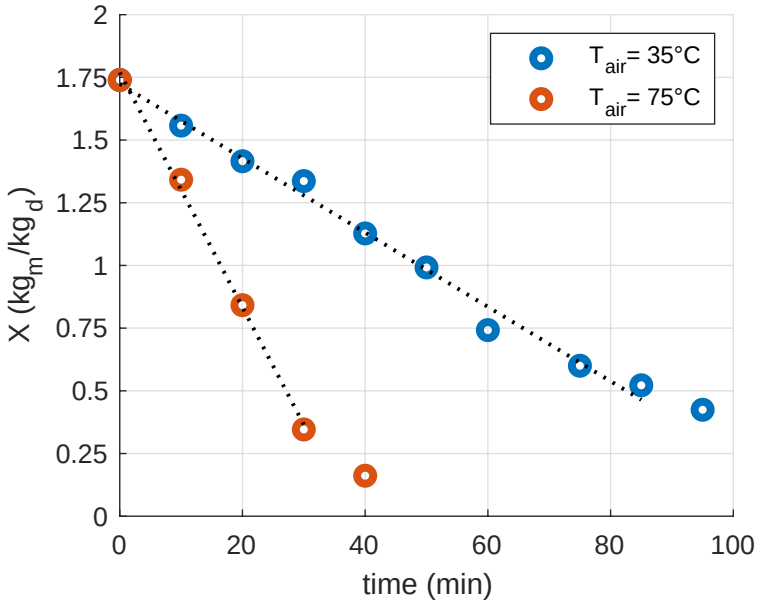

Figure 3.28: Effect of air temperature on manure moisture content X in through-circulation rotary dryer at $180\,m^3\,h^{-1}$, *H=7%.*

surface thanks to the rotation. The air flows in axial direction like in the cascade configuration. The external drilled surface is covered with the PE film to ensure the air sealing.
To guarantee a rolling regime in the cross section plane the rotational speed is set at 4 rpm while the temperature, the flow rate and the holdup are kept constant, Table 3.10.

Figure 3.29 shows the drying curves of moisture content u for the two configurations. Both the curves show a uncertainly of measurement due to the sampling mode. The through-circulation configuration dries the manure in 29 min while the cross-circulation in 41 min. There is only a difference of 10 min. It is true that, in the C-C the drying time is 30% greater than in the T-C but this is not an unsatisfactory result: here the air does not flow through the whole bed but the heat and mass

Table 3.10: Experimental conditions for manure drying investigation in two different rotary dryer configurations.

Test	**Config.**	$\mathbf{w_0}$ g	$\mathbf{u_0}$ $\frac{kg_m}{kg_m+kg_d}$	$\dot{\boldsymbol{V}}_{\boldsymbol{air}}$ m^3/h	$\mathbf{T}_{\boldsymbol{in}}$ °C	$\mathbf{Y}_{\boldsymbol{in}}$ $\frac{kg_m}{100kg_{da}}$	$\boldsymbol{\omega}$ rpm	**H** %	**flights** #	$\mathbf{t}_{\boldsymbol{SP}}$ min	**N** $\frac{kg_m}{m^3h}$
O	T-C	900	0.63	180	75	1.2	4	7	2	29	20
P	C-C	900	0.63	180	75	0.9	4	7	2	41	14

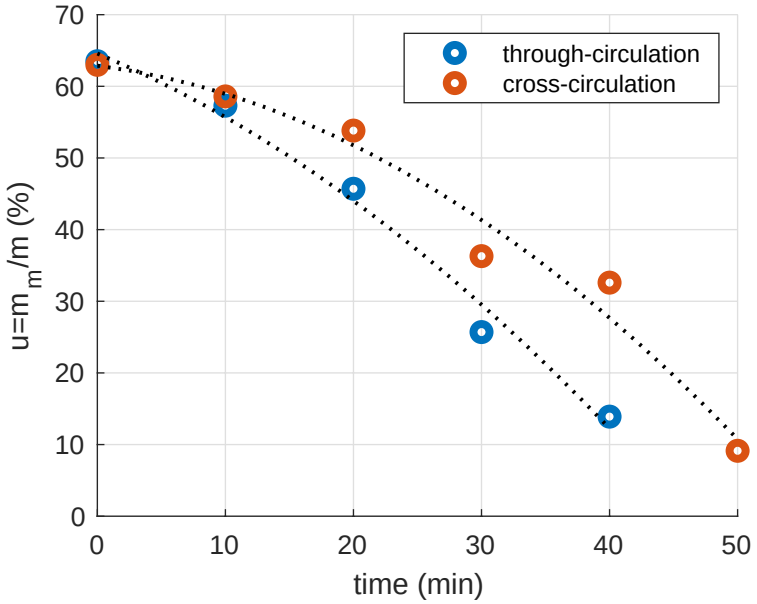

Figure 3.29: Effect of the dryer configuration on manure moisture content u at $180\,\mathrm{m^3\,h^{-1}}$, $75\,^{\circ}\mathrm{C}$, *H=7%, ω= 4 rpm.*

transfer occur only on the surface. The drying rate of test O is equal to $20\,\mathrm{kg\,m^{-3}\,h^{-1}}$ while the one of test P is $14\,\mathrm{kg\,m^{-3}\,h^{-1}}$ so their difference is of 30% too.
Nevertheless the airflow is not effectively exploited at all to dry the wet manure in the hybrid configuration, the performances are comparable to the through-circulation one. This means that the drying time could be drastically reduced if the air-wet manure contact was improved. Based on these considerations, the interest grows for the cascade rotary dryer where the close interaction between particles and airflow is maximized.

3.4.4 Conclusions

The rotary dryer ensures homogeneous dry material, which is not packed at the end of the process and it is easy to discharge from the dryer.
The temperature has a huge impact on the drying time so it is essential to keep it high. More investigations are required on its effects on the drying process.
The airflow-manure contact is also a key aspect. The through-circulation configuration ensures that all the air flows through the material bed thanks to the air-blade, while the air axial injection is more effective even though not all the air contributes to the drying process. Improving the axial configuration it is possible to increase the airflow effect on the heat and mass transfer. In fact the cascading rotary dryer configuration allows to spreads out the particles and creates strong contact between

particles and airflow. Indeed the material is fluidize by mechanical action.

3.5 Cascade rotary dryer

The experimental investigation on the cascading rotary dryer aims to evaluate the effect of the variable that affect the drying in this configuration. The investigated variable are collected into two main groups: the one concerning the solid motion regime inside the drum and the one related to the drying air. The former contains the rotation speed, the number of flights and the shape of flights. While the latter involves the air temperature, the air absolute humidity and the air flow rate. In the experimental setup the air enters in the drum from the centre of the inlet-outlet cross-section and exits through the drilled disc on the other side. The air inlet temperature is measured by a thermocouple that is fixed in the centre of the inlet tube. A PE film is fixed on the whole external drilled surface of the cylinder to force the air flow only where needed. The rotation speed is drastically increased compared to the previous cases.
Since the device is actually similar to the through-circulation configuration, the procedure is the same.
A numerical investigation follows the experimental results to predict the drying performances. Finally a first rough scale-up is carried out.

3.5.1 Investigation on the solid motion regime

The cascading rotary dryer is characterised by strong interaction between particles and air flow. This interaction is carried out by the internal shower of particles. It is due to the coupled effect of the rotation and the flights. The best is the curtain, stronger the interaction and faster the drying. The rotational speed, the number of flights and the shape of the flights are the variables that influence the cascade inside the drum. In order to evaluate their effect on the curtain creation an experimental campaign is carried out.
First of all the effect of the rotational speed is evaluated at different flow rates and temperature conditions. Then the number of flights effect is presented at different flow rates.

Effect of the rotation speed at low temperature

The experimental investigation focuses on the drying time at two different rotational speed: 30 and 50 rpm. In order to consider a broad range of operative conditions, their effect is evaluated at two different air flow rates: 100 and $50\,m^3\,h^{-1}$. The flights

Table 3.11: Experimental conditions for manure drying investigation at different rotation speed and low temperature.

Test	w_0	u_0	$\dot{V}_{air}$	T_{in}	Y_{in}	ω	H	flights	t_{SP}	N
	g	$\frac{kg_m}{kg_m+kg_d}$	m^3/h	°C	$\frac{kg_m}{100kg_{da}}$	rpm	%	#	min	$\frac{kg_m}{m^3h}$
Q	1350	0.64	100	75	1.5	30	10	2	35	26
R	1200	0.64	100	75	1.2	50	10	2	22	38
S	1200	0.64	50	65	1.3	30	10	2	67	12
T	1200	0.64	50	65	1.1	50	10	2	50	17

inside the drum are two and the holdup is equal to 10%. In Table 3.11 are reported the experimental conditions of the following tests.

The drying curves of tests Q and R are shown in Figure 3.30. When the flow rate is high ($100\,m^3\,h^{-1}$), the drying time decreases only if the rotation speed increases. In fact, at 30 rpm the drying time is 35 min while at 50 rpm it is 22 min. This means that by creating a well developed cascade the energy and mass transfer is improved, thanks to the better contact between air and particles. This phenomenon impacts on the drying rate, that increases from $26\,kg\,m^{-2}\,h^{-1}$ at 30 rpm to $38\,kg\,m^{-2}\,h^{-1}$.
These consideration are still true at a lower airflow for tests S and T respectively at 30 and 50 rpm. Looking at Figure 3.31, it shows that the effect of the increase in the rotation speed allows to reduce the drying time of 26% from 67 min to 50 min. The drying rate is increased from $12\,kg\,m^{-2}\,h^{-1}$ to $17\,kg\,m^{-2}\,h^{-1}$.
The cascade mechanical creation is fundamental to have an efficient heat and mass transfer. The rotation speed strongly influences the drying process at the considered conditions (low temperature, 2 flights). 50 rpm are the best condition: in a minute the particles fall into the cascade a hundred times while only sixty times when the rotation speed is 30 rpm. Indeed an improved particles curtain ensures a better contact between the wet solid and the airflow, so that the dying process becomes faster. Note that, the increase in the rotation speed within reason affects only mechanical aspect of the system without increasing the operative costs.

Effect of the rotation speed at high temperature

The effect of the rotation speed on the mechanically fluidized particles regime is evaluated at an high temperature airflow, equal to 150 °C, since it is available in the plant. In this investigation the air flow rate is $30\,m^3\,h^{-1}$ and the number of flights is four. Table 3.12 holds the experimental conditions.
Figure 3.32 shows the two drying curves at 30 and 50 rpm. Their drying time difference is small, about 6 minute, and the drying rates are also close to each other.

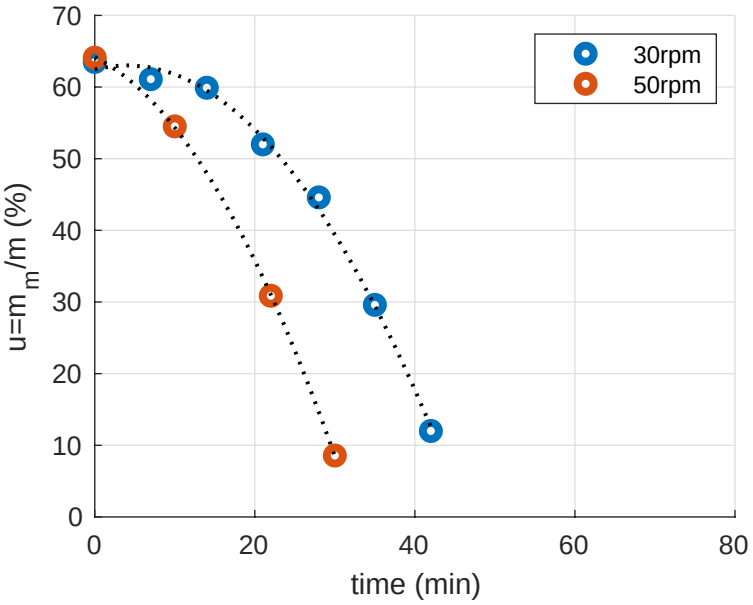

Figure 3.30: Effect of the rotation speed on manure moisture content u in cascade rotary dryer at $100\,\mathrm{m^3\,h^{-1}}$, $75\,^{\circ}\mathrm{C}$, *2 flights, H=10%.*

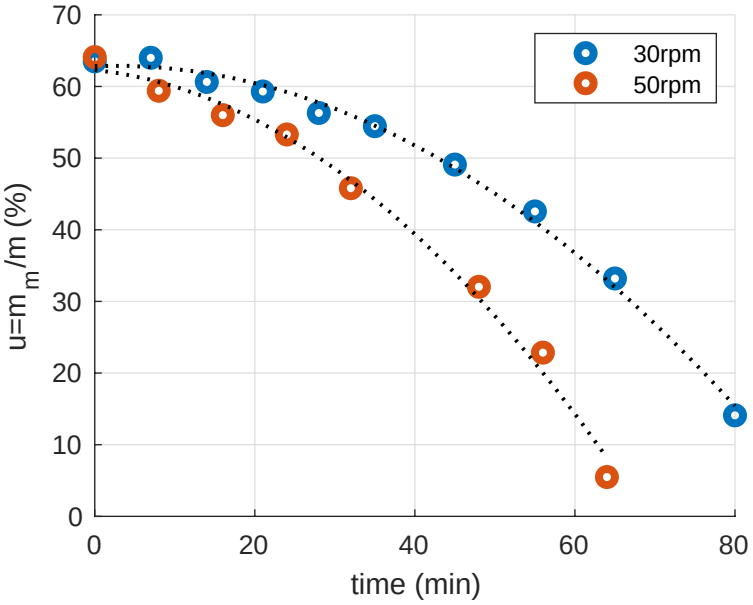

Figure 3.31: Effect of the rotation speed on manure moisture content u in cascade rotary dryer at $50\,\mathrm{m^3\,h^{-1}}$, $65\,^{\circ}\mathrm{C}$, *2 flights, H=10%.*

The improvement achievable by the increase in the rotation speed up to 50 rpm is not remarkable. Besides to the low temperature case, at high temperature the mass transfer rate at 30 rpm is already high and it does not control the process. In addition, there are 4 flights that take part in the creation of the curtain while in the previous Section they were only 2.
Moreover increasing too much the rotation speed can lead to the opposite direction: if the centrifugal force acting on the particles balances the gravitational one, the particles remain on the flights for the whole drum revolution. This aspect must be underlined in order to preserve the effectiveness of the cascading curtain. In addition, from a mechanical point of view, running the process at lower rotation speed reduces vibrations and mechanical stress on the dryer.
Hence, at high temperature and 4 flights, it is useful to run the drying process at 30 rpm to ensure an high mass transfer with a proper cascade, to reduce the mechanical stress and wear.

Table 3.12: Experimental conditions for manure drying investigation at different rotation speed and high temperature.

Test	$\mathbf{w_0}$ g	$\mathbf{u_0}$ $\frac{kg_m}{kg_m+kg_d}$	$\dot{\boldsymbol{V}}_{\boldsymbol{air}}$ m^3/h	$\mathbf{T}_{\boldsymbol{in}}$ °C	$\mathbf{Y}_{\boldsymbol{in}}$ $\frac{kg_m}{100kg_{da}}$	$\boldsymbol{\omega}$ rpm	**H** %	**flights** #	$\mathbf{t}_{\boldsymbol{SP}}$ min	**N** $\frac{kg_m}{m^2h}$
U	1200	0.64	30	150	2.5	50	10	4	26	32
V	1200	0.64	30	150	2.4	30	10	4	30	28

Effect of the number of flights

The effect of the number of flights is observed on the drying time keeping constant the others variables, which are reported in Table 3.13. This variable plays an important role in the generation of the mechanically fluidized particle regime and

Table 3.13: Experimental conditions for manure drying investigation at different number of flights.

Test	$\mathbf{w_0}$ g	$\mathbf{u_0}$ $\frac{kg_m}{kg_m+kg_d}$	$\dot{\boldsymbol{V}}_{\boldsymbol{air}}$ m^3/h	$\mathbf{T}_{\boldsymbol{in}}$ °C	$\mathbf{Y}_{\boldsymbol{in}}$ $\frac{kg_m}{100kg_{da}}$	$\boldsymbol{\omega}$ rpm	**H** %	**flights** #	$\mathbf{t}_{\boldsymbol{SP}}$ min	**N** $\frac{kg_m}{m^2h}$
R	1200	0.64	100	75	1.2	50	10	2	22	38
W	1200	0.64	100	75	1.1	50	10	4	17	49
T	1200	0.64	50	65	1.1	50	10	2	50	17
Y	1200	0.64	50	65	1.2	50	10	4	44	19

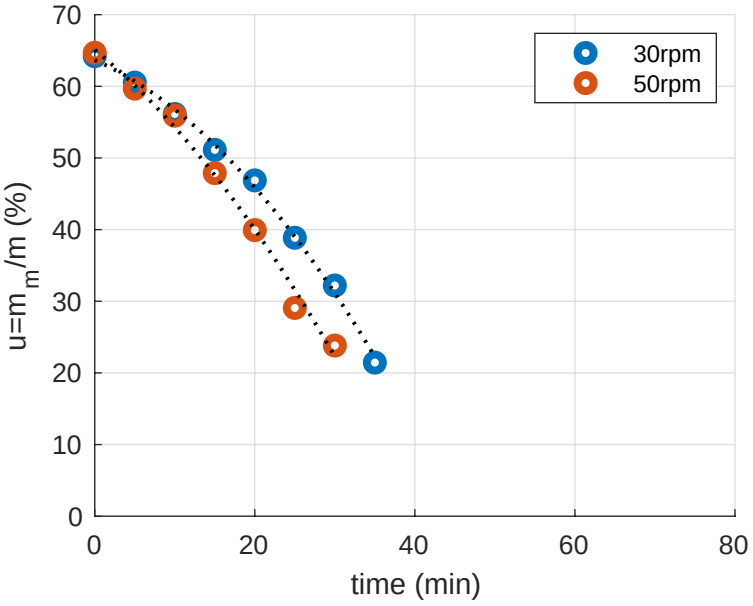

Figure 3.32: Effect of the rotation speed on manure moisture content u in cascade rotary dryer at $30\,m^3\,h^{-1}$, 150 °C, *4 flights, H=10%.*

plays a similar role to that of the rotation speed. The tests investigate the effect of 2 and 4 flights at 50 rpm, since it is the best condition at low temperature (65 to 75 °C). The evaluation is carried out at two different flow rates: 50 and $100\,m^3\,h^{-1}$. Despite there is a strong visible improvement on the cascade by doubling the number of flights, a significative difference on the drying curves does not occur. The results of T and Y tests at low flow rate are shown in Figure 3.33 where the curves are almost overlapped. This means that at these low conditions ($50\,m^3\,h^{-1}$ and 65 °C) the drying is not limited by the air-material contact since the cascade is well developed. The drying rates are extremely small, both of them are lower than $20\,kg\,m^{-3}\,h^{-1}$.
At high flow rates ($100\,m^3\,h^{-1}$), the effect of the number of internals appears as in Figure 3.34. Increasing the number of flights, the drying time is 23% reduced and the drying rate increases from 38 to $49\,kg\,m^{-3}\,h^{-1}$ reaching the order of magnitude suggested by the industrial rotary dryer manufacturers. Since an increase in the number of flights generates a huge effect in the drying rate, 4 internals for this pilot-scale rotary dryer are set. A better mechanically fluidized particle regime is obtained.
It is important to observe that, at high flow rates, the drying performance is great thanks to the improved mass transfer (both the rotation speed and the number of flights) and the higher energy provided by the airflow. This highly fluidized regime makes the particles extremely subjected to the air drag. In fact, in R and W ($\dot{V}_{air}$=$100\,m^3\,h^{-1}$, v_{air}=$0.4\,m\,s^{-1}$) the particles entrainment are huge: from 10

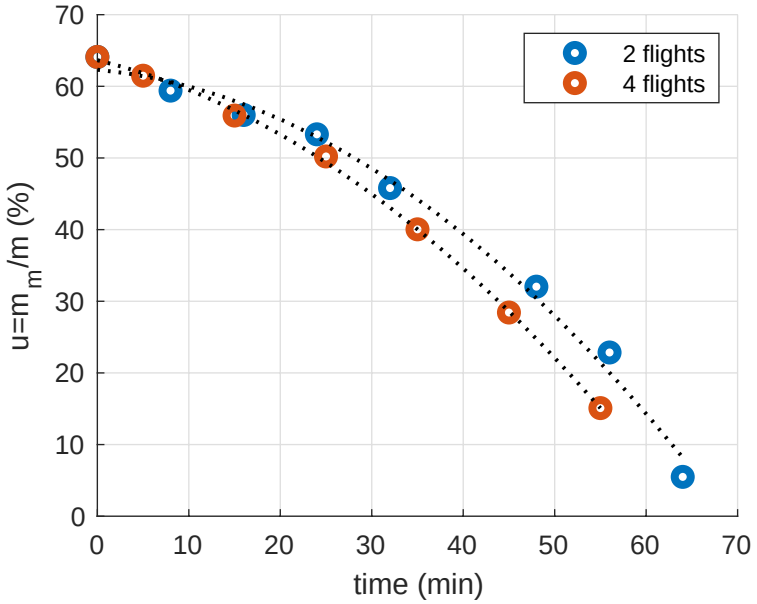

Figure 3.33: Effect of the number of flights on manure moisture content u in cascade rotary dryer at $50\,m^3\,h^{-1}$, 65 °C, *50 rpm, H=10%.*

min after the test beginning there is an important accumulation of material on the bottom of the drum towards the air outlet section. A small drag of particles is observed at $50\,m^3\,h^{-1}$ too (v_{air}=$0.2\,m\,s^{-1}$) . So the v_{air}=$0.2\,m\,s^{-1}$ is the maximum air rate possible to avoid entrainments.

Effect of the flights shape

The shape of the flights plays an important role in the detailed optimization of the curtain creation. Its investigation is carried out by manufacturing and testing three different shapes, sketched in Figure 3.35. The 3 spoons flight (b) create an adequate cascade in the first half of the cross sectional plane, in which the material is lifted up by the spoons. When the flight reaches the vertical position no manure remains on it, so the shower does not cover the entire section. The 1 palette flight (c) has an opposite behaviour: they create the cascade only while crossing the vertical position; during the lifting all the particles are contained in the palette. The smaller palette flight (d) allows the creation of a cascade that starts during the material lifting and ends overcoming the vertical position. The flights aim is to spread out the curtain in all the cross section of the drum in order to increase the contact between air and particles.

The same amount of manure is tested at $30\,m^3\,h^{-1}$ to avoid entrainments, at high temperature 150 °C and at 50 rpm. The flights are four(Figure 3.35a), as reported

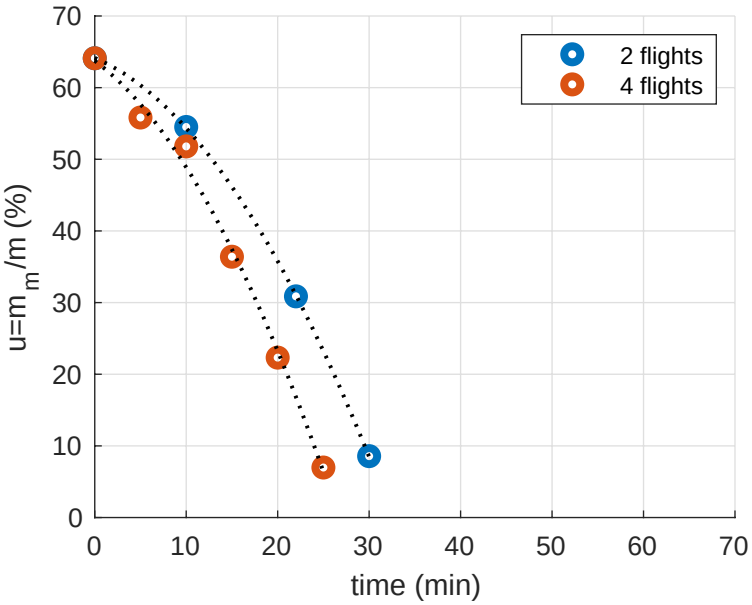

Figure 3.34: Effect of the number of flights on manure moisture content u in cascade rotary dryer at $100\,\mathrm{m^3\,h^{-1}}$, $75\,^{\circ}\mathrm{C}$, *50 rpm, H=10%.*

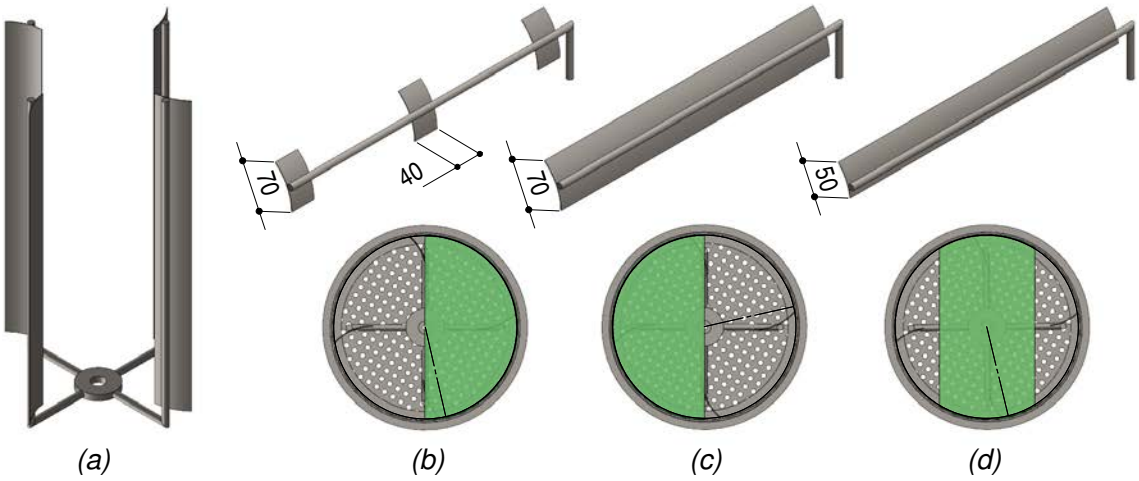

Figure 3.35: Flight shape and zone interested by the material curtain (green): four flights structure (a); 3 spoons flight (b); 1 palette (c); 1 smaller palette (d). UOM=mm.

Table 3.14: Experimental conditions for manure drying investigation at different shapes of flights.

Test	shape	w_0 g	u_0 $\frac{kg_m}{kg_m+kg_d}$	$\dot{V}_{air}$ m^3/h	T_{in} °C	Y_{in} $\frac{kg_m}{100kg_{da}}$	ω rpm	H %	flights #	t_{SP} min	N $\frac{kg_m}{m^2h}$
U	smaller palette	1200	0.64	30	150	2.5	50	10	4	26	32
Z	palette	1200	0.64	30	150	1.7	50	10	4	25	33
AA	3 spoons	1200	0.64	30	150	1.8	50	10	4	23	36

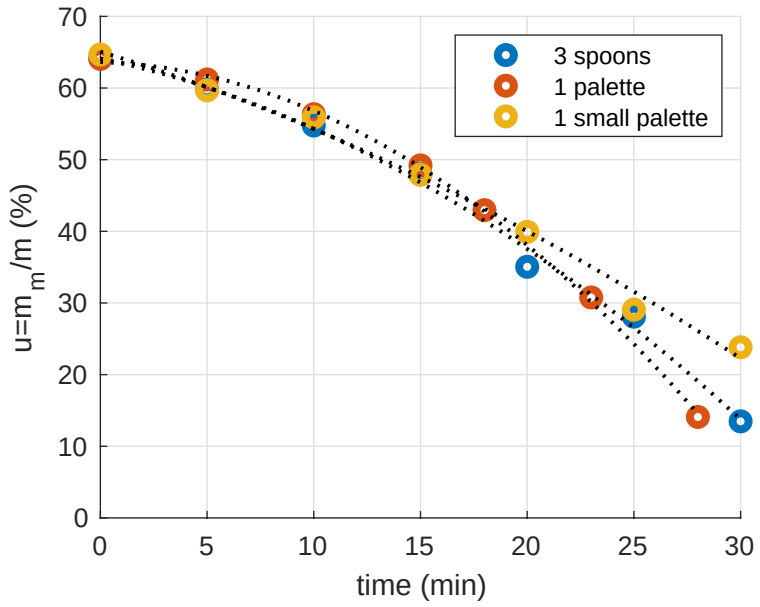

Figure 3.36: Effect of the shape of flights on manure moisture content u in cascade rotary dryer at 30 $m^3\,h^{-1}$, 150 °C, 50 rpm, 4 flights, H=10%.

in Table 3.14.

Figure 3.36 shows the manure drying curve: they are almost overlapped. The time to reach the set point is between 23 and 26 min for all the tests and the drying rate is in the range of 32 and 36 $kg\,m^{-3}\,h^{-1}$. Since the shape of the flights has not a visible impact on the drying performances the choice falls on the simplest device to produce and on the one that covers the largest area with the cascade. For these reasons the small palette flights is chosen for the following tests.

Conclusions

The curtain creation in the cascade rotary dryer is the crucial issue to improve the mass transfer between the wet manure and the airflow. The desired curtain configuration is the one that cover more cross section as possible. The coupled effect of the rotation speed and the number of flights compete in the generations of

the shower. At a low temperature (and 2 fights), the increase in the rotation speed from 30 to 50 rpm improves the cascade and consequently the mass transfer. At an high temperature (and 4 flights) the beneficial effect of the rotation speed on the drying performances is less pronounced so that it is possible to run the drying at lower rpm without increasing the drying time. This means that at these condition it is pointless to perform the drying at 50 rpm. Moreover, decreasing the rotational speed to 30 rpm the rotary dryer is subjected to lower mechanical stress and wear. The flights are extremely important to lift up the material and their number contributes to the creation of shower. Increasing their number up to four the curtain is well developed.
Combining these results, the flights need to be increased up to four while the rotation speed can be reduced at 30 rpm performing the drying at high temperature, in the pilot-scale dryer.
The tested shapes have not shown any relevant effect on the drying performances, hence the simplest is chosen. Needless to say that other unconventional shapes might improve the process.
$50\,\mathrm{m^3\,h^{-1}}$ which correspond to (v_{air}=$0.2\,\mathrm{m\,s^{-1}}$) is the maximum air flow rate reachable to preserve the cascade, while avoiding entrainments, which reduce the manure residence time. Hence improving the cascading regime, the particles are more dispersed and more affected by the air drag so the airflow needs to be reduced.

3.5.2 Investigation on the drying air

The air flow supplies the energy for the moisture evaporation. The air effectiveness in the drying process depends on three variables: its specific humidity ($\mathrm{kg}_m/\mathrm{kg}_{da}$), its temperature and its flow rate. These variable are clearly investigated in the pilot-scale cascade rotary dryer set-up, equipped with four small palette shaped flights and ω=30 rpm. Taking into consideration the previous results, the best drying performances are obtained at high temperature so the investigation is carried out at air temperature greater than 100 °C. For this reason, the PE film on drilled metal cylinder external surface is replaced with an aluminium.

Effect of the specific humidity

The specific humidity is the vapour content per mass unit of dry air. The test aims to compare the drying performances of two airflows with a strong difference in the specific humidity. The experimental conditions are reported in Table 3.15.
The airflow of test V directly comes from the chimney of a commercial pellet stove and it is directed injected in the dryer . The flue gasses have an high specific

Table 3.15: Experimental conditions for manure drying investigation at different air specific humidity.

Test	$\mathbf{w_0}$ g	$\mathbf{u_0}$ $\frac{kg_m}{kg_m+kg_d}$	$\dot{\boldsymbol{V}}_{\boldsymbol{air}}$ m^3/h	$\mathbf{T}_{\boldsymbol{in}}$ °C	$\mathbf{Y}_{\boldsymbol{in}}$ $\frac{kg_m}{100kg_{da}}$	$\boldsymbol{\omega}$ rpm	**H** %	**flights** #	$\mathbf{t}_{\boldsymbol{SP}}$ min	**N** $\frac{kg_m}{m^2h}$
V	1200	0.64	30	150	2.45	30	10	4	30	28
BB	1200	0.64	30	150	0.66	30	10	4	28	30

humidity equal to Y_V=2.45 $kg_m/100kg_{da}$ and their temperature is 150 °C. This test aims to simulate the drying using a recirculation of the furnace flue gasses coming from the manure combustion. Instead, in the BB test ambient air electrically heated by an heat gun is used. Its specific humidity is equal to Y_{BB}=0.66 $kg_m/100kg_{da}$. The air flow rate is 30 $m^3\,h^{-1}$ and the dryer holdup is equal to 10% in both tests.
The two drying curves are almost overlapped in Figure 3.37. At this temperature condition, the effect of the specific humidity seems negligible. This result could be surprising because it could be expected that humid air is unfit to a drying process. However, the flow with an higher specific humidity has also an higher saturation condition so that the difference between Y^{sat} and Y_{in}, which is the real driving force for the mass transfer, could be slightly reduced.
To better explain this concept the thermodynamic states of tests V and BB are reported in Figure 3.39. Test BB (the blue one) enters in the drum at 150 °C and Y_{BB}, proceeding along the wet bulb temperature line ($T_{wb,BB}$=41 °C) until the saturation curve, the saturation relative humidity can be determined (Y^{sat}_{BB}=5.2 $kg_m/100kg_{da}$). The mass transfer driving force is their difference which is 4.54 $kg_m/100kg_{da}$.
On the other hand, test V airflow at the inlet condition is at the same temperature as BB and at an higher moisture content since they are flue gasses (Y_V). The corresponding saturation condition at the particle interface is Y^{sat}_V=7.0 $kg_m/100kg_{da}$ and $T_{wb,V}$46 °C. The mass transfer driving force is 4.55 $kg_m/100kg_{da}$. In fact, the two drying processes have the same driving forces. This is the reason why the two curves are overlapped.
As demonstrated in fig Figure 3.38, a constant drying rate occurs for both tests. Outcomes of test V demonstrate that a fraction of the furnace flue gasses can be directly used as drying medium in the full-scale process avoiding the need of a drying air-flue gasses heat exchanger. This results in a reduction of the component number, that is a simpler plant layout.

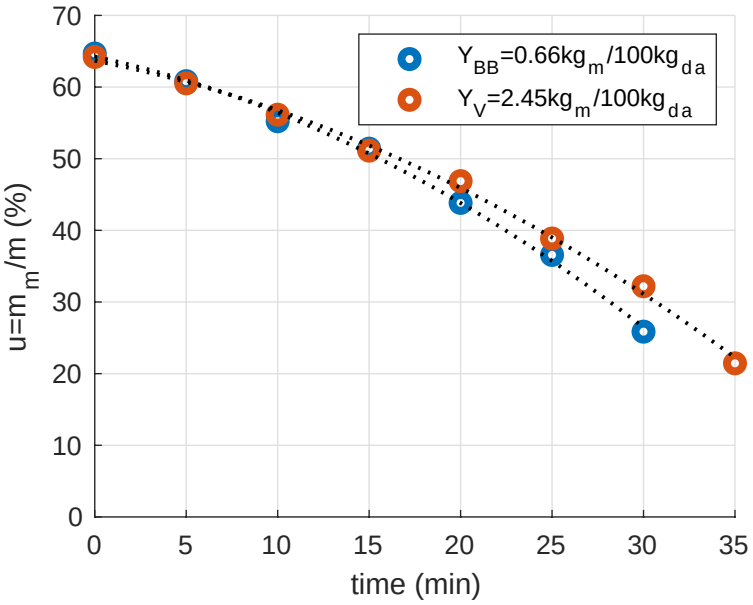

Figure 3.37: Effect of the air relative humidity on manure moisture content u in cascade rotary dryer at $30\,\mathrm{m^3\,h^{-1}}$, $150\,^{\circ}\mathrm{C}$, *30 rpm, 4 flights, H=10%.*

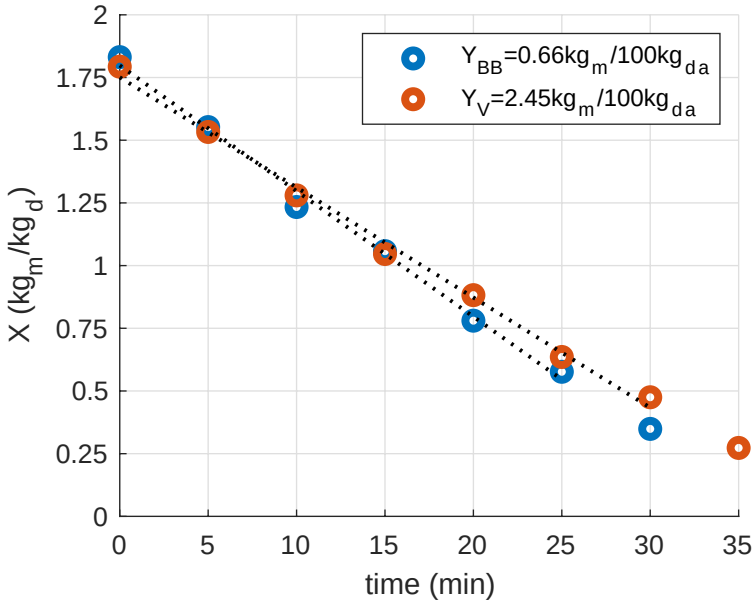

Figure 3.38: Effect of the air relative humidity on manure moisture content X in cascade rotary dryer at $30\,\mathrm{m^3\,h^{-1}}$, $150\,^{\circ}\mathrm{C}$, *30 rpm, 4 flights, H=10%.*

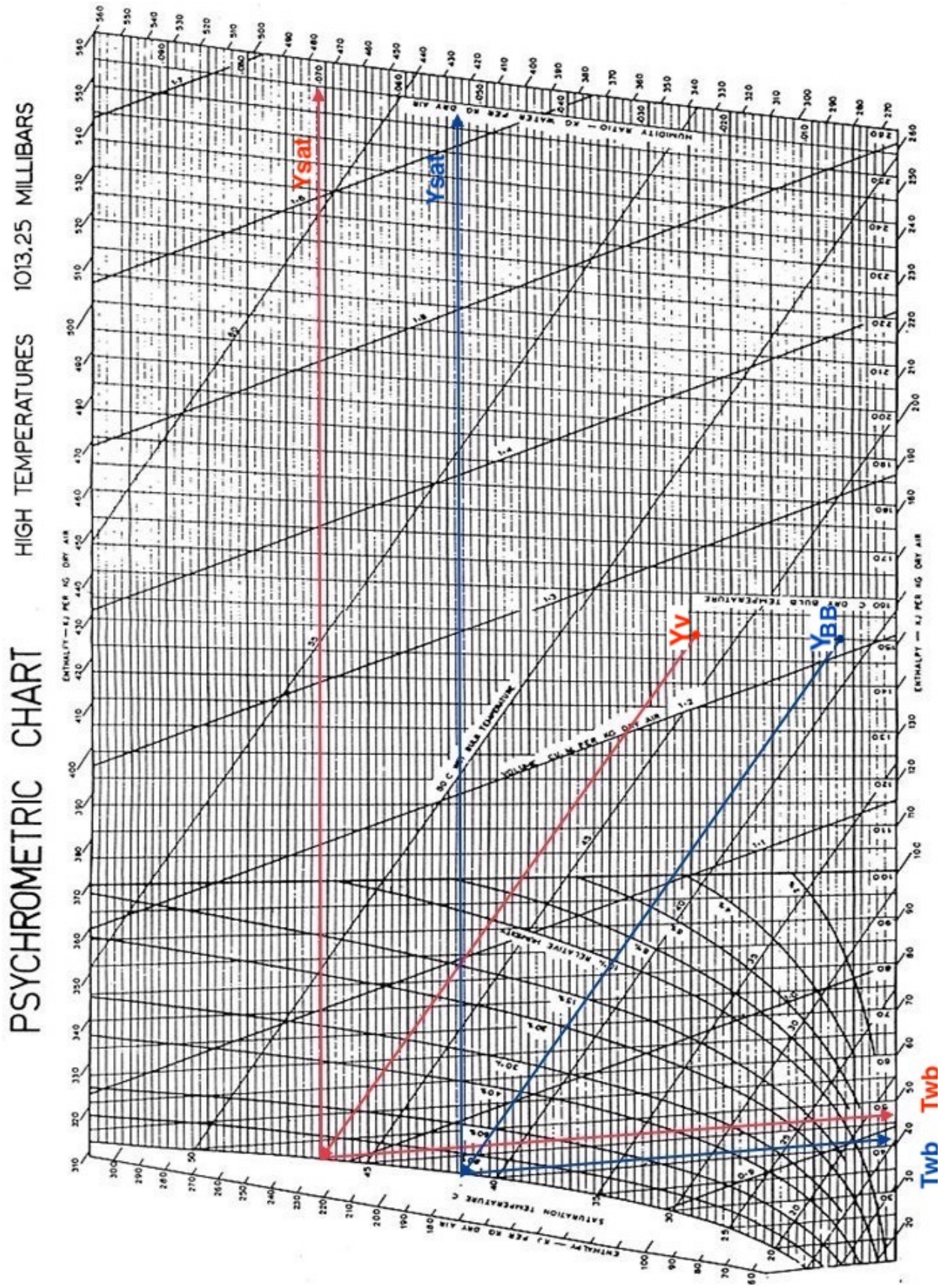

Figure 3.39: Thermodynamic states for tests V and BB in psychrometric chart at$30\,\mathrm{m^3\,h^{-1}}$, $150\,^{\circ}\mathrm{C}$, *30 rpm, 4 flights, H=10%.*

Table 3.16: Experimental conditions for manure drying investigation at different air temperature.

Test	w_0	u_0	$\dot{V}_{air}$	T_{in}	Y_{in}	ω	H	flights	t_{SP}	N
	g	$\frac{kg_m}{kg_m+kg_d}$	m^3/h	°C	$\frac{kg_m}{100kg_{da}}$	rpm	%	#	min	$\frac{kg_m}{m^2h}$
BB	1200	0.64	30	150	0.66	30	10	4	28	30
CC	1200	0.64	30	200	0.66	30	10	4	24	34
DD	1200	0.64	30	260	0.65	30	10	4	17	48
EE	1200	0.64	30	320	0.64	30	10	4	15	56
FF	1200	0.64	30	380	0.64	30	10	4	12	68

Effect of Temperature

The temperature effect on the drying process is here investigated, by varying it in the interval 150 to 380 °C. In this range of operability, five temperature (150, 200, 260, 320 and 380 °C) are tested keeping all the others variables constant. The cascading configuration is provided by ω=30 rpm and 4 small palette flights while the flow rates is $30\,m^3\,h^{-1}$. The experimental conditions are summarized in Table 3.16.
The temperature effect on the drying process is clearly shown in Figure 3.40: increasing the air temperature, the drying time is reduced and the the drying process is improved. Indeed, the drying time is halved from 150 to 380 °C. The decrease in moisture content is regular in all five tests. The drying rate is constant until the set point moisture content (i.e., 30%) as shown in Figure 3.41 where all the drying curves are straight lines. When the air temperature is higher than 260 °C, the corresponding constant drying rate falls in a range similar to that of industrial dryer (50 - $70\,kg\,m^{-3}\,h^{-1}$). Since the rate is constant, the temperature improves the moisture release mechanisms, such as diffusion, from the inside out refreshing continuously the water external layer on the particle. Moreover, during the constant drying period, the temperature of the solid particles remains constant and equal to the wet bulb temperature of the drying air. This allows to perform the drying at temperature higher than the dry manure auto ignition temperature (T_{ai}=210 °C), preventing from biomass ignition risk. It is still suggested to implement the co-current continuous configuration to prevent undesirable material overheating.
In Figure 3.42 the drying time is shown in function of the air temperature. The fitting curve slope shows the effect of a variation in temperature on the drying time: around 200 °C a slide variation in temperature leads to an higher effect than at 350 °C. In fact, an increase of 20 °C in the air temperature at 200 °C produces 3 min reduction in the drying time while only 1 min reduction at 320 °C. The same behaviour occurs in presence of a decrease in temperature. So a good compromise

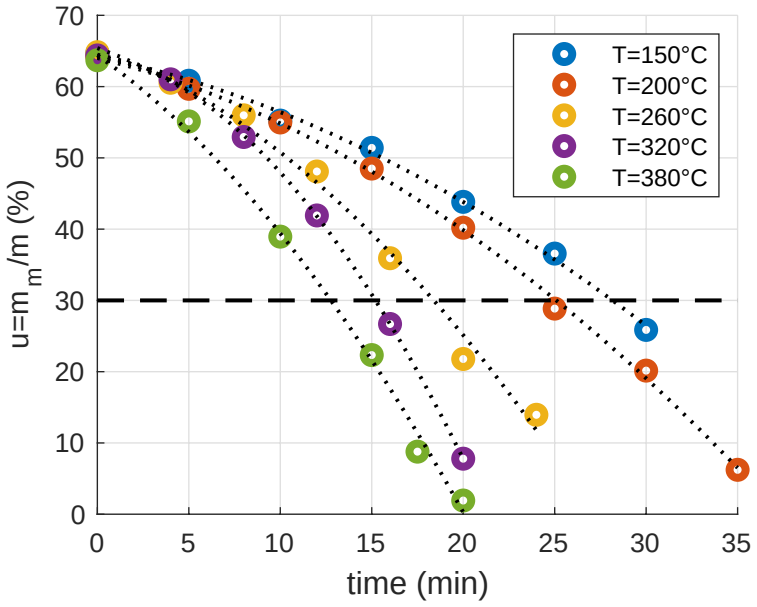

Figure 3.40: Effect of the air temperature on manure moisture content u in cascade rotary dryer at 30 $m^3\,h^{-1}$, 30 rpm, 4 flights, H=10%.

between short drying time, high temperature and low variability is 260 °C.

Effect of the volumetric flow rates

The effect of the air flow rates on the process of manure drying is further investigated. The rotary dryer performances are evaluated at 30, 22.5 and 15 $m^3\,h^{-1}$. The tests are carried out at constant temperature (260 °C); the other experimental conditions are collected in Table 3.17.
The moisture content (u) in time is shown in Figure 3.43. The air flow rates have a strong impact on the drying time, by doubling it the drying time is reduced more than an half. In fact, when the flow rates increases, the relative velocity between the particles and the air increases too, so that the mass transfer is improved. This

Table 3.17: Experimental conditions for manure drying investigation at different air flow rates.

Test	$\mathbf{w_0}$ g	$\mathbf{u_0}$ $\frac{kg_m}{kg_m+kg_d}$	$\dot{\boldsymbol{V}}_{\boldsymbol{air}}$ m^3/h	$\mathbf{T}_{\boldsymbol{in}}$ °C	$\mathbf{Y}_{\boldsymbol{in}}$ $\frac{kg_m}{100kg_{da}}$	$\boldsymbol{\omega}$ rpm	**H** %	**flights** #	$\mathbf{t}_{\boldsymbol{SP}}$ min	**N** $\frac{kg_m}{m^2h}$
DD	1200	0.64	30	260	0.65	30	10	4	17	48
GG	1200	0.64	22.5	260	0.80	30	10	4	24	34
HH	1200	0.64	15	260	0.80	30	10	4	37	22

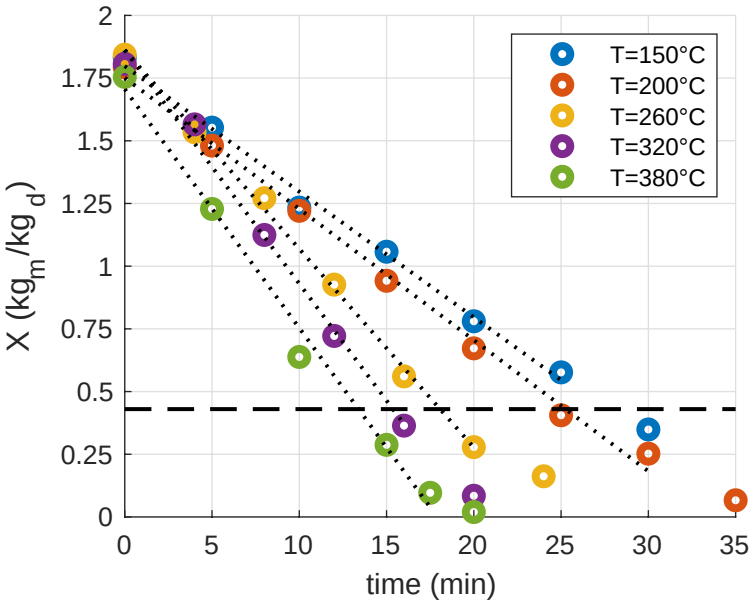

Figure 3.41: Effect of the air temperature on manure moisture content X in cascade rotary dryer at $30\,\mathrm{m^3\,h^{-1}}$*, 30 rpm, 4 flights, H=10%.*

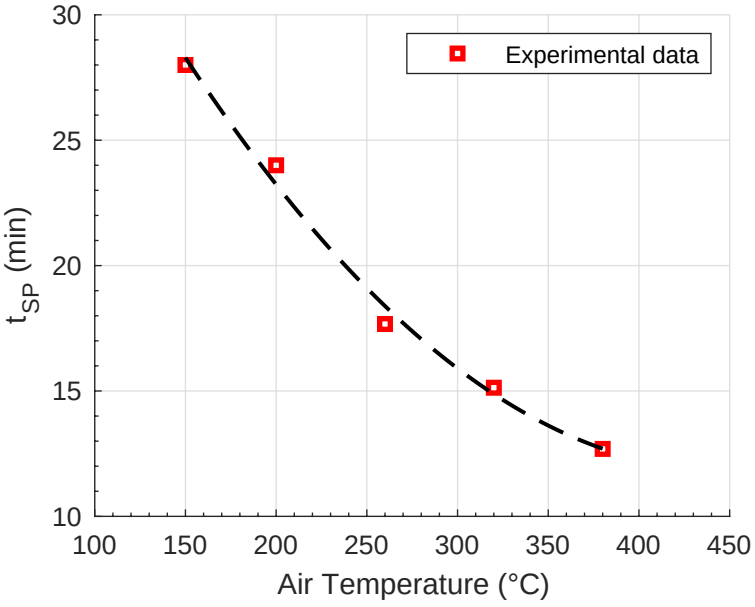

Figure 3.42: Air temperature effect on the drying time in cascade rotary dryer at $30\,\mathrm{m^3\,h^{-1}}$*, 30 rpm, 4 flights, H=10%.*

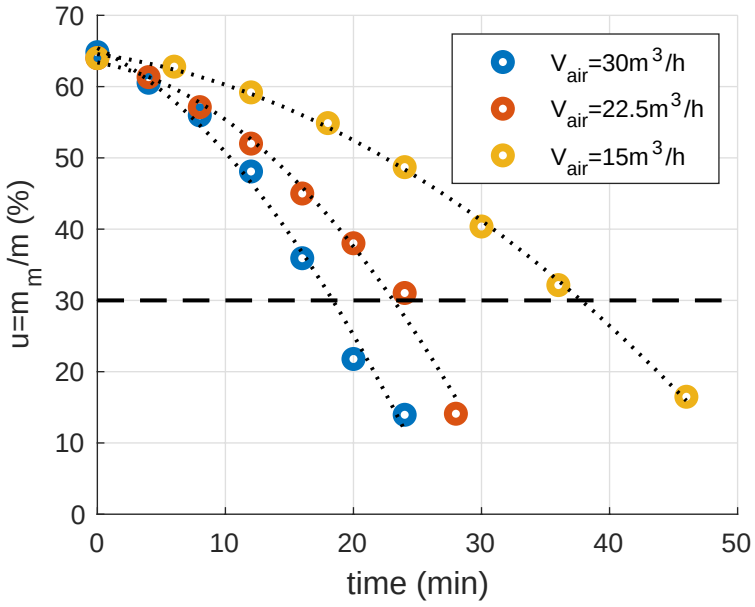

Figure 3.43: Effect of the air flow rates on manure moisture content u in cascade rotary dryer at 260 °C, 30 rpm, 4 flights, H=10%.

means that the air flow rate must be maximised to reduce the drying time without crossing the upper limit of 50 $m^3\,h^{-1}$ to avoid particles entrainment in the air stream. The constant drying rate persists in the whole drying process. They are N=22, 34 and 48 $kg\,m^{-3}\,h^{-1}$ respectively for 15, 22.5 and 30 $m^3\,h^{-1}$. In Figure 3.44 the air flow effect on the drying time is shown. The fitting curve slope is higher proceeding from 15 to 22.5 $m^3\,h^{-1}$ compared to the one in the range of 22.5 - 30 $m^3\,h^{-1}$. This means that the process is more sensible to a flow rate variation in the former range than in the latter. In fact, a 3 $m^3\,h^{-1}$ (Δv=0.01 $m\,s^{-1}$) increase in the volumetric flow rates at 15 $m^3\,h^{-1}$(v=0.06 $m\,s^{-1}$) produces 7 min reduction in the drying time, which is 30% less time. While the same increase at 25 $m^3\,h^{-1}$ (v=0.1 $m\,s^{-1}$) improves the drying time of only a 3 min which is 12% of the total.

Conclusions

The air impacts on the drying process with its specific humidity, its temperature and its flow rate. In order to perform efficiently the drying, the air temperature must be higher than 100 °C. The effect of the specific humidity does not affect the drying performances in the temperature range 150 - 380 °C which is the one suitable for the drying process. This is an important result because it allows to use the hot and wet, flue gasses coming from the furnace for an effective drying.
The effect of the air temperature is very significant on the drying process. It affects on both the mass and the heat transfer: increasing the temperature, the mass

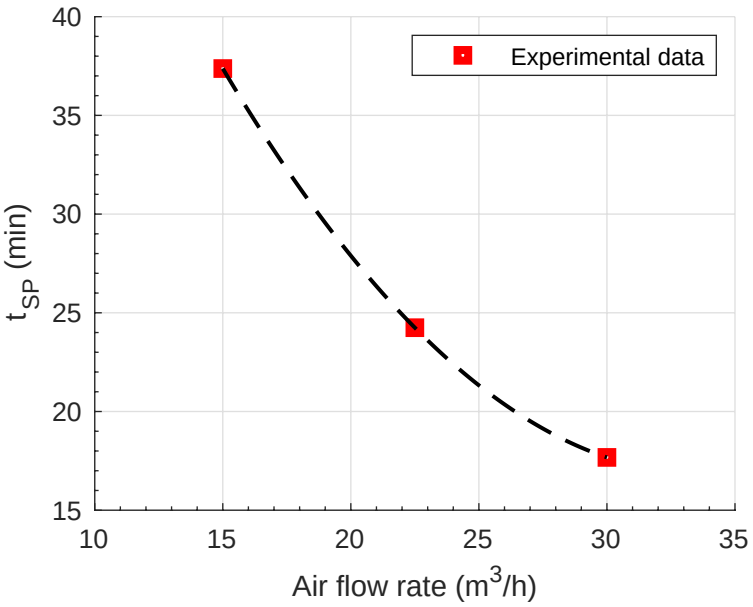

Figure 3.44: Air flow rates effect on the drying time in cascade rotary dryer at 260 °C, *30 rpm, 4 flights, H=10%.*

transfer coefficient, the saturation condition, and the driving force increase. The drying phenomenon takes place at constant drying rate. The preferred operative point is around 260 °C because it is a good compromise between 150 and 380 °C.
The air flow rate impacts on the drying performances since relative velocity between particles and air affects the heat and mass transfer coefficients. The air flow rate needs to be high to provide an effective drying, taking into consideration the entrainments reduction and the energy required to the hot air production.

Chapter 4

Drying model and preliminary design of rotary dryer

This Chapter focuses on the drying modelling in rotary dryers. The modelling of drying process is a complex challenge because the physical phenomena involve simultaneously heat and mass transport, resulting in an highly non-linear set of governing equations. Depending on the goal, different models can be developed. Usually their purposes are to design a new dryer, or to evaluate the performances at different conditions from the experimental one or to scale-up the dryer. The drying can be modelled in a simple way considering only constant drying rate or in a more complex one, modelling also the decreasing rate period. Different levels of complexity are needed for different stages of the design process.
Firstly the analysis of the first principle is presented to investigate the thermodynamic feasibility of the process. Then a 0D numerical model to predict manure drying behaviour is developed and tuned on the experimental results. The numerical results are critically evaluated. Finally, preliminary rough scale-up indications for a real industrial application are provided.

4.1 First principle analysis

This section deals with the thermodynamic analysis of the drying process and aims to investigate the energetic feasibility of the integrated manure drying, i.e., if the heat absorbed by the evaporation can be supplied by the hot flue gases from the manure combustion itself. In addition, this analysis permits to give some hints on the economic attractiveness of the cascaded drying and combustion in the same furnace.

Figure 4.1 shows the material and energetic flows in a counter current rotary dryer. The dry manure mass flow rate $\dot{m}_{s,d}$ enters in the dryer and it is dried from

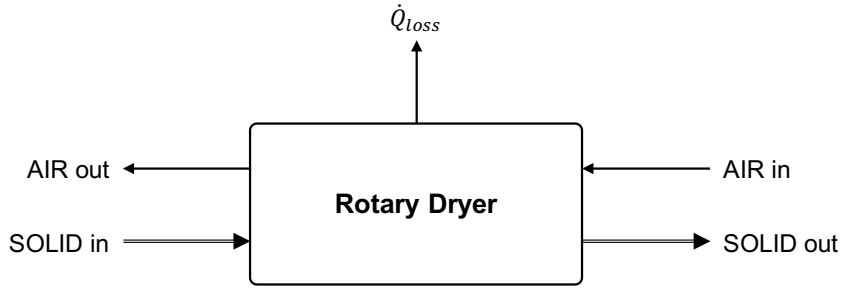

Figure 4.1: Schematic representation of counter current rotary dryer.

its initial moisture content X_{in} to the desired one, X_{out}. The solid increases its temperature from $T_{s,in}$ to $T_{s,out}$. The hot air flow rate $\dot{m}_{g,d}$ increases its specific moisture content from Y_{in} to Y_{out}. $T_{g,in}$ and $T_{g,out}$ are the inlet and outlet air temperatures, respectively.
The material balance on the moisture involves both wet solid and dry air.

$$\dot{m}_{s,d}X_{in} + \dot{m}_{g,d}Y_{in} = \dot{m}_{s,d}X_{out} + \dot{m}_{g,d}Y_{out} \tag{4.1}$$

The enthalpy balance requires the expressions for the enthalpy of the wet solid and the one for the air:

$$\dot{m}_{s,d}H'_{s,in} + \dot{m}_{g,d}H'_{g,in} = \dot{m}_{s,d}H'_{s,out} + \dot{m}_{g,d}H'_{g,out} + \dot{Q}_{loss} \tag{4.2}$$

where H'_s is the enthalpy of the wet solid, H'_g the one of the drying air (dry mass basis), and $\dot{Q}_{loss}$ is the net heat loss from the dryer and can be estimated as a fraction of the total heat $\dot{Q}_{tot}$ supplied to the dryer by the hot air ($\dot{Q}_{tot} = \dot{m}_{g,d}H'_{g,in}$). The enthalpy of wet solid at the temperature T_s is related to the reference state of solid and the liquid temperature T_0:

$$H'_s = c_s(T_s - T_0) + Xc_w(T_s - T_0) + \Delta H_w \tag{4.3}$$

where c_s and c_w are the heat capacity of dry manure and of moisture as liquid. ΔH_w is the integral heat of wetting which is generally neglected.
The enthalpy of the gas stream at the temperature T_g is related to the reference state of gas temperature T_0. This stream is composed by the air and the vapour.

$$H'_g = (c_g + c_v Y)(T_g - T_0) + \lambda_0 Y \tag{4.4}$$

where c_g and c_v are the heat capacity of dry air and of vapour. λ_0 is the heat of vaporization at reference temperature T_0.

Table 4.1: Variables of thermodynamic model

Design specifications		
$\dot{m}_{s,d}$	18	$\mathrm{kg\,h^{-1}}$
X_{in}	1.5	$\mathrm{kg}_m\ \mathrm{kg}_d^{-1}$
X_{out}	0.429	$\mathrm{kg}_m\ \mathrm{kg}_d^{-1}$
$\mathrm{T}_{s,in}$	10	°C
$\mathrm{T}_{g,in}$	150	°C

Properties		
c_g	1005	$\mathrm{J\,kg^{-1}\,K^{-1}}$
c_v	1884	$\mathrm{J\,kg^{-1}\,K^{-1}}$
λ_0	2502300	$\mathrm{J\,kg^{-1}}$
ρ_g	1.2	$\mathrm{kg\,m^{-3}}$
c_s	1500	$\mathrm{J\,kg^{-1}\,K^{-1}}$
c_w	4186	$\mathrm{J\,kg^{-1}\,K^{-1}}$
$\mathrm{T}_{g,amb}$	10	°C
$\mathrm{RH}_{g,amb}$	70	%

Assumptions		
$\dot{Q}_{loss}$	0.1 $\dot{Q}_{tot}$	$\mathrm{J\,kg^{-1}}$
$\mathrm{T}_{g,out}$	60	°C
$\mathrm{T}_{s,out}$	30	°C

Calculated variables	
$\dot{m}_g$	$\mathrm{kg\,s^{-1}}$
Y_{out}	$\mathrm{kg}_v\ \mathrm{kg}_{da}^{-1}$
P_g	kW

The values of the above variables are collected in Table 4.1. The manure flow rate is the one needed to guarantee a furnace power of 70 kW, (see Section 2.2). A typical winter day is assumed as the initial condition ($\mathrm{T}_{s,in}$, $\mathrm{T}_{g,amb}$, $\mathrm{RH}_{g,amb}$). It is possible to calculate the power required for heating the air stream,

$$P_g = \dot{m}_g(H'_{g,in} - H'_{g,amb}) \tag{4.5}$$

which is definitely the power required for the drying process.
The result of this calculation shows that the power required to drying the manure (P_g) is equal to 26.8 kW while the one delivered during the combustion is 70 kW. Thus the integrated process is energetically feasible and the resulting effective power is 43.2 kW,approximately equal to 62% of the delivered one.

4.2 0D model

A simple first principle analysis disregards the kinetic aspect of the drying, that is neither heat transfer from air to particle, neither mass transfer from particles to air are modelled. Conversely, the core of the 0D model here presented is the moisture transfer from fixed isolated particles to the hot airflow and the relative heat transfer. The model aims to describe the process evolution in time in terms of moisture content and solid temperature.

4.2.1 Model definition

The particle behaviour is assumed like the one of a wet bulb thermometer. The air at the interface is at saturated condition and its temperature corresponds to the wet bulb temperature of the inlet air. Constant rate for the overall drying duration is assumed.
Input variables are the solid amount and its moisture initial content, the air flow rates and its thermo-hygrometric properties. While the output variables are the mass of manure and the solid temperature in time.

The material balance for the solid is:

$$\frac{d\dot{m}_{wb}}{dt} = -\dot{m}^{ev} \tag{4.6}$$

where $\dot{m}_{wb}$ is the gross manure mass, $\dot{m}^{ev}$ is the evaporation rate.

The evaporation rate:

$$\dot{m}^{ev} = -\alpha h_m (y_w^{sat} - y_w^{in}) \tag{4.7}$$

where α is an fitting parameter in ($\mathrm{kg\,m^{-1}}$), h_m is the mass transfer coefficient ($\mathrm{m\,s^{-1}}$), y_w^{sat} and y_w^{in} are the molar fraction of moisture in air phase respectively at the particle interface (where the air is assumed saturated) and at the inlet condition.

The mass transfer coefficient h_m is estimated by using dimensionless numerical correlation for a single spherical particle fixed in the space and hit by the air flow rate. According to the Chlinton Colburn analogy, the mass transfer in convective regime is function of the Reynolds and Schmidt number, and using the correlation by Fyhr and Kemp [23].

$$Sh = 3.5 + 1.05 Re^{1/2} Sc^{1/3} \tag{4.8}$$

The Sherwood number is the ratio between the convective material transport and the diffusive one so the mass transfer coefficient can be easily obtained.

$$h_m = \frac{Sh \cdot \mathscr{D}_i}{d_p} \tag{4.9}$$

Here,$\mathscr{D}_i$ is the diffusive coefficient of vapour in air ($\mathrm{m\,s^{-1}}$) and d_p is the particle diameter (m). The particle diameter is assumed equal to 1 mm.

The mass transfer driving force is the difference between the two molar fractions. y_w^{sat} is the vapour molar fraction surrounding the manure particle surface. It is obtained by the ratio of the saturation pressure and the atmospheric one ($\mathrm{y}^{sat} = p^{sat}(T)/p$). The saturation pressure is function of the temperature and it is calculated

Table 4.2: Antoine coefficients for water.

A	**B**	**C**
-	K	K
4.6543	1435.264	-64.848

from Antoine equation with the specific parameters for the vapour, which are reported in Table 4.2.

$$P^{sat} = 10^{A-B/(T+C)} \tag{4.10}$$

The temperature T is the wet bulb temperature T_{wb} of the inlet dry air. This assumption is in accordance with the constant drying rate period physical phenomena described in section 1.2, where the wet bulb temperature is kept constant. The wet bulb temperature of the dry air (T_{db}) can be obtained by the relation:

$$T_{db} - T_{wb} = \frac{\lambda(T_{wb})(Y^{sat}(T_{wb}) - Y)}{950} \tag{4.11}$$

The vapour molar fraction in the bulk, y_w^{in}, depends on the inlet air thermo - hygrometric conditions. These conditions are assumed constant during the whole drying process.
The 0D model implies that there is not an inlet section nor an outlet one. The air that hits the particles has always the same conditions during the whole process; these conditions are the initial one. In fact, the model does not consider that the air increases its moisture content while drying the wet particles. This assumption is supported by the fact that it is supposed to use an high air flow rate compared to the removed vapour, hence the variation of moisture content in the airflow is negligible.

The energy balance is:

$$(m_{wb}c_{s,wb})\frac{dT_s}{dt} = \dot{q}^{g\to s} - \dot{m}^{ev}\lambda \tag{4.12}$$

m_{wb} is the mass of the manure (kg) and $c_{s,wb}$ is the specific heat of the solid ($\mathrm{J\,kg^{-1}\,K^{-1}}$). The variation of solid temperature dT_s/dt is related to the difference between the energy provided by the gas to the solid $\dot{q}^{g\to s}$ and the heat required for the moisture vaporization. In the constant rate period it is expected that all the energy provided to the solid is absorbed by the evaporation keeping the solid temperature constant.
The heat provided to the solid is:

$$\dot{q}^{g\to s} = \beta h_t(T_g - T_s) \tag{4.13}$$

where β is an adjustable parameter (m^2), which contains some geometrical particle properties, h_t is the heat transfer coefficient ($W\,m^{-2}\,K^{-1}$), T_g is the inlet gas temperature while T_s the solid one.
The previous discussion on the mass transfer followed the heat transfer analogy so, again the correlation refers to a spherical isolated particle fixed in the space and hit by the airflow.

$$Nu = 3.5 + 1.05Re^{1/2}Pr^{1/3} \tag{4.14}$$

$$h_t = \frac{Nu \cdot k}{d_p} \tag{4.15}$$

The Nusselt correlation is used [23] to obtain the heat transfer coefficient h_t. Since the Nusselt number is the ratio of the convective to conductive heat transfer, in Equation 4.15 k is the air thermal conductivity ($W\,m^{-1}\,K^{-1}$).
The model requires to solve the two differential equations:

$$\begin{cases} \frac{dm_{wb}}{dt} = -\alpha h_m (y_w^{sat} - y_w^{in}) \\ (m_{wb} c_{s,wb}) \dfrac{dT_s}{dt} = \beta h_t (T_g - T_s) - \dot{m}^{ev} \lambda \end{cases} \tag{4.16}$$

The two parameters α and β are used to tune the model to obtain a prediction in accordance with the experimental evidence. These adaptive parameters include the effect of the rotational speed and the flights. In fact, the mass transfer coefficient is obtained considering a correlation for a condition that is similar to the real one, but not the same one. Some considerations need to be done. First of all the particle is not spherical while the model assumes that. The model assumes a fixed particle that meets the air flow for the whole time. In spite of what happens in the drum, where the particle is dried only while falling in the cascade. Moreover the particle is not isolated during the drying process.

When α and β are set, it is possible to evaluate the dryer performances in different operative conditions. Since the parameters are specific for the particle motion regime, the model can predict the drying behaviour at different air inlet conditions and flow rates, keeping constant the rotational speed and the flights number and shape.

4.2.2 Numerical results

The 0D model requires to be tuned by experimental results. The tests DD is chosen in accordance with the previous considerations on the drying performances obtained at 260 °C. It occurs in constant rate up to u=20% as shown in Figure 3.41. The input variable of the model are the initial amount of manure, its moisture content, its temperature (20 °C) and the air characteristics which are collected in test DD

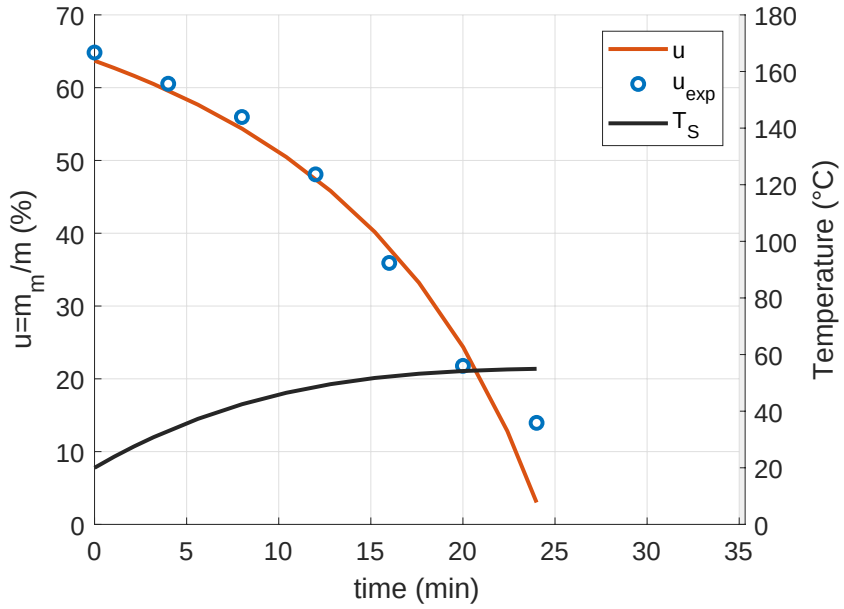

Figure 4.2: Numerical vs experimental evaluation of manure drying at 260 °C, 30 $m^3\,h^{-1}$, *30 rpm, 4 flights, H=10%:* α*=1.75e-2* $kg\,m^{-1}$; β*=3.75e-2* m^2.

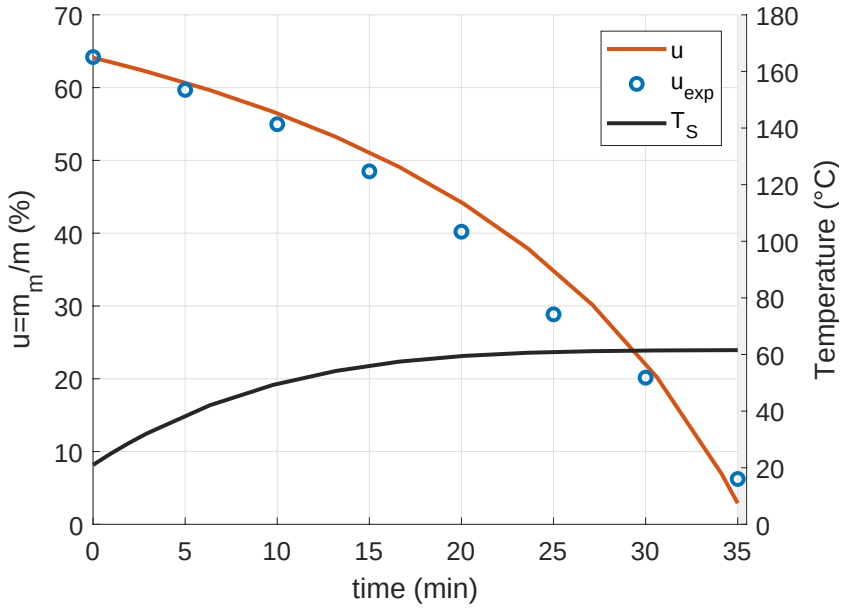

Figure 4.3: Numerical vs experimental evaluation of manure drying at 200 °C, 30 $m^3\,h^{-1}$, *30 rpm, 4 flights, H=10%:* α*=1.75e-2* $kg\,m^{-1}$; β*=3.75e-2* m^2.

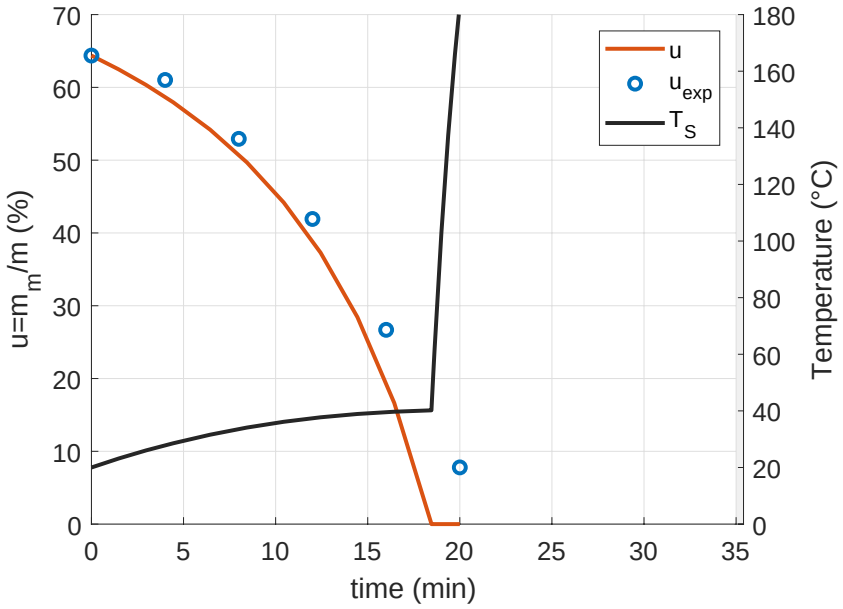

Figure 4.4: Numerical vs experimental evaluation of manure drying at 320 °C, 30 $m^3\,h^{-1}$, *30 rpm, 4 flights, H=10%:* α*=1.75e-2* $kg\,m^{-1}$; β*=3.75e-2* m^2.

row in Table 3.16.
The adjustable parameters α ($kg\,m^{-1}$) and β (m^2) are obtained by trial and error procedure. They are specific for the particle motion conditions inside the dryer and their tuning is crucial to fit the experimental data. In fact, they allow to relax the strong assumptions of fixed isolated particle taking into account the rotation speed, the shape and the number of flights, the particle swarming effect during the cascade and the airborne-dense phase ratio inside the drum. The couple which ensure a good fitting is:α=1.75e-2 $kg\,m^{-1}$ and β=3.75e-2 m^2. The numerical result fits pretty well the experimental points up to u=20% which is already beyond the interval of interest (see Figure 4.2). The solid temperature increases up to the wet bulb temperature of the drying air, which is the surface one. There are not experimental measurement on the solid temperature but the numerical result could be reasonable because the manure could be handle with hands at the end of the test without gloves.

The tuned model can predict the drying behaviour in different conditions if the motion conditions are kept constants. To verify it, two model runs at 200 °C and 320 °C are performed. Then they are compared to the experimental test CC and test EE. (Table 3.16). In Figure 4.3 the predicted numerical drying curve is compared to the experimental one at 200 °C. The model fits fairly good the experimental data although it underestimates a bit the effect of the temperature on the mass transfer, in fact the calculated curve stays over the experimental points for a while. While

overestimates the temperature effect on the heat transfer, showing an increase in the solid temperature faster than in the previous simulations (260 °C).
Increasing the temperature at 320 °C the numerical drying curve follows the experimental data as shown in Figure 4.4. The result is adequate despite the effect of air temperature on the mass transfer is overestimated by the model. In fact, the model predicts a little bit better performances than the experimental one. Moreover the temperature increases lower than the previous cases during the drying. Clearly the model is no more predictive when the drying is in decreasing rate. Whereas its interesting to observe that when the drying process is concluded (u=0% after 18 min), the solid temperature increases rapidly since the heat provided to the material is no more used by the moisture evaporation. This behaviour is coherent with the material physical behaviour. In first approximation, this means that until the material is not completely dry it does not drastically increase its temperature. If the material comes out the dryer at the set point the risk of undesired combustion is drastically reduced.
Besides from what expected, the model is not able to predict the effect of the air flow rates although its effect is included in the Reynolds number which appears, under square root, in both the mass and the heat transfer coefficient. It clearly appears that the flow rates impacts on the internal motion of particles.
The numerical model developed, is able to predict the manure drying behaviour for a batch process in different air inlet conditions. It is a very simple model that provides preliminary indications on drying performances for fixed internal motion regime, i.e., it allows to predict the temperature effect on the drying process.

4.3 Scale-up

This Section aims to provide a first rough estimation of the diameter, the length and the rotation speed of the full-scale rotary dryer. The scale-up is characterized by lot of empiricism. In fact, it could not be cautious to entrust the scale-up only to a physical based numerical modelling. The full scale rotary dryer must be tuned experimentally in order to adjust the operative parameters.

4.3.1 Model definition

The scale-up of cascading rotary dryer is supported by both the experimental and the numerical results. The input values are the volumetric manure flow rate and the specification of bot the air and the manure inlet and outlet conditions. The total holdup, the length-diameter ratio and the residence time are design specifications.
From pilot-scale to full-scale, the number and the shape of flights are kept constant

[24]. The ratio between centrifugal and gravitational forces acting on the particle is kept constant too [7].
The tested pilot-scale dryer is unable to continuously discharge material because it works in batch configuration. Even if the pilot-scale can continuously charge and discharge material, the dryer axial inclination angle must be determined experimentally on the full-scale dryer in order to reduce the scale effect [24]. The angle is increased from the horizontal until the residence time match the specification.
The air flow rate is estimated by solving simple mass and energy balances reported in Section 4.1. Geometrical specifications choices follows good design practical rules derived from the industrial past experience (see Table 1.2).

The dryer size (m^3) is estimated in function of the material residence time τ, the manure flow rate $\dot{V}$ and the total holdup H, as follows.

$$V_{drum} = \frac{\tau \cdot \dot{V}}{H} \tag{4.17}$$

In the industrial practice, the diameter and the length of the dryer have often been chosen simply by using a standard L/D ratio, since the dryer volume is already known.

$$D = \left(\frac{4 \cdot V_{drum}}{\pi \cdot LD} \right)^{1/3} \tag{4.18}$$

$$L = LD \cdot D \tag{4.19}$$

The desired axial velocity of the manure is obtained by a geometrical consideration.

$$v_z = L/\tau \tag{4.20}$$

In a full-scale dryer, this velocity needs to be achieved by varying the axis inclination from the horizontal: increasing the angle the velocity increases while reducing it, the effect is the opposite.

The rotation speed needs to be experimentally defined in pilot-scale (ω_p). It is the one that ensures the best cascade. It is transported in a full-scale (ω_f) keeping constant ν, which is the ratio of centrifugal to gravitational forces acting on the particle.

$$\nu = r_{e,p} \frac{\omega_p^2}{g} = r_{e,f} \frac{\omega_f^2}{g} \tag{4.21}$$

where r_e is the distance of the flight from the axis, ω is the angular speed (s^{-1}) and g is the gravity constant ($m^2\,s^{-1}$).

Table 4.3: Scale-up input variables.

Design specifications			**Assumptions**		
$\dot{m}_{s,wb}$	45	$kg\,h^{-1}$	$T_{s,out}$	30	°C
X_{in}	1.5	$kg_m\ kg_d^{-1}$	$T_{g,out}$	60	°C
X_{out}	0.429	$kg_m\ kg_d^{-1}$	$\dot{Q}_{loss}$	$0.1 \cdot \dot{Q}_{tot}$	$J\,kg^{-1}$
$T_{s,in}$	10	°C	tau	12	min
$T_{g,in}$	260	°C	H	10	%
Y_{in}	0.0245	$kg_v\ kg_{da}^{-1}$	L/D	4	-

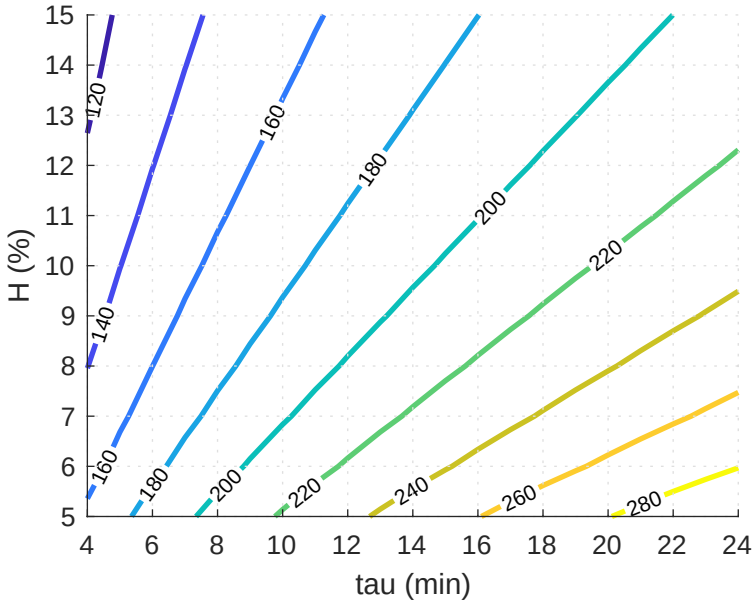

Figure 4.5: Rotary dryer length (cm) for L/D=4.

Table 4.4: Scale-up results.

L	**D**	$\boldsymbol{\omega}$	$\mathbf{v}_g$	$\mathbf{v}_s$
m	m	rpm	m/s	cm/min
1.9	0.47	22	0.38	15.6

4.3.2 Numerical results

The preliminary investigation starts setting the productivity to achieve: since the furnace size is 70 kW, the wet manure flow rates is 45 kg h^{-1} at 60%.
The input variables are the air inlet conditions and the manure conditions which are summarized in Table 4.3. It is assumed to use flue gasses at 260 °C and to collect them in the outlet at 60 °C as experimentally observed in test DD. An indicative information on the air flow rates is obtained by solving the thermodynamic balances.
In order to determine the rotary dryer size it is necessary to assume the internal solid holdup (H), the length-diameter ratio (L/D) and the residence time (τ). A compact dryer can be obtained by assuming a low L/D ratio. Assuming it equal to 4, the pattern of H vs τ possibilities can be obtained. Figure 4.5 shows the drum length in function of the holdup and the residence time. Fixing the residence time, the length of the drum decreases by increasing the holdup. In fact, the holdup is inversely proportional to the drum volume, in turn, the length as shown in Equation 4.17. A residence time around 12 min is assumed in accordance with the experimental results obtained during the investigation of the air temperature effect. The holdup is set equal to 10% to remain in the middle of the good design practice. This couple identifies the drum which is 1.90 m length and 0.47 m diameter.
From this preliminary geometrical estimation, the corresponding velocity of the hot air flow inside the drum is 0.38 m s^{-1}, obtained from the first principle calculation ($\dot{V}_g$=240 m^3 h^{-1}), while the manure axial velocity is 15.6 cm min^{-1}.
The rotation speed is 22 rpm and its estimation starts from the experimental values since the centrifugal to gravitational force ratio ν acting on the particles and the flights shape are kept constant from pilot to full scale. The results are collected in Table 4.4.
The choice of the axis inclination needs to be experimentally determined to ensure the residence time. Moreover the number of flights could be the same of the pilot scale but they are essential for the cascade creation so their number needs to be adjusted.
To sum up, this scale-up provides a general indication on the size of the full-scale rotary dryer. Then the dryer optimization will be experimentally carried out to determine the best set of duty parameter.

Chapter 5

Conclusions

In this work an experimental investigation on horse manure drying is performed in order to make this biomass suitable to combustion in customized furnaces where drying and burning are cascaded and integrated.

The aim of this work is two-fold: (i) to comparatively select the proper drying device and (ii) to evaluate the impact of the design variables (i.e, dryer geometry and drying air condition) on drying performance.

It was experimentally demonstrated that:

- The drying section must be separated from the storage section. As for the aerated hopper, a low drying bed height is to be preferred. In fact, there are air preferential paths that determine strong inhomogeneity in the moisture final distribution. Low bed heights guarantee more homogeneity in the moisture content, more homogeneous progression of the front of drying and less pressure drop through the bed.

- The wet material handling between the storage and the drying section is critical due to the inherent extreme variability of the material properties and stickiness: a dynamic device is required. Moreover in the static dryers, the dry material results in a unique solid mass like a monolith, impossible to discharge. For instance an economic and mature technology suitable to this aim could be the manure spreaders used in agriculture.

- The rotary dryer is selected as the most suitable drying device because it keeps the material mixed and fluffy during the drying and ensures an homogeneous moisture content in both time and space. In addition, it can be easily scaled within a wide range of productivities.

The variables influencing the drying can be grouped in two classes: (i) those affecting the degree of contact between the air and the material and (ii) the characte-

ristics of the drying air (i.e, temperature, absolute humidity, flow rate).

The air-material contact depends on the dryer configuration and it is the core of the drying process. The comparative investigation on different devices showed that:

- In the static devices (i.e. aerated hopper, packed fixed bed) the "flow through bed" configuration is realized. All the air flows through the material bed without dispersion. However the creation of preferential paths and the wall effect are diffuse due to the heterogeneity of the material.

- In the rotary dryer, the cascading rotary dryer configuration ensures a stronger interaction between the air and the material than the through circulation one. The creation of a material curtain hit by the dryer airflow is crucial. It depends on the coupled effect of the rotation speed and the number of flights: the drying time is reduced up to 25% by increasing the rotation speed from 30 to 50 rpm with 2 flights; while increasing from 2 to 4 their number the drying time is not affected by the increase in the rotation speed from 30 to 50 rpm.

The analysis of the drying curves have been carried out to quantitatively investigate the effect of the drying air characteristics on the drying process.
In particular, the experimental analysis on the drying air has highlighted that:

- The air temperature strongly impacts on both the heat and the mass transfer. Ambient air (around 30 °C) performs the drying in the order of 2 hours. While at higher temperatures (75 °C), the drying time is reduced up to 66%. For instance, an increase of temperature from 150 to 380 °C (at constant particles motion condition and air flow rate) reduces the drying time from 28 to 12 min.

- The hot combustion flue gasses with high specific humidity can be used in the drying process because the high performances achieved are the same of the dry air at the same temperature. This allows to simplify the plant layout since avoids the need of a drying air-flue gasses heat exchanger, reducing the number of unit operations.

- The air flow rates carry the enthalpy to the system. The general trend is: the higher the flow rates and the shortest the drying time. The airflow cannot be increased too much because it becomes too energy consuming and increases the particles entrainment. It is suggested to keep the air velocity lower than $0.2\,\mathrm{m\,s^{-1}}$ to preserve the cascade.

Moreover a 0D rotary dryer model was developed. The numerical investigation highlighted that the air effect on the manure drying process can be predicted quite well for fixed internal motion conditions and air flow rates.

Bibliography

[1] Treybal R. E. *Mass transfer operations*. McGraw - Hill, 1980.

[2] Reay D. A scientific approach to the design of continuous flow dryers for particulate solids. *Multiphase Science and Technology*, 4:1–102, 1989.

[3] Lewis W.K. The rate of drying of solid materials. *Industrial Engineering*, 13:427–443, 1921.

[4] Marshall W. R. Jr. Hougen O. A. The rate of drying of solid materials. *Am. In. Chem. Eng.*, 38:91–121, 1942.

[5] Purlis E. Modelling convective drying of foods: A multiphase porous media model considering heat of sorption. *Journal of Food Engineering*, 263:132 – 146, 2019.

[6] Mujumdar A. S. *Handbook of Industrial Drying*. CRC Press, 2014.

[7] Kemp C. I. Oakley D. E. Modelling of particulate drying in theory and in practice. *Drying Technology*, 20(9):1699–1750, 1989.

[8] Bengtsson P. Experimental analysis of low-temperature bed drying of wooden biomass particles. *Drying Technology*, 26(5):602–610, 2008.

[9] Lerman P. Wennberg O. Experimental method for designing a biomass bed dryer. *Biomass and Bioenergy*, 35:S31–S39, 2011.

[10] Tiina Myllymaa, Henrik Holmberg, and Pekka Ahtila. Techno-economic evaluation of biomass drying in moving beds: The effect of drying kinetics on drying costs. *Drying Technology*, 37(10):1201–1214, 2019.

[11] Klavina K. Cinis A. Zandeckis A. Experimental study on the effects of air velocity, temperature and depth on low-temperature bed drying of forest biomass residue. *Energy Procedia*, 72:42–48, 2015.

[12] Pang S. Mujumdar A.S. Drying of woody biomass for bioenergy: Drying technologies and optimization for an integrated bioenergy plant. *Drying Technology*, 28:690–701, 2010.

[13] Xu Q. Pang S. Modelling of rotary drying of woody biomass. *Drying Technology*, 26:1344–1350, 2008.

[14] Silva M.G. Lira T.S. Arruda E.B. Murata V.V. and Barrozo M.A.S. Modelling of fertilizer drying in a rotary dryer: parametric sensitivity analysis. *Brazilian Journal of Chemical Engineering*, 29(02):359 – 369, 2012.

[15] Baker C.G.J. The design of flights in cascading rotary dryers. *Drying Technology*, 6(4):631–653, 1988.

[16] Perry R.H. Green D.W. *Perry's chemical engineers' handbook.* New York: McGraw-Hill, 2008.

[17] ALMOIT s.r.l. https://www.almoit.com, 2020, 1 settembre.

[18] Da Lio L. Castello P. Gianfelice G. Cavalli R. Canu P. Effective energy exploitation from horse manure combustion. *Waste management - under review.*

[19] M. Nitsche, F. Hensgen, and M. Wachendorf. Energy generation from horse husbandry residues by anaerobic digestion, combustion and an integreted approach. *Sustainability 9, 358*, 2017.

[20] Z. Cui, J. Shi, and Y. Li. Solid-state anaerobic digestion of spent wheat straw from horse stables. *Bioresource Technology 102: 9432-9437*, 2011.

[21] J. Lundgren and E. Petterson. Combustion of horse manure for heat production. *Bioresource Technology 100: 3121-3126*, 2009.

[22] Boateng A. A. *Rotary Kilns: Transport Phenomena and Transport Processes.* Butterworth-Heinemann, 2008.

[23] C. Fyhr and I.C. Kemp. Evaluation of the thin-layer method used for measuring single particle drying kinetics. *Chemical Engineering Research and Design*, 76(7):815 – 822, 1998. Particle Technology.

[24] S. E. Papadakis, T. A. G. Langrish, I. C. Kemp, and R. E. Bahu. Scale-up of cascading rotary dryers. *Drying Technology*, 12(1-2):259–277, 1994.